Energetic Analysis and Optimisation Strategies of a Modern Northern European Supermarket

Von der Fakultät für Maschinenbau

der Technischen Universität Carolo-Wilhelmina zu Braunschweig

zur Erlangung der Würde

einer Doktor-Ingenieurin oder eines Doktor-Ingenieurs (Dr.-Ing.)

genehmigte Dissertation

von:	**Maren Titze**
aus (Geburtsort):	**Nürnberg**
eingereicht am:	**11.07.2016**
mündliche Prüfung am:	**30.06.2017**
Gutachter:	**Prof. Dr.-Ing. Jürgen Köhler**
	Prof. Petter Nekså

2017

Hereby, I’d like to thank everyone who supported and accompanied me during the development of this thesis. My particular thanks go to my doctoral supervisor Prof. Dr-Ing. Jürgen Koehler for the content-related mentoring and support. Moreover, I want to thank my second supervisor Prof. Petter Nekså for the assessment of my thesis. Special thanks go to Nicholas Lemke for all the helpful discussions and the encouragements during the development process. Moreover I want to thank Christian Schulze for the support in terms of the simulations models. Thank you Matthias Kwak for spending some evenings saving my data. Thank you Nicolas Fidorra and Armin Hafner for the support and several discussions about supermarket systems. I thank all my project partners, especially from Danfoss and SystemAir for helping me and providing useful information. Thank you also to all my students that helped me with their scientific work and the development of several models and evaluations. Thank you to all my colleges from the Institut für Thermodynamik and from SINTEF for the conversations, support and help. Thanks to all my lunch break and fruit break friends and to all colleagues for giving me such a pleasant time at the IfT. And last but not least, I want to thank my family and all my friends that emotionally supported me during this intensive time, believed in me and affirmed me to finish this work.

Content

List of symbols

Latin symbols

A	area	$[m^2]$
c	concentration	$\left[\frac{g_{CO2}}{g_{air}}\right]$
A_S	sales area	$[m^2]$
c_p	specific isobaric heat capacity	$\left[\frac{J}{kg\ K}\right]$
E	emissions	$\left[\frac{m^3_{CO2}}{s}\right]$
$\Delta\overline{F}$	mean overall error	$[-]$
h	specific enthalpy	$\left[\frac{J}{kg}\right]$
I	radiant intensity	$\left[\frac{W}{m^2 * \mu m}\right]$
l	length/ thickness	$[m]$
$\dot{m}$	mass flow	$\left[\frac{kg}{s}\right]$
$K(\lambda)$	luminous efficacy	$\left[\frac{lm}{W}\right]$
p	pressure	$[Pa]$
P	power (consumption)	$[W]$
$\dot{Q}$	heat flow	$[W]$
R	thermal resistance	$\left[\frac{K}{W}\right]$
R_S	solar radiation	$\left[\frac{W}{m^2}\right]$
T	temperature	$[K]$

V	volume	$[m^3]$
$\dot{V}$	volume flow	$\left[\frac{m^3}{s}\right]$
W_e	energy intensity	$\left[\frac{kWh}{m^2}\right]$
x	absolute humidity	$[-]$
$\Delta\overline{x_1}$, $\Delta\overline{x_2}$	mean individual error	$[-]$
y	measured value	$[-]$
$\hat{y}$	simulated value	$[-]$

Greek Symbols

α	heat transfer coefficient	$\left[\frac{W}{m^2\,K}\right]$
λ	thermal conductivity	$\left[\frac{W}{m\,K}\right]$
λ	wavelength	$[nm]$
ρ	density	$\left[\frac{kg}{m^3}\right]$
τ	transmittance factor	$[-]$
φ	relative humidity	$[\%]$

Indices and abbrevations

AE	aerogel
AEW	aerogel window
$AirCu$	air curtain
$AHXC$	air heat exchanger cooling

$AHXH$	air heat exchanger heating
AHU	air handling unit
$AHUSR$	air handling unit staff room
amb	ambient
$AUWH$	additionally usable waste heat
BC	base case
BHX	borehole heat exchanger
BP	bypass
CO_2e	CO_2 equivalent
$comp.ref.$	compressors of the refrigeration plant
DC	dry cooler
DO	door openings
EE	extra evaporator
$el.dev.$	electrical devices
exh	exhaust
F	fruits
FH	floor heating
GC	goods delivery area
GDA	gas cooler
GHG	greenhouse gas
GWP	global warming potential
HFC	hydrofluorocarbon
HP	high pressure
HPC	high pressure compressor
$HVAC$	heating, ventilation and air conditioning
HXC	heat exchanger for cooling
IHX	internal heat exchanger
ins	insulation

LED	light emitting diode
liq	liquid
LP	low pressure
LPC	low pressure compressor
LT	low temperature
LTC	low temperature cabinet
MAE	mean average error
$MAPE$	mean average percentage error
max	maximum
$meas$	measurements
MT	medium temperature
MTC	medium temperature cabinet
NAE	natural air exchange
$NAER$	natural air exchange rate
opt	optimal
P	people
PE	polyethylene
PFC	perfluorocarbons
ret	return
RW	rotary wheel
RWS	rotary wheel supply air side
SFA	sales floor area
sim	simulations
$subs.$	sub system
sup	supply
SM	snow melt
UWH	usable waste heat
vap	vapour

VLE	vapour-liquid-equilibrium
WH	waste heat
WD	window

List of figures

List of tables

1. Introduction

The task of this thesis was the analysis of the energy efficiency and the investigation of energetic saving potentials in northern European supermarkets. For this purpose, field measurements were carried out in a test supermarket in Norway. Furthermore, a simulation model of the supermarket was designed and validated.

1.1. Motivation

Supermarket refrigeration systems are responsible for more than 30 % of the refrigerant greenhouse gas consumption in Europe [1]. The worldwide contribution of supermarkets to greenhouse gas emissions is 33 % and estimations suggest that by 2050 overall food production will have increased by 70 % [2], of which a considerable part will probably be consumed by supermarket systems. The share of supermarkets in the total power consumption in Europe is about 3 % [3]. Due to the 20-20-20 goals of the European Union, greenhouse gas emissions are to be reduced by 20 % compared to 1990, energy efficiency is to be increased by 20 % and 20 % of energy should come from renewable sources by 2020 [4]. In addition, power savings in supermarkets have a direct positive impact on profits and a “green image” can help to attract customers.

Supermarkets and their energy efficiency differ considerably. They range from convenience stores with less than 280 m^2 sales floor area (SFA) to hypermarkets with more than 10,000 m^2. So-called discount stores with an SFA of about 1,000 m^2 are increasingly popular in Europe. In Norway, 55 % of the turnover is achieved by discounters, as compared to 41 % in Germany and Belgium [5]. One advantage is their unique design and product range. Discount stores are often located in stand-alone buildings that are designed only for this purpose and can be built fast and at low cost. However, their energy efficiency can be poor due to cheap equipment and the lack of an energy efficiency strategy. The power consumption in supermarkets comprises several end-users that influence each other, such as refrigeration, heating, ventilation and air conditioning (HVAC) or illumination. This means that individual consideration of each sub-system does not automatically lead to an improvement of the overall power consumption. If the efficiency of one component is improved, this can affect the efficiency of another component. Consideration of the overall system, heat recovery and the development of an advanced control system are key parameters for achieving a minimum energy supermarket.

1.2. Background

This thesis was developed as part of a cooperation of the Institut für Thermodynamik of Technische Universität Braunschweig and SINTEF, the largest independent research organisation in Scandinavia. The thesis was mainly realised within the CREATIV project [6]. The main objective of this project was the development of new energy efficient heating and cooling technologies

in industry applications and strategies for reducing primary power consumption and greenhouse gas emissions of Norwegian industries. A consortium of 17 partners from industry and research and development worked together on the topics of “Electricity production from surplus heat”, “Utilisation of thermal energy” and “Efficient heating and cooling”. In addition, four PhD positions and two postdoctoral positions were created and several master theses and student works were incorporated. Beyond the research part of the project, case and innovation processes were carried out in direct collaboration with industrial partners. In this way, the newly developed models and approaches could be validated. These cases were divided into three groups: “Energy effective industry clusters – Utilization of surplus heat at various temperatures”, “Supermarkets – Total integrated energy systems and component development” and “Food industry – Control and heat pump systems”.

This thesis was undertaken as part of the second group named above. A discount store of the Norwegian merchandise retailer REMA 1000 was designed and built in Trondheim (Kroppanmarka). Danfoss, Carrier and Systemair, among others, contributed to the technical implementation. An overall monitoring system was installed in the supermarket, providing access to about 600 measurement values, which were continuously logged and saved. The shop was opened in August 2013.

1.3. Purpose and method

Supermarkets are complex systems with a range of factors that influence power consumption. Overall power consumption is often measured in supermarkets, but detailed information about the power consumption of the sub-systems is rarely available. In addition to the efficiencies of the installed sub systems, such as the refrigeration plant and HVAC, the interaction between them plays a major role. Heat recovery can be implemented in different ways in a supermarket. Apart from a proper design, the key to minimum power consumption is an advanced control strategy. The aim of this work was to analyse the power consumption in a reference supermarket, to evaluate the relationship between control and energy efficiency, and to develop a control strategy that leads to reduced power consumption. This thesis consists of two parts. In the first part, a detailed analysis and disaggregation of the supermarket's power consumption was carried out. For this purpose, the available measurement data for the major part of the year 2014 were evaluated. Conclusions were drawn about the influence of ambient and internal conditions on the power consumption of the supermarket. In the second part, these conclusions were used as a basis for developing a control strategy and identifying measures to increase energy efficiency. A dynamic model was created in order to test the control strategies and measures. Unlike other simulative approaches which produce different smaller or steady-state models, one highly dynamic overall model was developed. The building, the technical equipment including the refrigeration system, HVAC and secondary

loops were considered within one model. This was crucial for investigating the internal interactions, but made the approach challenging, due to the complexity of the modelled supermarket, very different time constants of the sub-systems and the presence of several controllers. A complex model with high simulation times was built.

1.4. Scientific relevance and novelty of the work

Different works were carried out in order to analyse the power consumption in supermarkets and to deviate savings strategies. These analyses were usually either done by measurements or simulations.

The advantage of measurements is that the gained results are often more reliable compared to simulations. The disadvantage is that, in many cases, it is difficult or impossible to test and compare different scenarios like control strategies or technical equipment for equivalent ambient conditions. Moreover, the amount of measured data is often limited. In some cases, only the overall power consumption is available without disaggregation. Detailed information about temperatures, humidities and mass flows are often not available. Thus, assumptions have to be made that can distort the results.

The advantage using simulations is that a lot of scenarios can be tested quickly. Cases that cannot be tested in a real supermarket out of safety reasons or because they might have a negative impact on the indoor climate or refrigerated goods can be simulated and evaluated. The disadvantage of simulations is that, dependent on the model quality, high simulation errors can occur, which, again reduces the reliability of the results.

Besides this, in some approaches, both methods are combined. Anyway, usually the used models are very simple in order to make sure that the overall supermarket system can be simulated in a short time. If more complex and detailed models were used, they usually only include parts of the system, like the refrigeration system or the building. Sometimes, different models are combined post-processing. In these cases, either the processes in the different sub systems or the interactions between the sub-systems are nor considered properly.

In this thesis, both methods, simulation and measurements, were combined. Over 600 measurement devices were installed in a test supermarket. The measured values during one year were proved and missing values were calculated in a complex evaluation process. These evaluations could not only be used to analyse the annual energy efficiency of the supermarket, but also to create a base on which a model could be developed and validated. The developed model included all the sub systems in a detailed way, including pressure drops, mass flow distributions and controllers as well as interactions with each other. The building, refrigeration plant, air handling unit as well as secondary loops were considered. By the combination of these both methods, a reliable statement about the power consumption of the test supermarket could be made. Subsequently, different optimisation strategies were developed and

evaluated. Even though only one specific supermarket was considered, some of the results can be transferred to other systems as well. Especially because the considered supermarket was a discount store in a stand-alone building, which is a widespread system all over Europe.

2. Technical supermarket systems

Across the globe, supermarket systems vary in size, product range, building type, technical equipment, staff and customer behaviour etc. In many cases, low energy efficiency refrigeration and HVAC systems were incorporated due to low acquisition prices. However, in recent years, the interest in energy efficiency has grown, including in supermarkets. This has led to the interaction between refrigeration and HVAC system, including heat recovery, being considered and more efficient equipment being used. This chapter gives an overview of the most common technical equipment in supermarkets.

2.1. Refrigeration

The refrigeration system is one of the main energy consumers in many supermarkets and among the most important technical equipment. Depending on the type and size of supermarket as well as the amount of chilled goods, the cooling capacity can vary from zero to several hundred kW. Display cabinets are normally used to store chilled food, but some supermarkets are also equipped with completely chilled rooms. Before being placed in the display cabinets, the food has to be stored in storage rooms. There are two temperature levels for the storage of goods: normal temperature cooling or chilling is used for vegetables or dairy products, for instance, and the temperature level of the chilled goods is about 2°C to 4°C; frozen goods, such as ice cream or frozen pizza, are usually stored at temperatures of -12°C to -18°C. The evaporation temperature is usually between –15°C and 5°C for normal temperature cooling and between -30°C and -40°C for low temperature cooling [7].

There are several technical possibilities for providing the required cooling capacity. The refrigeration systems can be divided into two different types: plug-in units and centralised systems. Plug-in or stand-alone units are display cabinets with an internal refrigeration cycle, which operate independently of each other. The waste heat from the condenser is usually released directly into the sales area. Central or remote systems include a central refrigeration plant with one or more compressors, condensers and valves. The main part of the system is usually located in the machine room, with the condensers often placed on the rooftop. There are two different centralised systems: direct and indirect ones. In direct systems, the evaporators are located in the cabinets and the refrigerant is passed directly from the machine room into the evaporators via tubes. When it comes to indirect systems, there is a difference between completely and partially indirect systems and indirect cascade systems. In indirect systems, the evaporator is usually situated in the machine room and used to cool the brine in a secondary

loop that is connected to the cabinets. Combinations of direct and indirect systems are commonly used in supermarkets. In many cases, separate refrigeration plants are installed for cooling and freezing. Sometimes, plug-in units are used for freezing and remote refrigeration for chilling, while in other cases chilling is realised with a direct remote system and freezing with an indirect system. A detailed description of the different systems can be found in the doctoral thesis of Arias [7].

The main advantage of stand-alone units is the small amount of refrigerant required. In addition, many supermarket owners appreciate the flexibility, easy maintenance and exchangeability, although they are often inefficient. Moreover, waste heat recovery cannot be controlled and waste heat is simply released into the sales area throughout the year. This can be advantageous in winter, but can lead to a high cooling demand in the building during the summer. Direct centralised systems have a much higher refrigerant demand due to long tubes which are necessary to circulate the refrigerant between the machine room, the sales area and the rooftop. 4-5 kg of refrigerant are typically used per kW cooling capacity in a centralised direct system [8]. This leads to more leakages and, consequently, to a higher direct global warming potential (GWP). On the other hand, the efficiencies of direct centralised systems are usually high and the indirect greenhouse gas (GHG) emissions lower. In order to reduce leakages, indirect systems with much lower refrigerant charge can be used. The disadvantage of indirect systems is the low efficiency compared to direct systems due to additional temperature differences [9] and the pump work necessary to circulate the brine [10]. Nevertheless, centralised systems provide a flexible way of handling waste heat. Heat recovery is possible in wintertime, while the waste heat can be rejected to the ambient during the summer. In systems with high refrigerant charges, the GWP of the refrigerant is crucial. Refrigerant leakage can be very different depending on the system. According to Cortella et al., direct emissions account for a share of 20 % in HVAC systems and 60 % in refrigeration systems [11]. Leakage rates of 1 - 5 % per year for integral equipment and 10 % - 30 % for remote systems were reported [3], [12]. The high leakage rates in centralised systems are mainly due to the large number of fittings. The direct GWP in a system depends on the leakage rate, the kind of refrigerant used and the electricity mix of the respective country.

Due to the banning of CFCs and HCFCs in the late 1980s [13], those refrigerants were often replaced with hydrofluorocarbons (HFC) or fluorocarbons (PFC). R-404a is still widely used for supermarket refrigeration [14]. HFCs and PFCs have no ozone-depleting potential, but their GWPs are several thousand times higher than those of CO_2. Different regulations were put in place to reduce their use [15], [16]. The objective of the latest regulation was to ban refrigerants with GWPs higher than 150 in centralised systems (>40 kW) from 2022 onwards, with the exception of the primary cycle in cascade systems, where GWPs up to 1500 are allowed. Some countries, such as Sweden, also put heavy taxes on HFC in order to promote the use of natural refrigerants [17]. This shows that, for a long term solution, an alternative to HFCs and PFCs

has to be found. Natural refrigerants have negligible GWPs, but many are flammable or toxic. Using CO_2 as a refrigerant has several advantages: the GWP is minimal, the ozone-depletion potential is zero and it is neither flammable nor toxic. Though, it is suffocating at concentrations of 4-8% or higher. Moreover, the heat transfer performance is superior to HFC refrigerants due to its high density, latent heat, specific heat, thermal conductivity and volumetric cooling capacity, and its low viscosity. Smaller components and tubes can be used and the pressure drop is much lower than in equivalent remote systems. The main disadvantages in comparison with other refrigerants are the high operating pressure and the low critical temperature.

The development of supermarket CO_2 refrigeration systems started in Scandinavia and is now becoming increasingly popular across Europe, North America and Australia [3]. Around 3,000 trans-critical CO_2 supermarket refrigeration systems are currently installed in Europe. The number of CO_2 systems has grown considerably in the last few years. Especially in Denmark, UK, Germany, Switzerland, Norway and Sweden CO_2 is a popular refrigerant for supermarket applications [18]. Due to this spread, components for CO_2 refrigeration systems can be produced in much larger quantities, become much cheaper and can consequently compete with those of conventional systems.

In supermarkets, CO_2 can be used either in indirect [19], cascade [20] or all CO_2 trans-critical systems [21]. In overall CO_2 systems, the system operates in trans-critical or sub-critical mode, depending on the ambient temperature. In the trans-critical mode, “gas cooling” takes place after compression instead of condensation.

2.2. HVAC

Power consumption for heating, cooling and ventilation in supermarkets can vary considerably and depends on several factors. The geographic location and the size of the market influence the heating or cooling demand. Furthermore, supermarkets are extremely complex buildings with many heat sources and sinks. The north-south-orientation, condition and insulation of the building and windows determine the space heating requirements, as well as internal loads from illumination, plug-in units and other electrical devices. Lower efficiencies of the technical internals lead to higher heat loads and reduce the heating demand of the building in winter but increase the cooling demand in summer. Air infiltration can occur in traffic doorways, depending on the type of door and the frequency of door openings. Air curtains, automatic doors and sluices with two sets of doors are often installed in order to reduce infiltrations. Air leakage can also occur when all doors and windows are closed, depending on the tightness of the building envelope.

The size and especially the type of refrigeration plant has a significant impact on the heating and cooling demand. Integral refrigeration units release heat into the building, whereas centralised systems absorb heat from the shop. The amount of heat load depends on the size and design of the plant and the presence of glass doors or air curtains. In addition, the control of the HVAC system also determines the heating or cooling demand. Depending on the heating demand, the volume flow can be set constant and the fans can be controlled. The ratio of fresh air to recirculated air supplied to the shop can be controlled via the CO_2 content in the sales area [22], [23], [24], which leads to a reduction of the exhaust air fan speed. Nevertheless, the volume flows are often kept constant [3], possibly because this is easier to control. Some countries, such as the UK, have regulations about minimum fresh air volume flow [25], whereas in other countries, such as Germany, indoor air requirements refer to the CO_2 content in the air [26]. The power consumption of the fans also depends on internal and external pressure drops of the HVAC. Internal pressure drops are caused mainly by filters and heat exchangers, external pressure drops by the ducts of the distribution system. Internal pressure losses can be reduced, for example, if components are bypassed while they are not in use.

3. Power consumption in supermarkets

There are different challenges in determining and assessing the energy performance of supermarkets. Power consumption depends on several conditions and factors. A completely fair comparison of different markets would take into consideration all boundary conditions, including weighting factors, which is almost impossible. Capturing measurement data is another challenge. In many supermarkets, power consumption is measured, but not necessarily disaggregated into individual consumers. For a detailed analysis, the power consumption of all end users, ambient and indoor climate conditions, number of customers and personnel and refrigeration load would have to be measured. The installation of detailed measurement equipment is complicated and expensive and would be hard to afford for owners of very small shops. Moreover, physical data, such as geographic location, but also details about the building such as structure, materials, insulation and window area, have to be known for a comparison. Nevertheless, different analyses of supermarket systems have been carried out, either by measurement, simulation or both. Some of the research results will be presented in the following.

3.1. Overall consumption and disaggregation

The composition of power consumption in supermarkets is complex. Figure 3-1 shows the influencing factors and interactions between factors. Internal equipment, control strategies, location and type of building, weather conditions, size and kind of supermarket are some of the parameters which determine the energy performance.

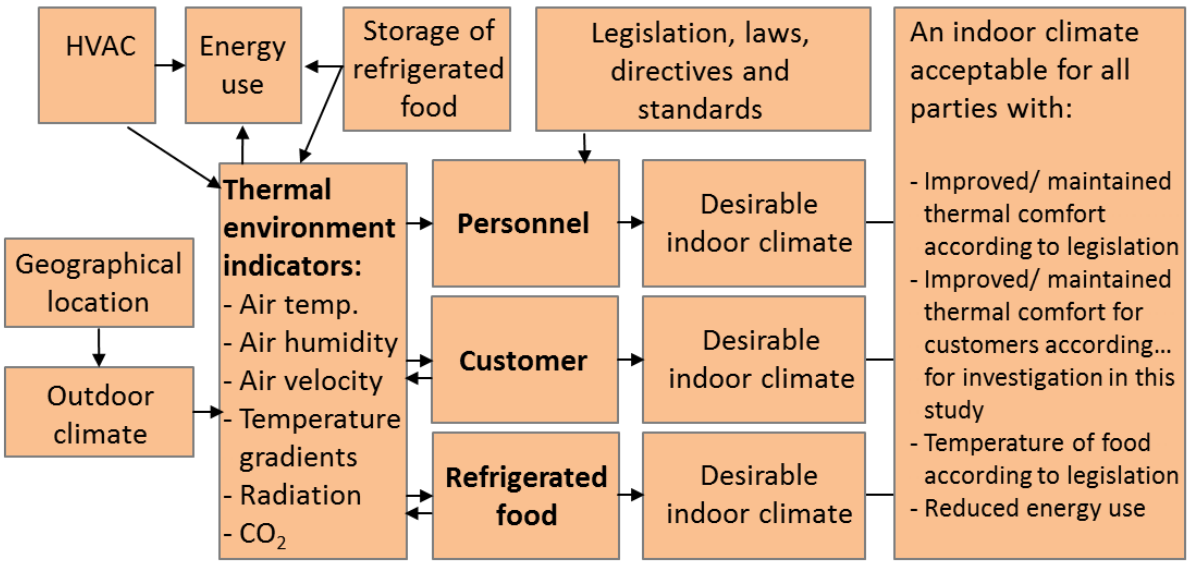

Figure 3-1: Complexity the supermarket's power consumption **[27]**

In industrial countries, the power consumption of supermarkets accounts for about 3 - 4 % of the overall power consumption and 1% of greenhouse gas emissions [23], [28], [29], [3], [30].

The contribution of the refrigeration plant to the overall power consumption in supermarkets accounts for about 25 - 60 % [31], [32], mainly depending on the size and efficiency of the refrigeration system and the location of the shop.

A British study showed that the average power consumption in supermarkets using predominantly integral refrigeration equipment is about 300 kWh/m^2 higher than in those using remote refrigeration. With an average power consumption of 1480 kWh/m^2, this is equivalent to a share of 20 % [3].

The efficiency of trans-critical systems is often lower than in an equivalent R-404a cycle. However, at low ambient temperatures the efficiency of CO_2 systems can be higher than that of R-404a systems [33], [34], [35]. In northern European countries like Norway, Sweden, Denmark, Germany or even Switzerland, it can be advantageous to use CO_2 as a refrigerant, if the system can be operated in subcritical mode for most of the time [33]. Several publications have compared CO_2 systems to conventional systems. One study showed that CO_2 trans-critical systems have a higher performance than R-404a systems for ambient temperatures below 21°C and a similar performance in the crossover region between 25°C and 21°C [34]. Sawalha measured a crossover point at 23°C [36]. Sharma et al. suggest that for the northernmost two thirds of the US, the performance of a well-designed CO_2 system is equal to or higher than that of an R-404a system [37]. Another study showed that in a cold climate, an energy reduction of up to 18 % is possible using a CO_2 trans-critical booster system, as compared to a conventional R-404a system. In hot climates, by contrast, savings of 11 % can be achieved with a cascade NH_3-CO_2 system [38]. Girotto et al. investigated a parallel CO_2 refrigeration plant in northern Italy and found that power consumption was 10 % higher than in a conventional

R-404a system [33]. Measurements in a German supermarket [39] and simulations in a typical UK supermarket [35], both for one year, showed a similar energy efficiency of CO_2 and conventional systems. Besides this, one advantage of CO_2 plants is their heat recovery potential. A reduction in space heating of 30 % in winter and 100 % in summer was determined by Ge et al. [29]. When CO_2 refrigeration plants are compared to conventional systems, the reduction in space heating should always be taken into account. Recent developments, such as the incorporation of ejectors, can further increase the performance of trans-critical systems [40]. Improvements in energy efficiency of up to 30 % have been shown [41]. In addition to the improved efficiency of refrigeration systems, different measures that lead to a reduction of the heat load to the cabinets are getting more common. In vertical display cabinets, 60 - 70 % of the cooling load is caused by infiltration [42]. Glass doors [43], night blinds and air curtains can significantly reduce the heat load to the cabinets and consequently the power consumption for compressors and fans of the refrigeration systems.

The power consumption of the HVAC system, which is about 8 - 28 % [3], [32] is influenced in part by the geographic location, but also to a considerable extent by the control strategy and the application of heat recovery. The cost for heating and cooling depends not only on the demand but also on the deployed heat sources. Gas or electrical heating are commonly used. One study showed that in British supermarkets, gas has a share of about 20 % in the total power consumption [44]. If heat recovery from the refrigeration plant is employed, these costs can be reduced considerably. In the literature, savings of 40 % to 80 % have been described [7], [35], [45]. The amount of recoverable heat from the refrigeration plant depends on the refrigeration system, the control and the recovery system. Heat storage can be used for balancing the heat supply of the refrigeration system and the heat demand of the building. If floor heating loops are installed, the waste heat can be used at a lower temperature level, which leads to an increase of the usable share of the waste heat from the refrigeration system. By using a heat recovery wheel in the HVAC unit, the heating demand can be reduced by more than 70 % [46]. The disadvantage of this wheel are higher pressure losses which have to be overcome by the fans. Other control strategies, such as free night cooling or floating temperature set points, can lead to a reduction of HVAC energy cost [46]. However, it has to be taken into account that measures which reduce the power consumption of the HVAC are not always advantageous for the supermarket's overall energy balance. Low indoor air temperature and relative humidity can be achieved through a higher effort of the HVAC, but lead to considerably lower heat loads to the cabinets and a reduction of refrigeration costs [47].

15 - 35 % of the energy consumed is spent on illumination [3], [32], depending on the efficiency of the artificial lighting, the use of daylight and daylight-dependent control. High lighting levels of around 1000 lux [48] are commonly used to attract customers. Fluorescent lighting is widely used [3], with light emitting diodes (LED) also becoming increasingly popular, especially in cabinets [49]. The low energy cost of LEDs can lead to savings of up to 66 % [50]

and the low heat production causes a reduction of the heat load in the cabinets. However, it should be noted that an increase in illumination efficiency leads to a potentially significant reduction of heat load to the building. In winter, this heat sometimes has to be replaced by the HVAC, which entails higher heating costs. In summer, this heat load reduction can be advantageous and further savings can be achieved by daylight use, combined with matt and high reflecting room colours [51]. In addition to energetic advantages, natural light has a positive psychological effect on customers [52]. Light sensors can be used to reduce artificial illumination in correlation with natural light intensity. Occupancy sensors can be installed in storage rooms and low traffic areas [3]. The set points for lux levels in 24 hour shops can be reduced at night and a minimum lux level can be set while stores are closed [53].

Apart from the equipment and the amount of chilled goods, the power consumption depends on factors such as the store format, business practices and shopping activity [2]. The presence of additional consumers, such as an internal bakery, raises the energy intensity significantly. In the US, the average energy intensity in supermarkets was about 549 kWh/m^2 per year in 2011 [54]. According to Arias [7], 256 Swedish supermarkets with an average annual consumption of 421 kWh/m^2 were investigated in 1998, where the consumption in hypermarkets (about 7000 m^2) with 326 kWh/m^2 was considerably lower than in small shops (about 600 m^2) with 471 kWh/m^2 per year. A study carried out in the UK in 2010 compared 2570 stores and showed much higher annual energy intensities: between 700 kWh/m^2 in hypermarkets and 2000 kWh/m^2 in convenience stores for electrical energy and zero to 250 kWh/m^2 for gas. It also showed that convenience stores using plug-in units for refrigeration consume about 300 kWh/m^2 more energy than those with a centralised refrigeration system [3].

In a UK study from 2012, Kokolotroni et al. found that an average of 1026 kWh/m^2 SFA was consumed for electricity and 261 kWh/m^2 SFA for natural gas [2]. Another British study from 2007 stated values around 1000 kWh/m^2 [55]. In Germany, 458 kWh/m^2 SFA were detected for small independent shops (SFA < 500m^2) and 396 kWh/m^2 SFA for retail shops (SFA mostly > 500m^2) in 2015 [56]. It is evident that the energy intensity varies considerably with the size of the store. In most cases, small shops, such as convenience stores, have a high share of chilled food on total goods, whereas hypermarkets primarily sell non-chilled goods. Moreover, different types of shops exist in different countries. Shops are usually classified in terms of size, but the ranges and reference system (total floor area or sales floor area) are individually set in each study. Moreover, the influence of the weather needs to be included in such considerations. In addition, the type of equipment (refrigeration system, ventilation system or heat recovery) differs according to the location and date of the study, due to EU or national regulations.

However, supermarkets of the same size and comparable location can show extreme differences in energy intensities, up to a factor of three [3]. One reason for this could be the building

situation: some shops are part of a shopping mall or a row of houses, while others are stand-alone buildings. The age and type of insulation also plays a major role. A study from 2015 demonstrated that in Germany independent shops which are not part of a retail chain are usually located in stand-alone buildings (60 %) or part of a row of houses (38.8 %) and only 1.3 % are located in a shopping mall. Stand-alone buildings are also common for retail shops (<55 %), more than 25 % are part of a row of houses and over 20 % are located in shopping malls. 46 % of the buildings of independent shops were built before 1945, 27 % between 1946 and 1977, 19 % between 1995 and 2001 and only 4 % after 2002. Retail shop buildings are much more modern: 62 % of the buildings are older than 1995, 22 % were built between 1995 and 2005 and 15 % after 2005 [56]. Different EU directives from recent years concern the improvement of the energy performance of buildings. The European Energy Performance of Buildings Directive [57], which was renewed in 2010 [58], states that buildings constructed in 2021 or later, as well as existing buildings that are refurbished, should include 10 % renewable energy sources. In addition, high energy efficiency standards are prescribed with regards to insulation, air-tightness and heat transmittance. In the EU directive from 2010 recast, buildings such as supermarkets or restaurants are required to display energy performance certificates [58]. In England, it is obligatory to test the air-tightness of supermarkets larger than 1,000 m^2. The maximum air exchange rate permitted is 10 $m^3/h/m^2$ at 50 bar differential pressure [59].

Apart from the building, the efficiencies of the internals, such as refrigeration plant, HVAC and artificial light, as well as the realisation of heat recovery, have a significant influence on power consumption. The quality of the internals and buildings primarily depends on the decision-making structures. A German study from 2015 showed that in 43 % of small independent shops and in 79 % of retail chain shops, the shop operator did not own the building [56]. The operator of the shop is usually interested in low energy costs, whereas the landlord tends to be more interested in low acquisition costs. In small independent shops, 99 % of decisions are made by the owner or manager of the shop, whereas in retail chain shops 50 % of decisions are made by the energy commissary or department, 38 % by the technical purchase or expansion department, 31 % by the facility management, 23 % by the controlling and energy purchase department, 19 % by the company headquarters and 15 % by external consultants [56]. Thus, in small shops, the person interested in low power consumption has considerable freedom of choice, although they may not have the skills to decide which technical equipment is the best for his shop and hiring a planning company might be too expensive. In retail shops, the decision is rarely made by the shop manager. Sometimes, energy departments with good technical knowledge exist, but they are not the only ones to make decisions. Supermarkets are highly complex systems with sub-systems that influence each other. Manufacturers usually work on the improvement of the efficiency of one component without considering the interaction with other components. For example, if a floating, shop set temperature is chosen, this

can reduce the power consumption of the HVAC, but it increases the power consumption of the refrigeration plant. If heat recovery is applied, the amount of gas or electrical heating is reduced, while the power consumption of the refrigeration plant increases. The reduction of illumination costs through the use of natural light can cause high solar radiation heat load in the summer, increasing the energy effort for refrigeration and air conditioning. A remote refrigeration plant is usually more efficient than stand-alone units, but in the case of plug-in systems, the waste heat is rejected into the shop, considerably lowering the heating demand. This can be advantageous in cold climates and disadvantageous in hot or temperate climates, especially during the summer. Finding the most efficient overall system is a challenge, as the efficiency of each component depends on the behaviour of the other components. Accepting lower efficiencies for one sub-system can sometimes improve the efficiencies of one or several other systems. Installing a proper interconnection between the sub-systems, which means secondary loops and control, is one of the most important tasks. This can be difficult as companies usually don't specialise in the construction of individual secondary loops. Moreover, maintaining and servicing the secondary loops requires specific skills. As a consequence, systems that are cheap and easy to maintain are often more popular than energy efficient systems.

Energy only accounts for about 2 % of the overall turnover [56]. Thus, return on investment in energy efficiency might not be too high, while other investments might promise bigger and faster profits. Decision makers are more interested in high turnover and profit, thus prioritising high flexibility (plug-in units), customer friendly systems (no glass doors on cabinets) or even investment in marketing strategies over energy efficient equipment. Still, it is worth thinking about energy efficient systems, even from an economic point of view. Margins are also only around 1 - 4.2 % [60], [56], so energy costs constitute about 25 – 200 % of the profit. US Energy Star estimated an increase of sales by $59 for a $1 reduction in energy costs [61]. Moreover, a green image is increasingly important for attracting customers.

3.2. Assessment and approaches for power savings

The benchmarking of supermarket systems is a challenging topic. Supermarkets are normally assessed by their energy intensity, which can be useful if stores of similar size and location are compared. But the size of the supermarket, the amount of chilled goods, location, weather conditions and much more have an immense influence. Thus, a comparison of different supermarkets is only partially possible.

Buildings are often classified according to their size or location. The Department for Environment, Food and Rural Affairs (Defra) and the Institute of Grocery Distribution (IGD) in the UK created a classification mainly related to store size. According to this classification, convenience stores are very small shops (<280 m^2) that can be part of a building and are usually

located in dense urban areas. Supermarkets are small shops (280–1,400 m^2) and can be part of a building or stand alone, usually found in urban areas. Superstores are more often located in suburban regions, in stand-alone buildings with a size of 1,400–5,000 m^2 and hypermarkets are larger than 5,000 $m^{2,}$ usually located out of town and seldom sell food [62], [63].

Instead of the total floor area, the sales floor area is often used as a reference value [44]. Sometimes, the building's age is considered [44], [64]. Sankar et al. call for model-based benchmarking where an ideal power consumption is calculated according to the building's age and, as a consequence, the ideal value can be compared to the actual value [65].

In a study by Spyrou et al., physical parameters, such as sales floor area, year of building construction, ceiling heights or food:non-food ratio, were considered, as well as operational parameters such as opening hours or sales per SFA and regional parameters such as cooling and heating degree days [66] and geographical position. It could be shown that the SFA accounted for 44.6 % of variability of the power consumption, the volume of sales for 26.3 %, the food:non-food ratio for 3.7 % and the pre-post 2002 factor relative to the year of building construction or refurbishment for 1.2 % [44].

Lindberg et al. defined several goodness factors in order to compare supermarkets with different refrigeration systems and sizes, whereas the sales and total floor area were less important. The goodness factors for freezing, cooling and total refrigeration were defined as the energy consumed relative to the chilled volume. They highlighted the importance of standardised measuring and testing methods for cooling capacity and power consumption of refrigeration systems. Year-round monitoring is recommended in order to record seasonal variations. Moreover, different approaches for control volumes were proposed for comparing supermarkets. The boundaries differ depending on whether the refrigeration system, opening hours, geographic location or indoor environment are included [23].

Due to government regulations, energy labelling and a growing awareness of the impact of global warming, the interest in power saving concepts is growing among supermarket operators.

The Carbon Trust estimates that high power savings can be achieved by improving the subsystems and their efficiencies, such as refrigeration and HVAC systems, but also heat recovery from the refrigeration plant, thermal energy storage, demand side management and trigeneration. Moreover, energy efficient buildings, lighting systems and the integration of renewable energy sources were recommended [67].

Evans et al. estimate that in the UK, 44 % CO_2 equivalent (CO_2e) could be saved by retrofitting components, 54 % by refitting components, especially refrigeration systems, and 66 % for new stores, compared to a current baseline store [14].

According to Ge et al., power savings in recent years were due to several factors: energy monitoring and the development of control strategies, as well as doors on display cabinets and advanced defrosting processes have become more common. More innovative equipment has been installed, such as LED illumination, more energy efficient refrigeration and HVAC, as well as a higher number of renewable energy sources. In addition to the technical improvements, staff training and increasing energy awareness are reasons for reduced power consumption [29]. Another study investigated different ventilation systems and control strategies in supermarkets and showed that huge savings in costs and CO_2 emissions could be achieved through improved envelope air-tightness, natural ventilation, ventilative cooling, specific fan power reduction, CO_2 refrigeration systems with heat recovery and storage with phase change materials [2]. According to Kolokotroni, Hill et al. called for similar measures, such as the increased use of daylight, LED lighting, natural ventilation, more efficient refrigeration cabinets, renewable energy sources and improved control systems [2].

A 2015 study by the German energy agency (DENA) investigated which kind of measures were taken in order to improve the energy efficiency in supermarkets. 45 % of owners of small independent shops exchanged the windows, 29 % renovated the roof, 20 % the façade and 16 % the ambient insulation of the building. In terms of internal equipment, the heating system was updated in 20 % of cases, electrics in 5 % and illumination in 2 % [56].

In a British study, power saving strategies A, B and C were tested and compared to a base case supermarket in terms of CO_2e savings, change in capital costs and net-present value. Package A consisted of composite internal floors, high efficiency illumination, fan power reduction by control, improved chiller and boiler efficiencies and south-facing glazed façade. In package B, illumination, chillers and fan power control was even more efficient, roof lights and ventilation heat recovery were used and the air tightness of the building was improved. In package C, the fan power control and chiller efficiencies were higher than in case B, more roof lights were installed and the building's air tightness was higher. In addition, an active chilled beam/radiant ceiling and advanced thermal bridging were installed and an improved wall u-value could be achieved. Measurements resulted in a CO_2e reduction of 27 %, 51 % and 46 % respectively [68].

Different power saving approaches were tested in two UK studies, both comparing advanced techniques to a base case supermarket. Both recommend initiatives such as reduction of illumination costs by using daylight and more efficient lamps, reduction of HVAC power consumption by heat recovery and partially using natural ventilation, reduction of refrigeration power consumption through improved cabinets with doors and LED lighting, as well as improved control of the sub-systems, higher efficiencies of components and the use of renewable energy. Through these measures, a reduction in power consumption of about 50% down to around 400 kWh/m² were achieved compared to the base case [2], [68].

3.3. Case studies and research projects

Due to the growing interest in power savings for both environmental and economic reasons, more and more companies, research centres and universities are commissioned to develop overall concepts including building, refrigeration plant, HVAC, heat recovery and illumination. Some of the research projects that were carried out in recent years will be presented in the following.

Much of the research on power consumption in supermarket systems was carried out by KTH for several years, especially focusing on the use of CO_2 refrigeration systems and heat recovery. The simulation software CyberMart was developed as part of the doctoral thesis of Jaime Arias [7]. This software calculates the heating performance of a supermarket. The HVAC system and different refrigeration systems were considered in the model; heat recovery and the interaction between refrigeration, illumination and HVAC were modelled; control strategies, especially of the refrigeration plant and the heat recovery potential, were investigated in computer simulations; a sensitivity analysis was carried out to find out which parameters had the highest influence on the power consumption in supermarkets; field measurements were carried out in seven Swedish supermarkets; new CO_2 refrigeration systems were compared to standard systems, the developed models were evaluated, and the influence of different factors such as ambient temperature, humidity and night covering of display cases on the overall power consumption were evaluated. The simulation results predicted that all necessary heat can be recovered from the refrigeration plant, whereas measurements indicated that only a part of the heating demand can be satisfied by heat recovery. It was assumed that some reasons for the worse measurement results were the poor performance of heat recovery systems and the fact that HVAC and refrigeration system were controlled separately. An overall approach was recommended where the whole supermarket is taken into consideration, including interactions between the sub-systems.

Sawalha investigated supermarket refrigeration systems in his doctoral thesis and publications [69], [70], [36]. Computer models were developed using EES to compare CO_2 indirect, NH_3/CO_2 cascade and trans-critical systems with a direct R-404a system. To evaluate the theoretical results, a scaled-down supermarket was rebuilt and tested in the laboratory. In addition to the performance of the systems at different ambient conditions, the leakage rates were investigated. It could be shown that the CO_2 systems under investigation were efficient solutions without causing exceptional health risks. The CyberMart and EES models were further used for other simulations of heat recovery from CO_2 trans-critical refrigeration systems in supermarkets [71], [72], which investigated the influence of parameters such as gas cooler subcooling and evaporation temperature on system performance. Annual simulations showed that the systems performed better when applying the proposed control strategy than an equivalent R-404a system with separate heat pump.

In a master thesis, the control strategy of two existing supermarket systems was analysed and compared to a theoretical case. The amount of recovered heat was measured and the potential of heat recovery was modelled using EES. The investigated systems were compared to R-404a and CO_2/NH_3 cascade systems and heat pumps in a simulation, before considering the heat recovery rates and studying the possibilities of selling heat to the district heating network. Significant differences were found between measurements and simulations [73].

Further on, the efficiency of different CO_2 trans-critical systems was analysed using field measurements in five Swedish supermarkets. The results showed that the operating mode, the amount of sub-cooling, gas removal from the intermediate vessel, evaporation temperature, internal and external superheat and compressor efficiency have a significant impact on the system's performance [74]. Different internal heat exchanger arrangements in refrigeration systems were simulated and the influence on system performance was investigated [17].

At Brunel University in the UK, long-term experience in the supermarket area exists due to several investigations and studies. Power consumption data of 2,570 supermarkets of all major store categories and retail food chains were collected and evaluated. Results showed that power consumption in the stores varied widely. A power law could be found to describe the relation between energy intensity and sales floor area. The power saving potential was estimated to be 10 % or 840 GWh and 355,000 tonnes of CO_2 emissions if all supermarkets with an energy intensity above the mean value were reduced to the mean value. Different measures were suggested, such as heat recovery, adjusted control or the use of more efficient equipment [3]. The SuperSim model was developed and validated in order to test the performance of centralised refrigeration systems, as well as their interaction with the HVAC system and building. It was used for the comparison of performance and heat recovery of trans-critical CO_2 and R-404a systems and the optimisation of CO_2 systems [29].]. One-year simulations were carried out with optimised control and it was concluded that in the case of heat recovery and at low ambient temperatures, the CO_2 system performs better than the conventional R-404a system. It was found that 40 % of space heating could be covered by heat recovery from the CO_2 system [35]. The effects of different parameters on the performance of a trans-critical booster system were analysed by means of a sensitivity analysis and a thermodynamic model with the objective of developing a high-side pressure control strategy for different operating conditions. Influencing parameters such as the effectiveness of the internal heat exchanger, medium pressure, low pressure and superheating on the overall efficiency were also investigated [75].

The German retail chain Aldi Süd and the Fraunhofer Insitut für solare Energiesysteme built a test supermarket in Rastatt that was opened in 2010. The German Federal Ministry of Economics and Industry (BMWi) funded the project to investigate the potential of power savings through an efficient overall concept and control strategy [39]. The store has a total floor area of 1,825 m^2 and a sales floor area of 1,103 m^2. A two-stage CO_2 refrigeration plant including

heat pump mode combined with six 100 m deep borehole heat exchangers was implemented. The building comprises heat recovery, a photovoltaic plant, floor heating and thermal activation of building structures. A CO_2-based control of the AHU fans was implemented. Simulations of the building were realised with TRNSYS to determine the demand of heating and primary energy of the supermarket in advance, during the planning phase. A reduction of energy costs for heating, cooling and refrigeration of 29 % compared to a standard branch was predicted, which corresponds to a reduction of the energy intensity from 501 kWh/m^2 to 357 kWh/m^2. The measured power consumption was 407 kWh/m^2 in 2011 and 378 kWh/m^2 in 2012, with a prediction of 413 kWh/m^2 for 2013. Using Modelica, a simplified refrigeration plant model was built to develop a control strategy for the trans-critical mode [22].

3.4. Simulation approaches

Case studies can be very helpful for the analysis of the power consumption of end-users in supermarkets, since actual modifications, for example of the technical equipment or control strategies, are often difficult or impossible. The safety of customers and staff could be endangered and interruptions of the daily business would be necessary, which can harm the supermarket's reputation. Moreover, a detailed analysis would require a sizeable set of measurement equipment and data logging. Simulations are a promising method for testing different system configurations or control systems that can be adjusted relatively easily. However, it has to be kept in mind that simulations cannot replace measurements and that they can differ significantly from reality [76]. Adequate validations have to be carried out in order to gain reliable results. Different approaches exist for simulation purposes, some of which will be presented and discussed in the following.

CyberMart was developed at KTH in Sweden [7]. The focus was on the development of a user-friendly software that can easily simulate different supermarkets. It permits the investigation of measures and methods to improve the energy efficiency, the comparison of different systems and the power saving potential. The model is a one-zone model in which the overall heat balance and thermal capacity of the supermarket are considered. It includes refrigeration and HVAC system, illumination and other equipment, as well as the building structure and weather conditions. The user can choose between seven different refrigeration systems, calculate heating and cooling loads and predict overall electricity consumptions. Even though the model structure is relatively simple, it could be validated on measurement data of five Swedish supermarkets with relatively good agreement. Long-time simulations over one year can be carried out with this software. However, detailed and individual control strategies, different heat transfer correlations or pressure drop of the components can only be simulated partially. CyberMart is a quasi-steady state model. It is assumed that the fresh air flow of the HVAC is controlled by the CO_2 content of the indoor air [7].

EnergyPlus is a software that was funded by the U.S. Department of Energy Building Technologies Office. In this quasi-steady state model, power consumption, HVAC, lighting, internal loads and water use are considered in the overall heat balance. Refrigeration plants including heat recovery, cold room and display cabinets can be modelled [32]. A multi-zone model approach facilitates a more realistic calculation of the indoor air conditions and the HVAC supply air. Radiant and convective effects are considered in the heat balance. It includes detailed models of different components, such as windows or HVAC, and allows the simulation of user-defined control. A wide range of weather data is available and sub-hourly or annual simulations are possible [77]. Cooling and heating loads are calculated dependent on the overall building loads and conditions. The interaction between the sub-systems such as HVAC and refrigeration plant building loads are considered [78].

The free clean energy software RetScreen was developed by the Government of Canada. The software provides energy, cost, emission, financial and sensitivity/risk analysis. A global database of weather data from 6,700 ground base stations and NASA satellite data are available, as well as a benchmark, project, hydrology and product database [79]. In the model, the building is considered as one temperature zone, with heating and cooling loads calculated in a steady state mode using monthly average climatic data. The amount of fresh air is not calculated but has to be set as an input by the user [29].

The model SuperSim, developed at Brunel University in the UK, is based on the simulation software TRNSYS and provides the opportunity to simulate the performance of centralised refrigeration systems and the interaction with the building and HVAC. The fresh air supply flow is treated as an input value. Hourly simulations can be carried out with the quasi-steady state model. It was validated using data from a supermarket with reasonable accuracy [29].

TRNSYS was developed by the University of Wisconsin [80]. Transient systems can be simulated with this model and it is primarily used to simulate buildings and technical plants, especially for thermal overall analyses. It is equipped with a large component library which includes, for example, multi-zone buildings, pumps, weather data and basic HVAC equipment. Users can modify the existing components or write their own models.

Another simulation approach is currently being developed at Technische Universität Braunschweig. The SuperSmart tool gives the opportunity to combine different simulation models using functional mockup units. The aim is to create a supermarket benchmark tool that is able to carry out annual simulations of overall supermarket systems. Different supermarkets and different technical solutions for one supermarket can be investigated and assessed [81], [82].

Apart from CyberMart and SuperSmart, none of the tools mentioned above is a model explicitly for supermarkets. Most of them are building models that can be adjusted to the case of a supermarket. The technical equipment, such as the refrigeration plant, the HVAC system and

the heat recovery system, are usually modelled in a drastically simplified way or even neglected and controllers are usually not considered. Most of the models were designed to carry out long term simulations. Supermarkets are very complex and heterogeneous systems that are difficult to model. Simplifications have to be made in order to achieve acceptable simulation times. Quasi-steady state models that give hourly values are often used and highly dynamic processes and different time constants are neglected, while different sub-systems are usually simulated in separate models. For instance, the heating demand of the supermarket is simulated with a building software such as EnergyPlus, the refrigeration plant with Energy Equation solver and the amount of recovered heat is calculated post-processing. The disadvantage in this case is that interactions between the sub systems are not correctly represented. Gas cooler return temperatures, efficiencies and heat recovery potentials can be wrong. Sometimes stationary operating points are simulated and the results are interpolated in order to obtain annual values. In other cases, values such as heat loads are assumed to be more rigid than they really are, or even constant. Simplified calculations are used for variables such as the refrigeration heat load as a linear function of the ambient temperature. Some of these measures are necessary to allow annual simulations while considering the interaction between different sub-systems. If the objective is the comparison of different systems, quick model creation and modification are essential.

If simulations are used for the investigation of an individual supermarket system with a focus on the control strategy, a highly dynamic simulation approach is obligatory. For a detailed analysis, control systems, thermal capacities, pressure drops and dynamics of all subsystems have to be taken into consideration in one single model. The disadvantage is that the development of these models is time-consuming and the simulation times are long. Annual simulations of complex systems like supermarkets are very time-consuming and not always possible.

The software TILSuite is a tool that allows a highly dynamic simulation of thermodynamic systems. It was developed by the Institut für Thermodynamik of the Technische Universität Braunschweig and the company TLK Thermo GmbH in Braunschweig, Germany. It is equipped with a library of several components of thermal systems, such as compressors, pumps, heat exchangers and tubes. Add-on packages for different applications such as storage tanks or vehicle cabinets are available. The components can easily be modified and adjusted by the user, if necessary. A broad range of fluid data are available in the library TILMedia, which enables an exact and fast simulation [83]. The models in TIL are written in the object oriented, equation-based modelling language Modelica, with which complex physical systems can be modelled. The most common simulation environments are Dymola, SimulationX and Wolfram SystemModeler.

4. Reference supermarket

Within the CREATIV project, an overall supermarket concept was designed and a test supermarket was built in Trondheim (Norway). The shop opened in August 2013 and more than 600 measurement values have continuously been logged since. The supermarket is a discount store of the Norwegian supermarket chain REMA 1000. It is located in a stand-alone building with a total floor area of 1,000 m^2 and a sales area of 800 m^2.

Figure 4-1: Sketch of the REMA 1000 supermarket in Kroppanmarka **[84]**

The supermarket is sketched in Figure 4-1. An overall energy concept was developed for the reference supermarket. An efficient heat recovery and control strategy was implemented. The overall concept is shown in Figure 4-2. The refrigeration plant is a direct CO_2-booster system that is primarily used for chilling. For freezing, plug-in units are used mainly. The waste heat from the refrigeration plant can be used by HVAC, floor heating or snow melting of the car park and truck ramp, and part of it can be stored in stratified tanks. The tanks are connected to the main air handling unit (AHU) in the sales area, a smaller air handling unit in the staff room (AHUSR), and the entrance air curtain (AirCu). The system includes a borehole heat exchanger (BHX) system. Thus, waste heat from the refrigeration plant can be rejected or used for cooling via the cooling heat exchanger in the air handling unit. The control strategy was designed in order to satisfy the heating demand of the building by heat recovery and to avoid electrical heating. When the waste heat is not sufficient, the refrigeration plant can be run in heat pump mode.

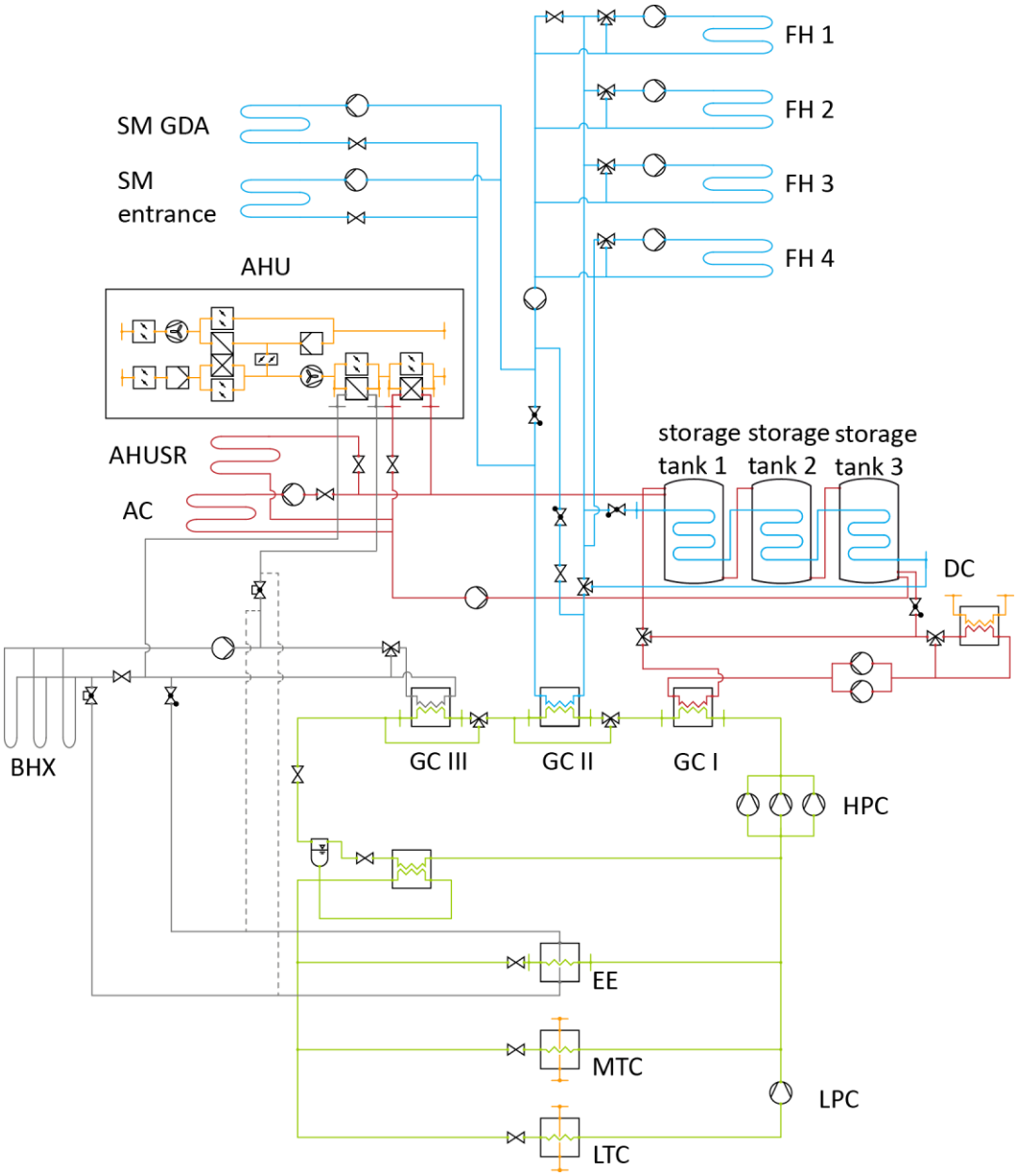

Figure 4-2: Schematic view of the technical systems in the reference supermarket

4.1. Building

The building has a total floor area of 1,000 m^2 and a height of 6.1 m. The ground plan of the building is shown in Figure 4-3. The sales floor area (1) has a size of 799 m^2 and represents the main part of the building. The entrance area (2) is separated from the outside and the sales area by sliding glass doors. The supermarket is equipped with cooling (6) and freezing storage (7). The other rooms are the staff room, toilets, bottle return room, machine room and storage room. The AHUs are located on the first floor.

The store is equipped with triple-glazed float glass windows on the north, east and south sides and aerogel windows on the west, east and south sides and the roof. The overall window area is 47 m^2 and the aerogel area is 229 m^2.

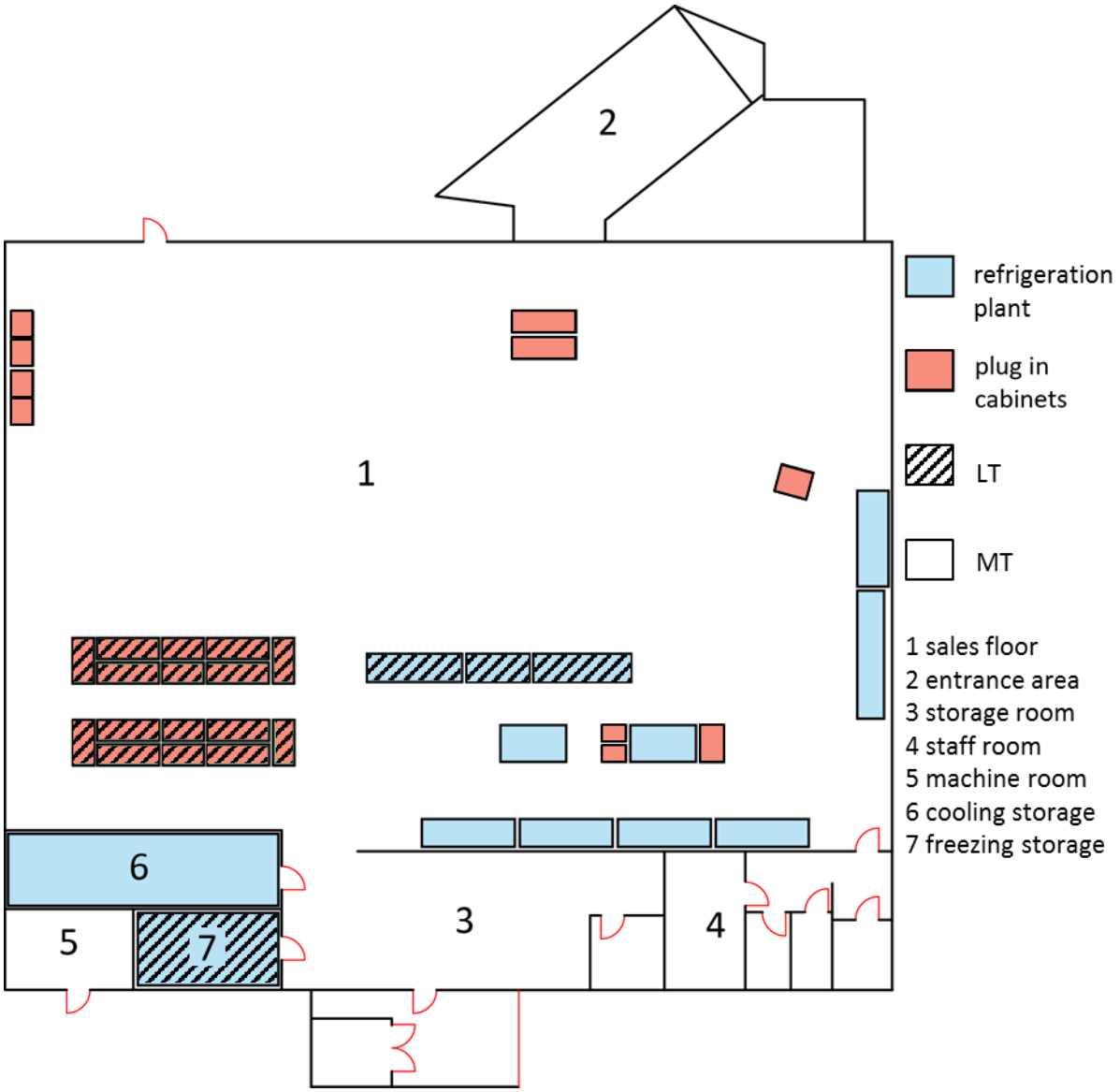

Figure 4-3: Ground plan

The walls were built from modules consisting of steel with a rock wool core. The roof is planted with sedum and the floor consists of ceramic tiles over a screed layer. Below the screed is an insulation layer of expanded polystyrene. The floor heating tubes sit on top of the insulation, below the screed. Three of the tubes are located in the sales area and one in the freezing storage room to avoid freezing and expansion of the floor. The snow melting tubes are located below the car park and the goods delivery area (GDA).

The illumination system is arranged in four rows, each row can be switched on or off separately depending on the daylight intensity. Fluorescent tubes are used and the supermarket is equipped with several lux meters.

The distribution of the cabinets is illustrated in Figure 4-3 and shows that approximately half of the cabinets are integral systems, while the other half are connected to the remote refrigeration system.

4.2. Refrigeration plant

The remote refrigeration plant is an overall CO_2 booster system. The plant is equipped with one low pressure (LP) compressor and three high pressure (HP) compressors. The low pressure compressor and one of the high pressure compressors are speed-controlled. It is designed for a total cooling capacity of 82 kW and a freezing capacity of 5.2 kW.

The high pressure of the plant can be controlled according to the gas cooler return temperature with a maximum pressure of 120 bars. The high pressure is usually kept as low as possible but can be raised during the winter to increase the amount of available waste heat.

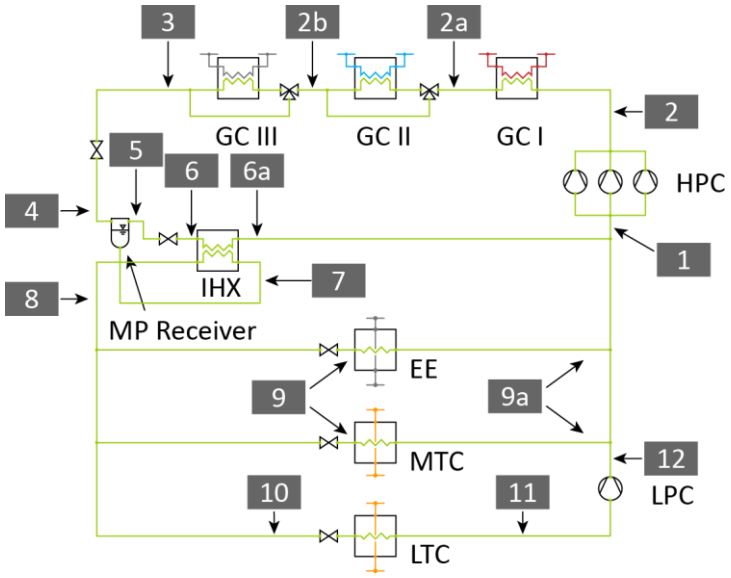

Figure 4-4: Schematic drawing of the refrigeration plant

A schematic drawing of the refrigeration plant is depicted in Figure 4-4 and the log p, h-diagram of a typical operation point is shown in Figure 4-5. After the high pressure compressors (2), three gas coolers are arranged in a row. Heat recovery can be realised in the first (2-2a) and second (2a-2b) gas cooler. The first gas cooler is connected to the tank cycle loop. The waste heat can be stored or used in the air handler unit and, if no heating is required, it can be released into the environment. In the second heat exchanger, the waste heat can be transferred to the floor heating (FH) and snow melt (SM) cycle. To achieve a high COP for the refrigeration plant, the gas cooler return temperature should be as low as possible. The refrigerant temperature can be lowered in the second heat exchanger, depending on the return temperature from the floor heating and snow melt loops. The return temperature of the second gas cooler was typically around 23°C in the supermarket. The temperature can be further decreased in the third gas cooler (2b-3), which is connected to the borehole heat exchanger.

The refrigerant returning from the third gas cooler is throttled to 35 bars (4) and ends up in the two-phase region. After the valve it is separated into gas and liquid in a medium pressure receiver. The gas part (5) is throttled to 28 bars (6) and used to sub-cool the liquid (7) in an internal heat exchanger (6-6a). Part of the subcooled liquid (8) is throttled to the medium

pressure of 28 bars (9) after the IHX and passed through the medium temperature (MT) cabinets (9-9a). The rest is expanded to the low pressure of 12 bars (10) and passed through low temperature (LT) cabinets (10-11). After the LT cabinets, it is compressed to the medium pressure of 28 bar (4).

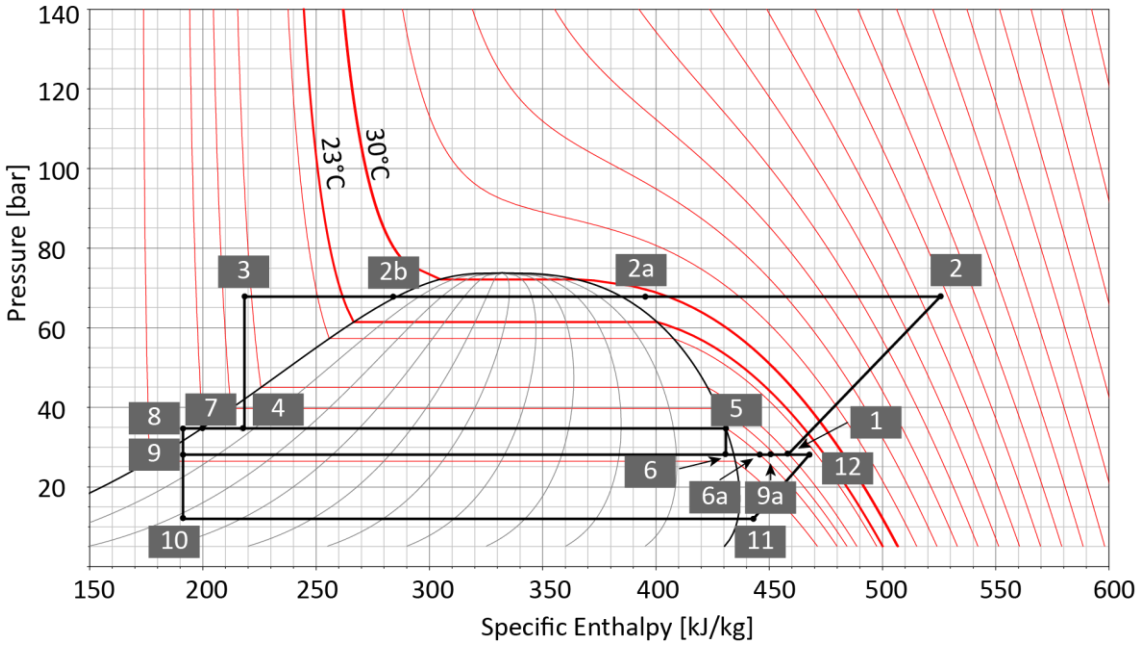

Figure 4-5: Log p, h diagram of a typical operation point of the refrigeration system

There is an extra evaporator (EE) arranged parallel to the MT cabinets. The EE has a capacity of about 30 kW and the evaporation pressure is equivalent to that in the MT cabinets. The evaporator is connected to the borehole heat exchanger cycle on the liquid side (see Figure 4-2). During winter, when the heating demand of the building is high, the EE can be used to increase the heat load and, consequently, the waste heat of the refrigeration plant. In this case, the refrigeration plant is also used as a heat pump. In summertime, the extra evaporator can be connected directly to the cooling heat exchanger of the AHU on the liquid side (dotted line in Figure 4-2) to cool the sales area.

The refrigerant from the LP compressors (12) is mixed (1) with the refrigerant from the medium pressure cabinets and extra evaporator (09a) and the gas from the IHX (6a) and compressed to high pressure (2).

4.3. HVAC, heat recovery and secondary loops

The heat recovery system consists of the tanks and tank cycle, AHUs and floor heating cycle. The BHX cycle can be used for gas cooling of the refrigeration plant and for heating or cooling of the building. The individual cycles will be described in this chapter.

Tank Cycle

The tank cycle system can be seen in Figure 4-2 (red lines). The operating fluid is a glycol water mixture. The heat is transferred from the refrigeration plant by the first gas cooler (GC I) and can be stored in three tanks which are arranged in a row. The tanks are stratified storage tanks with a volume of 550 l each, equipped with an internal tube heat exchanger. The liquid supplied from the gas cooler flows directly into the tanks. If the tank temperature is high enough or no heating is required, the tanks can be bypassed via a three way valve located before the inlet of the first tank. A smaller backup tank (198 l) with the option of thermal heating (capacity: 45 kW) is located after the third storage tank. This tank was installed only for emergencies and is not depicted in the drawings. The heat tanks are connected to the AHU, the AHUSR and the air curtain (AirCu) in the entrance area. The advantage of the direct tank system is that no extra temperature differences are caused by an internal heat exchanger in the tank. The tubes inside the tanks are connected to the floor heating cycle and are only used if the heat from GC II to the FH cycle is not sufficient.

A dry cooler (DC) was installed after the tanks. It is located on the roof of the building and is used to ensure a specific supply temperature to GC I. In summertime, when heating is not required, the heat can be totally or partially rejected by the DC into the ambient. If heating is required but the return temperature from the tanks is too high, the DC is also used. For safety reasons, it has a total capacity of 140 kW. It is also equipped with five fans that are controlled in groups of two and three, so it is possible to reduce the power consumption in cases of low heat load. The mass flow distribution in the tank cycle is controlled by several pumps and valves.

AHU

The air handling unit is designed in a way that the internal pressure drops are minimal to reduce the fan power. The AHU is depicted in Figure 4-6. The air that is sucked in from the ambient first passes a filter (F sup) before it can be preheated in an internal heat exchanger by the return air. The IHX is a rotary wheel (RW) that causes huge pressure losses and can be bypassed (Fl 1) if preheating is not necessary. The filtered air can be mixed with return air and heated or cooled in separate heat exchangers (AHXH, AHXC) before being supplied to the supermarket. Both heat exchangers can be bypassed. The return air can be recirculated totally or a part can be mixed with ambient air, depending on the CO_2 content in the shop. If the return air is recirculated or passed through the rotary wheel, it has to be filtered first. If not, the filter (F exh) can be bypassed and the air can be discharged directly to the ambient. Both fans are speed controlled. The exhaust air fan flow can be controlled according to the CO_2 content in the shop and the supply air fan according to the heating or cooling demand [24]. The bypassing of the components is controlled by the flaps Fl1-Fl6, while the fans and flaps Fl7 and Fl8 control the supply and exhaust air flow.

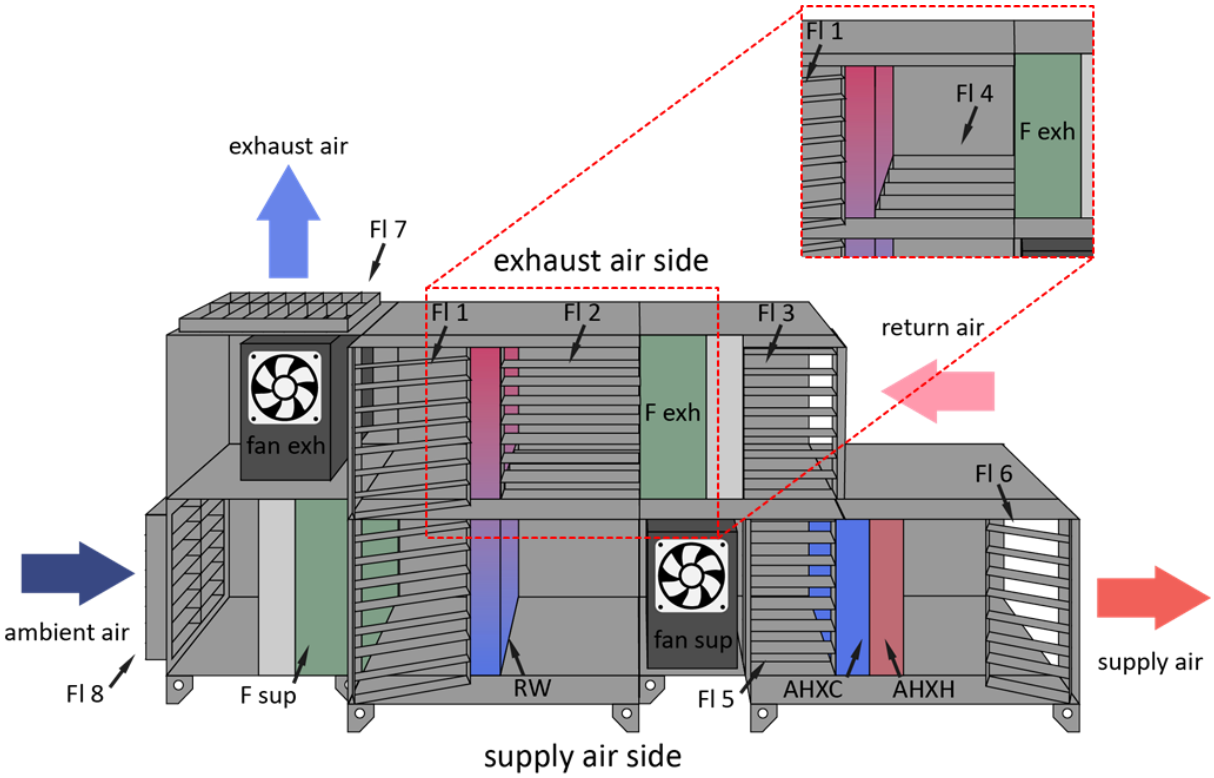

Figure 4-6: AHU including components and air flow

Floor Heating Cycle

If heat recovery is realised with the air handling unit, a liquid supply temperature above 30°C is required. Depending on the high pressure of the refrigeration plant, a considerable part of the waste heat is available at lower temperatures (see Figure 4-5). The floor heating cycle makes it possible to use the waste heat at a much lower temperature level, down to around 23 °C.

The working fluid in the FH loop is a water glycol mixture. The FH tubes in the sales area and the freezing room are polyethylene tubes. In total, there are three FH loops in the sales area (see Figure 4-2), each consisting of five parallel tubes. The heat is transferred from the refrigeration plant by the second gas cooler (GC II). If the supply temperature to the FH loops in the sales area is too low, heat can be extracted from the storage tanks. The snow melting loops can be used to melt the snow in the car park and the goods delivery zone. They can also serve as an additional heat sink to reduce the refrigerant temperature after GC II.

Borehole heat exchanger

The borehole heat exchanger cycle is connected to the third gas cooler (GC III) and the extra evaporator of the refrigeration plant (see Figure 4-2). A part of the waste heat from the refrigeration plant can be transferred to the BHX. For sales area cooling, the liquid can be extracted directly from the BHX and passed on to the AHU cooling heat exchanger (AHXC). The liquid can be cooled down to around 7-12 °C in the borehole heat exchanger. If the supply air temperature in the AHXC has to be reduced in order to raise the cooling capacity, the BHX cycle

can be run in summer mode (dotted lines) by switching a manual valve. In this case, the liquid is cooled in the EE before entering the AHU cooling HX. Supply temperatures of around 2°C can be reached. The mass flow in the AHU cooling HX is not controlled by a separate pump or valve but results from the pressure resistances in the system. Consequently, in summer mode, the mass flow in the AHU cooling HX is lower than in winter mode, due to the additional resistance of the EE. The borehole heat exchanger consists of three parallel probes, which are single u-tubes with a depth of 175 m. The ground holes are not filled and in the upper part the holes are surrounded by a layer of concrete. There is no information about the exact composition and thermal properties of the ground or ground water flow. An accumulation of rain water in the boreholes is possible.

5. Field measurements and evaluation

Comprehensive and detailed measurements were carried out in the described test supermarket. Data from January to December 2014 were collected and evaluated. The evaluation and calculation processes and the results will be presented in the following chapter.

5.1. Evaluation

In the supermarket described above, data from around 600 measurement points were recorded, around 80 of which could be used for the evaluations. The data were measured in one-minute-intervals. In fact, not all of the measured values were reliable for a variety of reasons. Temperature sensors, for instance, do not give reliable results if they are not placed properly. Heat flow meters usually detect the temperature difference and mass flow. The measurement device is equipped with a database of different fluid densities and heat capacities to calculate the heat flow, but if fluid data for the measured liquid are not available in the databank, a similar fluid has to be chosen instead. Consequently, errors of around 30 % can easily occur.

As a consequence, the measurement data used had to be verified by time consuming calculations. In order to gain reliable results, heat and mass balances were drawn up for the subsystems and the overall system. Not all relevant data were measured in the supermarket. In addition, some measurement devices failed partly. Around 80 values, such as mass flows, temperatures and heat flows, had to be calculated. Fluid data from the TILMedia library (see 3.4) were used for the calculations.

Some relevant values were missing across longer periods. Nevertheless, it was possible to carry out evaluations for eight months of the year 2014 and to draw significant conclusions from these results. In the following chapters, the calculation and evaluation methods will be described. The overall heat balance was subdivided into heat balances for the subsystems. The algebraic signs were related to the system in a way that all mass flows and heat flowing out of the subsystem have a negative sign.

5.1.1. Refrigeration plant

The refrigeration plant, including measurement sensors, is depicted in Figure 5-1. The power consumption was measured separately for the low pressure compressor and the high pressure compressors. The low pressure, medium pressure, receiver pressure and high pressure were also measured. Pressure losses in the heat exchangers and tubes were neglected in the calculations.

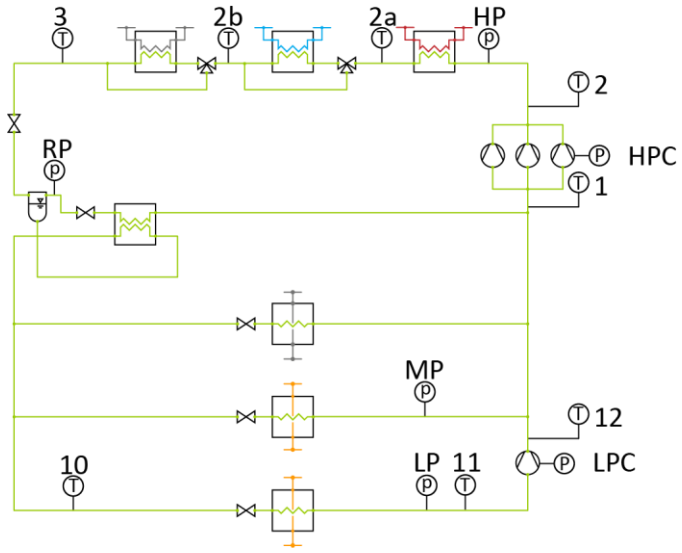

Figure 5-1 Measured data in the refrigeration plant

The temperature was measured before and after the compressors and after each gas cooler. The evaporation temperature of the LT cabinets was also measured.

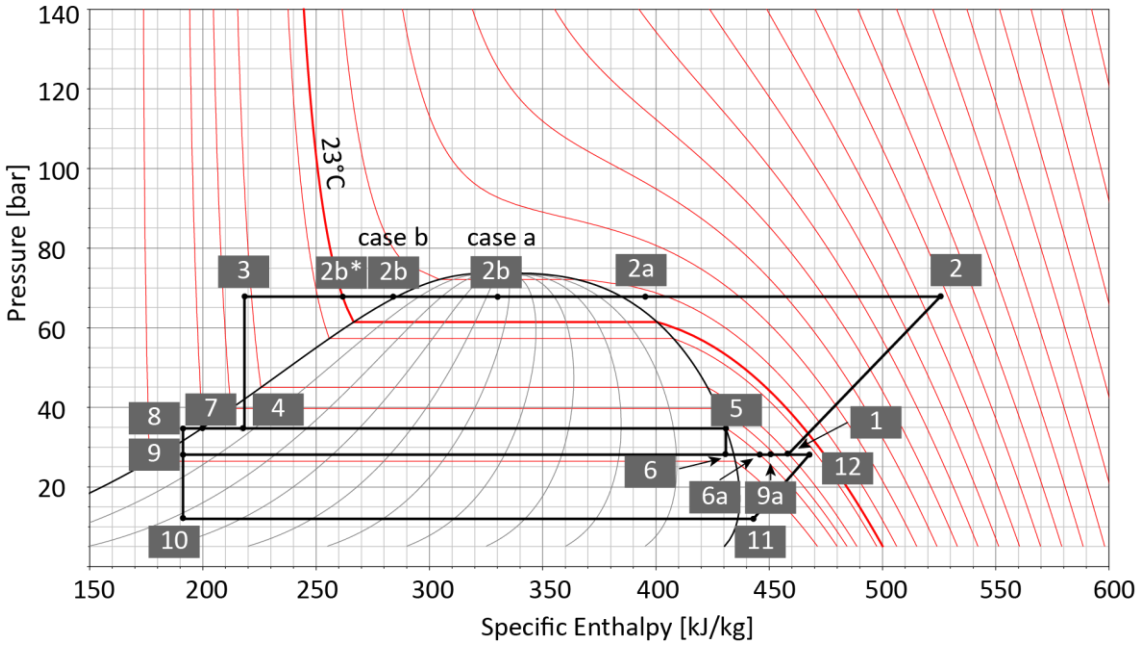

Figure 5-2: p,h – Diagram of the cycle with all relevant points

For the heat balances of the refrigeration plant, various mass flows, enthalpies and temperatures were calculated in the points plotted in Figure 4-4.

The heat flow extracted from the second gas cooler and the heat supplied to the extra evaporator were calculated in the energy balance of the floor heating cycle (see 5.1.3). The values were adopted in the refrigeration balance. An exception are the months January and February, where the heat in GC II was calculated in a different way, as described below.

The enthalpies for operating points 1, 2, 2a, 3, 11 and 12 could be determined by the pressure, the temperature and TILMedia fluid data [85].

The mass flow of the high pressure compressor was calculated according to the following equation:

$$\dot{m}_{HPC} = \frac{P_{HPC,fluid}}{(h_2 - h_1)} \quad \textbf{(5.1)}$$

P_{Fluid} is the total compressor power minus the heat losses via the compressor surface. It was assumed that the losses are equal to 5 % of the total power consumption.

The calculation of the GC II return enthalpy (2b) was challenging, as the operating point was partly located inside (case A) and partly outside (case B) of the two-phase area. Most of the time (except January and February), it was situated inside the two-phase region. As a consequence, the pressure and temperature were not sufficient for determining the value. Thus, the enthalpy in point 2b was calculated via the use of the heat flow extracted from GC II with $\dot{m}_{GCII} = \dot{m}_{HPC}$.

$$h_{2a} = h_{2b} - \frac{\dot{Q}_{GCII}}{\dot{m}_{GCII}} \quad \textbf{(5.2)}$$

For January and February, the operating point 2b was located outside the two-phase region (see Figure 5-2) and h_{2b} could be calculated as a function of the measured temperature 2b and the high pressure using fluid data.

The heat removed from GC I and GC III, as well as GC II in January and February, was calculated subsequently.

$$\dot{Q}_{GC,i} = \dot{m}_{GC} * (h_{ret} - h_{sup}) \quad \textbf{(5.3)}$$

For the throttling process after GC III 03, an isenthalpic change of state was assumed, which implies that $h_4 = h_3$. The pressure 4 in the receiver is known and, as the operating point is located in the two-phase region (see Figure 5-2), the associated temperature could be determined. After the receiver (4), the fluid is separated into a vapour part 5 and a liquid part 7. The enthalpies are equal to the bubble enthalpy and the dew enthalpy of the pressure 4 in the receiver. The mass flow distribution was calculated using the law of the lever and the mass balance.

$$\frac{\dot{m}_{vap}}{\dot{m}_{liq}} = \frac{(h_4 - h_7)}{(h_5 - h_4)} \quad \textbf{(5.4)}$$

$$\dot{m}_{GC,i} = \dot{m}_{vap} + \dot{m}_{liq} \quad \textbf{(5.5)}$$

The separated vapour 5 is throttled down to the medium pressure 6. Assuming isenthalpic throttling, h_6=h_5 follows. Temperature 6 is equal to the bubble temperature of the medium pressure. For the determination of IHX vapour return temperature 6a, it was assumed that the liquid mass flow exceeds the vapour mass flow considerably. Consequently, IHX vapour return temperature 6 is almost equal to IHX liquid supply temperature 7, T_{6a}=T_7. Enthalpy 6a could be determined using the temperature and the pressure. Knowing the vapour supply, return enthalpies and mass flow, the heat flow of the IHX could be calculated.

$$\dot{Q}_{IHX} = \dot{m}_{vap} * (h_{6a} - h_6) \quad \textbf{(5.6)}$$

Using the heat flow, the IHX liquid return enthalpy h_8 could be determined.

$$h_8 = h_7 + \frac{\dot{Q}_{IHX}}{\dot{m}_{liq}} \quad \textbf{(5.7)}$$

The IHX liquid return mass flow in operating point 8 is separated into the low temperature cabinet (LTC), medium temperature cabinet (MTC) and EE mass flows. The LTC and MTC mass flows are split into mass flows of the individual cabinets. For balancing, considering the LTC, MTC and EE mass flows was sufficient.

The throttling process reaches the two-phase region in both cases, so the end temperatures are equal to the bubble temperatures of the evaporation pressures, which can be determined using fluid data. It was assumed that isenthalpic throttling occurred. Consequently, evaporator supply enthalpies 09 and 10 are equal to IHX liquid return enthalpy 08.

Operating points 11 after the LTC and 12 after the LPC are both located outside the two-phase region (see Figure 5-2). The enthalpies could be calculated using the measured pressures and temperatures and fluid data. The LPC flow could be calculated according to the MPC flow described above.

A mass balance was drawn to determine the MTC mass flow.

$$\dot{m}_{liq} = \dot{m}_{MTC+EE} + \dot{m}_{LTC} \quad \textbf{(5.8)}$$

The sum of the transferred heat transferred in the MTC and EE $\dot{Q}_{MTC+EE}$ was derived from the overall heat balance of the refrigeration plant.

$$\dot{Q}_{MTC+EE} = \dot{Q}_{GCI} + \dot{Q}_{GCII} + \dot{Q}_{GCIII} + \dot{Q}_{LTC} + P_{HPC,fluid} + P_{LPC,fluid} \quad \textbf{(5.9)}$$

The value for the EE heat flow was adopted from calculations of the floor heating cycle (see 5.1.3), making it possible to calculate the heat flow in the medium temperature cabinets.

$$\dot{Q}_{MTC+EE} = \dot{Q}_{MTC} + \dot{Q}_{EE} \quad \textbf{(5.10)}$$

Finally, the MTC/ EE return enthalpy in operating point 9a could be calculated.

$$h_{9a} = h_9 + \frac{\dot{Q}_{MTC+EE}}{\dot{m}_{MTC}} \quad \textbf{(5.11)}$$

In addition, the usable share of the waste heat was calculated for further considerations. It was assumed that the waste heat could be used for heat recovery by floor heating until a refrigerant temperature of t_2*=23°C (see Figure 5-2). The corresponding enthalpy h_2* of the refrigerant was determined as the enthalpy at the condensing pressure and a temperature of 23°C. Thus, the maximum recoverable heat flow resulted in:

$$\dot{Q}_{UWH} = \dot{m}_{GC} * (h_2 - h_2^*) \quad \textbf{(5.12)}$$

In such a complex system, it is challenging to find a method to evaluate the efficiency of the refrigeration plant and heat recovery. The COP can usually only be used in order to compare the efficiency of a refrigeration plant or heat pump considering one temperature level. In the current case, the refrigeration load is extracted from the cabinets at two different temperature levels. Moreover, heat recovery takes place at different temperature levels. Nevertheless, as it is difficult to evaluate the systems efficiency any other way, it was decided to calculate three COPs. It should be noted, that these COPs were exclusively used to evaluate the system in different operation points and for different control strategies. They cannot be used to compare it to other refrigeration systems.

The refrigeration COP was calculated:

$$COP_{ref} = \frac{\dot{Q}_{MTC} + \dot{Q}_{LTC}}{P_{HPC} + P_{LPC}} \quad \textbf{(5.13)}$$

In addition, the total COP of the used heat was calculated:

$$COP_{total} = \frac{\dot{Q}_{MTC} + \dot{Q}_{LTC} + \dot{Q}_{HC}}{P_{HPC} + P_{LPC}} \quad \textbf{(5.14)}$$

Where $\dot{Q}_{HC}$ is the sum of the waste heat used for heating and cooling.

$$\dot{Q}_{HC} = \dot{Q}_{AHXH} + \dot{Q}_{AHXC} + \dot{Q}_{FH} + \dot{Q}_{AHUSR} + \dot{Q}_{AirCu} \quad \textbf{(5.15)}$$

Finally, the maximal possible overall COP was calculated for the case that all the available waste heat is recovered and used for heating:

$$COP_{max} = \frac{\dot{Q}_{MTC} + \dot{Q}_{LTC} + \dot{Q}_{UWH}}{P_{HPC} + P_{LPC}} \quad \textbf{(5.16)}$$

5.1.2. Tank cycle

In the tank cycle, temperature sensors were installed before and after all heat exchangers (see Figure 5-3) and the temperatures inside the tanks were measured. The thermocouples are located at the bottom and top of the tanks. The positions of the tank valve and the dry cooler valve were detected in percent. The heat flow in the AHU, the AHUSR and the AirCu were measured, as well as the capacity of the DC fans and the main pumps. The heat flow through the gas cooler (GC I) was calculated in the refrigeration plant balance (see 5.1.1). The heat flow that was extracted from the tanks by the floor heating cycle was calculated in the floor heating cycle balance (see 5.1.3). The calculated values were adopted in the tank cycle balance. The locations of the sensors in the tank cycle can be retraced in Figure 5-3.

The liquid mass flow in GC I was determined by the heat flow, return and supply temperatures. The isobaric heat capacity was determined using TILMedia fluid data and always for the mean temperature of the supplying and returning fluid. A fluid composition of 70 % water and 30 % glycol was assumed.

$$\dot{m}_{GCI} = \frac{\dot{Q}_{GCI}}{c_{p,GCI} * \left(T_{GCI,ret} - T_{GCI,sup}\right)} \quad \textbf{(5.17)}$$

The position of the three-way valve in front of the tank was known. It indicates whether the liquid passes through or bypasses the tanks. If the liquid flows into the tanks, $\dot{m}_{GCI} = \dot{m}_{Tanks}$ is valid. The heat supplied to the tanks was calculated with the GC I return temperature and DC supply temperature.

$$\dot{Q}_{tanks} = \dot{m}_{tanks} * c_{p,tanks} * \left(T_{DC,sup} - T_{GCI,ret}\right) \quad \textbf{(5.18)}$$

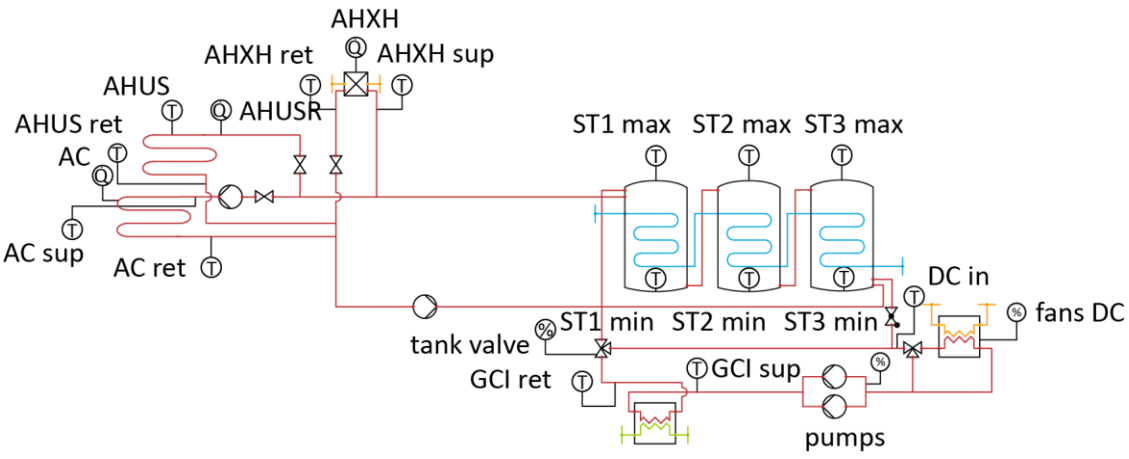

Figure 5-3: Measured data in the tank cycle

The heat extracted in the DC was calculated with $\dot{m}_{DC}=\dot{m}_{Tanks}$, if the tanks were passed through and $\dot{m}_{DC}=\dot{m}_{Tanks,BP}$, if they were bypassed.

$$\dot{Q}_{DC} = \dot{m}_{DC} * c_{p,DC} * \left(T_{GCI,sup} - T_{DC,sup}\right) \quad \textbf{(5.19)}$$

The mass flows in the AHU, AHUSR and AirCu were calculated with the respective mass flow, supply and return temperature.

$$\dot{Q} = \dot{m} * c_p * \left(T_{ret} - T_{sup}\right) \quad \textbf{(5.20)}$$

The overall heat fluctuation in the tanks was calculated in two ways. The first was to calculate the total fluctuation, which is equal to the sum of all supplied and extracted heat flows.

$$\dot{Q}_{Tanks,total} = \dot{Q}_{tanks} + \dot{Q}_{tanks,FH} + \dot{Q}_{AHU} + \dot{Q}_{AHUSR} + \dot{Q}_{AirCu} \quad \textbf{(5.21)}$$

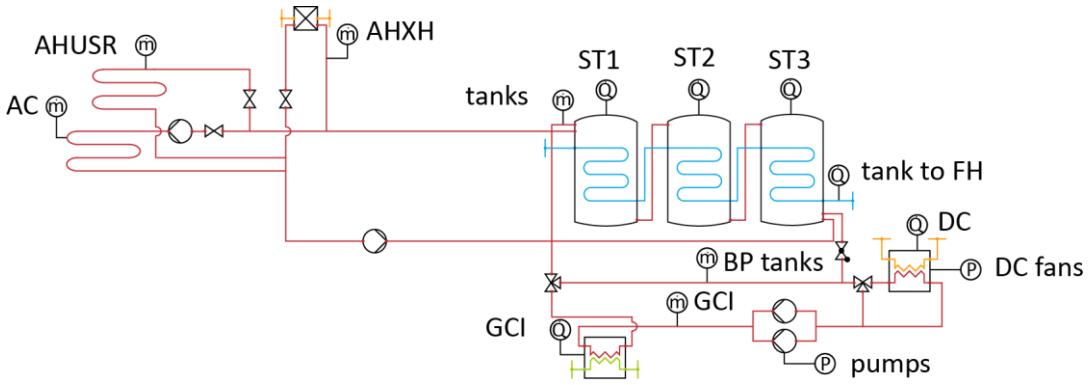

Figure 5-4: Calculated data in the tank cycle

The second way was to calculate the fluctuation in each individual tank. This was determined by the change of the tank average temperatures per time interval. Summarising the value for all three tanks also leads to the overall heat fluctuation.

$$\dot{Q}_{Tank,i,total} = V_{Tank,i} * \rho_{Tank,i} * c_{p,Tank,i} * \frac{\Delta T_{Tank}}{\Delta t} \quad \textbf{(5.22)}$$

The power consumption of the DC fans was calculated with the capacity. According to the manufacturer's data, the maximum power consumption per fan is 0.42 kW.

$$P_{Fans,DC} = n_{Fans,DC} * P_{Fans,DC,max} \quad \textbf{(5.23)}$$

$n_{Fans,DC}$ is the capacity of the fans (actual speed in relation to the maximum speed). The calculation of the main pump's power consumption was done in the same way. A maximum power consumption of 1.5 kW was stated by the manufacturer.

5.1.3. Floor heating cycle

The measurement sensors in the FH cycle are visualised in Figure 5-5. 14 temperature sensors were implemented. The extracted heat, as well as the supply and return temperature, were measured for each individual FH loop. The position of the three way valve in front of the tanks (tank valve) was recorded. All mass flows in the cycle were calculated. The calculated points are shown in Figure 5-6.

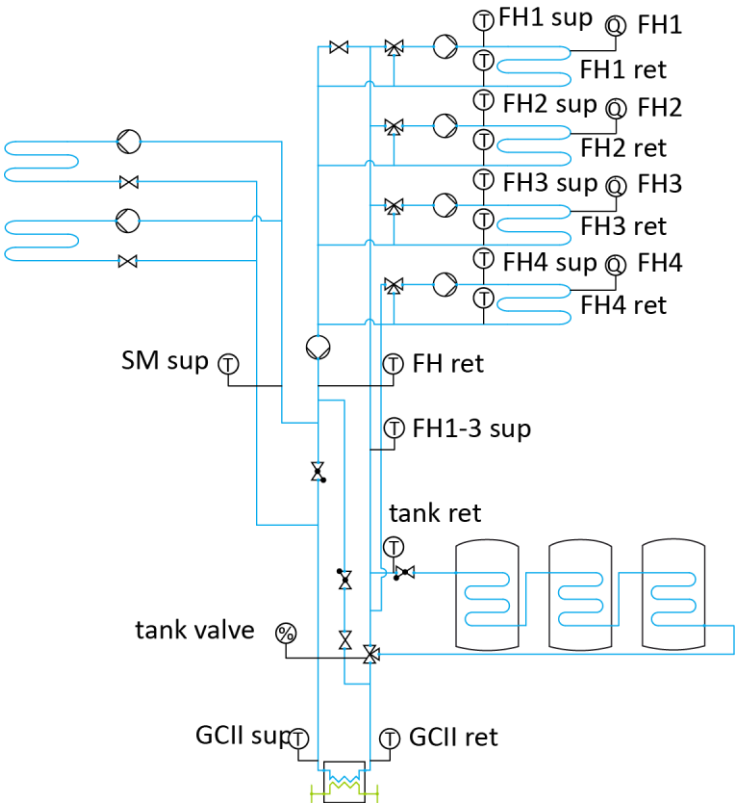

Figure 5-5: Measured data in the floor heating cycle

$\dot{m}_{FH,I}$, which is the total mass flow circulating in each tube (i=1,2,3), was calculated using the extracted heat as well as the supply and return temperature.

$$\dot{m}_{FH,i} = \frac{\dot{Q}_{FHi}}{c_{p,FHi} * (T_{FHi,ret} - T_{FHi,sup})} \quad \textbf{(5.24)}$$

The mass flow supplied to the individual FH loops $\dot{m}_{FH,i,sup}$ was calculated by drawing a mass and heat balance around the three way valves in front of the loops. Solving the equation for $\dot{m}_{FH,i,sup}$ resulted in:

$$\dot{m}_{FH,i,sup} = \dot{m}_{FH,i} * \frac{(c_{p,FHi,sup} * T_{FHi,sup} - c_{p,FHi,ret} * T_{FHi,ret})}{(c_{p,FH1-3,sup} * T_{FH1-3,sup} - c_{p,FHi,ret} * T_{FHi,ret})} \quad \textbf{(5.25)}$$

The measured and calculated points of an individual loop are depicted in Figure 5-7.

The same was done for the supply mass flow in FH4.

$$\dot{m}_{FH4,sup} = \dot{m}_{FH4} * \frac{(c_{p,FH4,sup} * T_{FH4,sup} - c_{p,FH4,ret} * T_{FH4,ret})}{(c_{p,GCII,ret} * T_{GCII,ret} - c_{p,FH4,ret} * T_{FH4,ret})} \quad \textbf{(5.26)}$$

As the temperature $T_{FH1\text{-}3,ret}$ was not measured, a challenging calculation method for $\dot{m}_{FH1\text{-}3}$ was necessary. A heat and mass balance was drawn around the control volume depicted in Figure 5-8. Liquid is supplied to the control volume in points 01 and 02 and leaves it in point 03. The heat extracted in the FH loops had to be considered in the energy balance.

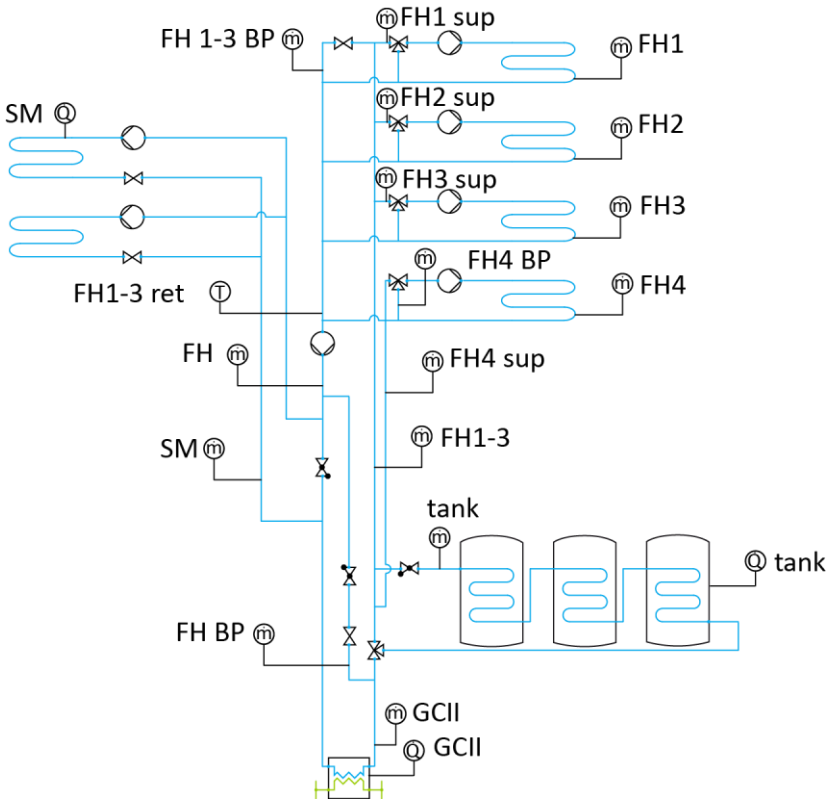

Figure 5-6: Calculated data in the floor heating cycle

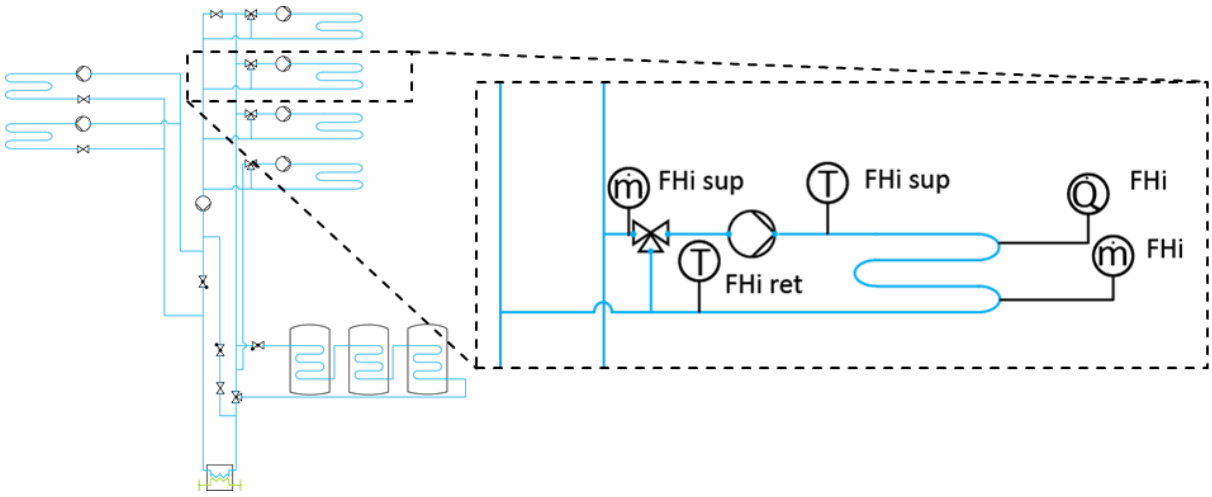

Figure 5-7: Calculated and measured data for one single FH loop

The mass balance

$$\dot{m}_{FH,1-3} + \dot{m}_{FH,4,sup} = \dot{m}_{FH} \quad \textbf{(5.27)}$$

and the energy balance

$$\dot{m}_{FH1-3} * c_{p,FH1-3,sup} * T_{FH1-3,sup} + \dot{m}_{FH,4,sup} * c_{p,GCII,ret} * T_{GCII,ret} + \dot{Q}_{FH1} + \dot{Q}_{FH2} + \dot{Q}_{FH3} + \dot{Q}_{FH4} = \dot{m}_{FH} * c_{p,FH,ret} * T_{FH,ret} \quad \textbf{(5.28)}$$

resulted in:

$$\dot{m}_{FH1-3} = = \frac{\dot{m}_{FH,4,sup} * \left(c_{p,GCII,ret} * T_{GCII,ret} - \dot{m}_{FH} * c_{p,FH,ret}\right) + \dot{Q}_{FH1} + \dot{Q}_{FH2} + \dot{Q}_{FH3} + \dot{Q}_{FH4}}{\dot{m}_{FH} * c_{p,FH,ret} - c_{p,FH1-3,sup} * T_{FH1-3,sup}} \quad \textbf{(5.29)}$$

The FH bypass mass flow for $\dot{m}_{FH,BP}$ could be determined by the mass

$$\dot{m}_{FH} + \dot{m}_{FH,BP} = \dot{m}_{FH,SM} \quad \textbf{(5.30)}$$

and heat balance at the point where the liquid enters the SM cycle (point 04 in Figure 5-8),

$$\dot{m}_{FH} * c_{p,FH,ret} * T_{FH,ret} + \dot{m}_{FH,BP} * c_{p,GCII,ret} * T_{GCII,ret} = = \dot{m}_{FH,SM} * c_{p,SM,sup} * T_{SM,sup} \quad \textbf{(5.31)}$$

which led to

$$\dot{m}_{FH,BP} = \dot{m}_{FH} * \frac{\left(c_{p,SM,sup} * T_{SM,sup} - c_{p,FH,ret} * T_{FH,ret}\right)}{\left(c_{p,GCII,ret} * T_{GCII,ret} - c_{p,SM,sup} * T_{SM,sup}\right)} \quad \textbf{(5.32)}$$

Next, the mass flow in the second gas cooler $\dot{m}_{GCII}$ was determined by a simple mass balance.

$$\dot{m}_{GCII} = \dot{m}_{FH} + \dot{m}_{FH,BP} \quad \textbf{(5.33)}$$

The mass flow into the tanks $\dot{m}_{tank}$, could be determined using the heat and mass balance drawn in point 05 (see Figure 5-8), resulting in:

$$\dot{m}_{tank} = \dot{m}_{FH1-3} * \frac{\left(c_{p,GCII,ret} * T_{GCII,ret} - c_{p,Tank,ret} * T_{tank,ret}\right)}{\left(c_{p,GCII,ret} * T_{GCII,ret} - c_{p,FH1-3,sup} * T_{FH1-3,sup}\right)} \quad \textbf{(5.34)}$$

The temperature $T_{FH1\text{-}3,ret}$ was identified using the heat and mass balance in point 06:

$$T_{FH1-3,ret} = \frac{\dot{m}_{FH} * c_{p,FH,ret} * T_{FH,ret} - \dot{m}_{FH4} * c_{p,FH4,ret} * T_{FH4,ret}}{\dot{m}_{FH1-3}} \quad \textbf{(5.35)}$$

With the calculated mass flows and temperatures, the heat flows in the gas cooler, snow melt and tanks were calculated.

$$\dot{Q}_{GCII} = \dot{m}_{GCII} * \ c_{p,GCII} * \left(T_{GCII,ret} - T_{GCIIsup}\right) \quad \textbf{(5.36)}$$

$$\dot{Q}_{SM} = \dot{m}_{GCII} * \ c_{p,SM} * \left(T_{GCII,in} - T_{SM,in}\right) \quad \textbf{(5.37)}$$

$$\dot{Q}_{Tank} = \dot{m}_{Tank} * \ c_{p,Tank} * \left(T_{Tank,out} - T_{GCII,out}\right) \quad \textbf{(5.38)}$$

with:

$$\dot{m}_{GCII} = \dot{m}_{FH} + \dot{m}_{FH,BP} \quad \textbf{(5.39)}$$

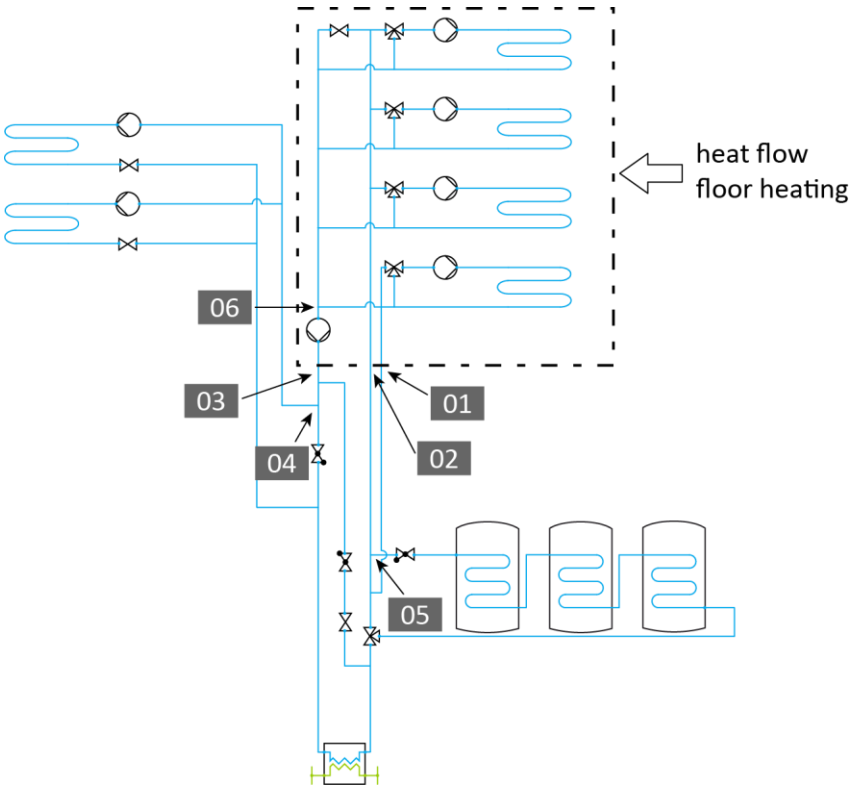

Figure 5-8: Balancing areas for the calculations of mass flows

5.1.4. Borehole heat exchanger cycle

Figure 5-9 shows the BHX cycle including measurement sensors. The BHX and EE supply and return temperatures were known. The AHU and GC III supply temperatures were also measured. The valve position of the extra evaporator valve (EEV) was recorded. The heat flow supplied to the AHU heat exchanger for cooling (AHXC) was detected. The GC III heat flow was calculated in the refrigeration plant cycle balance (see 5.1.1).

The position of the summer/winter valves (SWV) determine whether the BHX cycle runs in summer or winter mode. The summer and winter interconnections are both plotted in Figure 5-10. If the valves are open, winter mode is on (a). The liquid returning from the BHX flows directly into the AHXC. In winter mode, the evaporator can be used to transfer heat from the BHX to the refrigeration plant in the EE (heat pump mode). If the heat pump mode is off in

winter, the EE is bypassed. The mass flow into the evaporator is controlled by the evaporator valve. In summer mode, the SWVs are closed and the liquid returning from the BHX is forced to pass through the EE before entering the AHXC. The actual mode (S/W) was not measured but had to be determined by the position of the EE valve, supply and return temperature. Only if the valve is 100% open and $T_{EE,ret}$ is below $T_{EE,sup}$, this indicates the summer mode, otherwise winter mode is on.

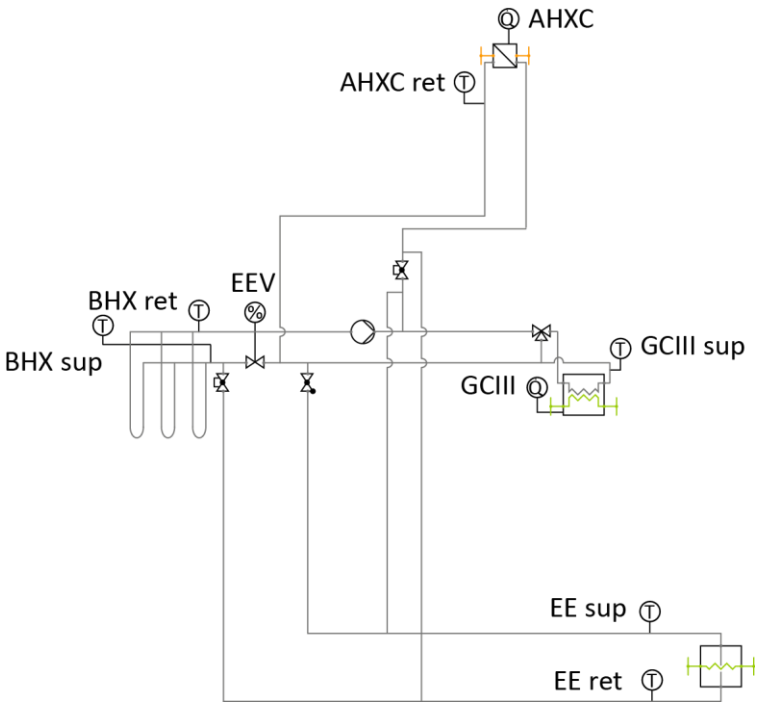

Figure 5-9: Measured data in the Borehole HX Cycle

Figure 5-11 shows the calculated values of the BHX cycle. The mass flow into the AHXC could be calculated using the heat flow, supply and return temperature. The supply temperature depends on the mode. In winter mode, $T_{AHXC,sup}$ is equal to $T_{BHX,ret}$ and in summer mode it is equal to $T_{EE,ret}$

$$\dot{m}_{AHU} = \frac{\dot{Q}_{AHU}}{c_{p,AHU} * \left(T_{AHXC,ret} - T_{AHXC,sup}\right)} \quad \textbf{(5.40)}$$

The GC III mass flow on the secondary side was calculated correspondingly.

$$\dot{m}_{GCIII} = \frac{\dot{Q}_{GCIII}}{c_{p,GCIII} * \left(T_{GCIII,ret} - T_{GCIII,sup}\right)} \quad \textbf{(5.41)}$$

For the calculation of the GC III bypass mass flow, it was necessary to calculate a theoretical BHX supply temperature $T_{BHX,sup,th}$. This temperature represents the BHX supply temperature in case the GC BP mass flow is zero. It was determined for both summer and winter mode. The heat and mass balance was calculated at the BHX inlet.

In case the winter mode is on and the evaporator is in use, the balance can be solved as follows:

$$T_{BHX,sup,th} = \frac{\dot{m}_{AHXC} * c_{p,AHXC,ret} * T_{AHXC,ret} - \dot{m}_{EE} * c_{p,EE,ret} * T_{EE,ret}}{\dot{m}_{AHXC} * c_{p,AHXC,ret} + \dot{m}_{EE} * c_{p,EE,ret}} \quad \textbf{(5.42)}$$

In all other cases, the balance resulted in the following equation:

$$T_{BHX,sup,th} = \frac{\dot{m}_{AHXC} * c_{p,AHXC,ret} * T_{AHXC,ret} - \dot{m}_{GCIII} * c_{p,GCIII,ret} * T_{GCIII,ret}}{\dot{m}_{AHXC} * c_{p,AHXC,ret} + \dot{m}_{GCIII} * c_{p,GCIII,ret}} \quad \textbf{(5.43)}$$

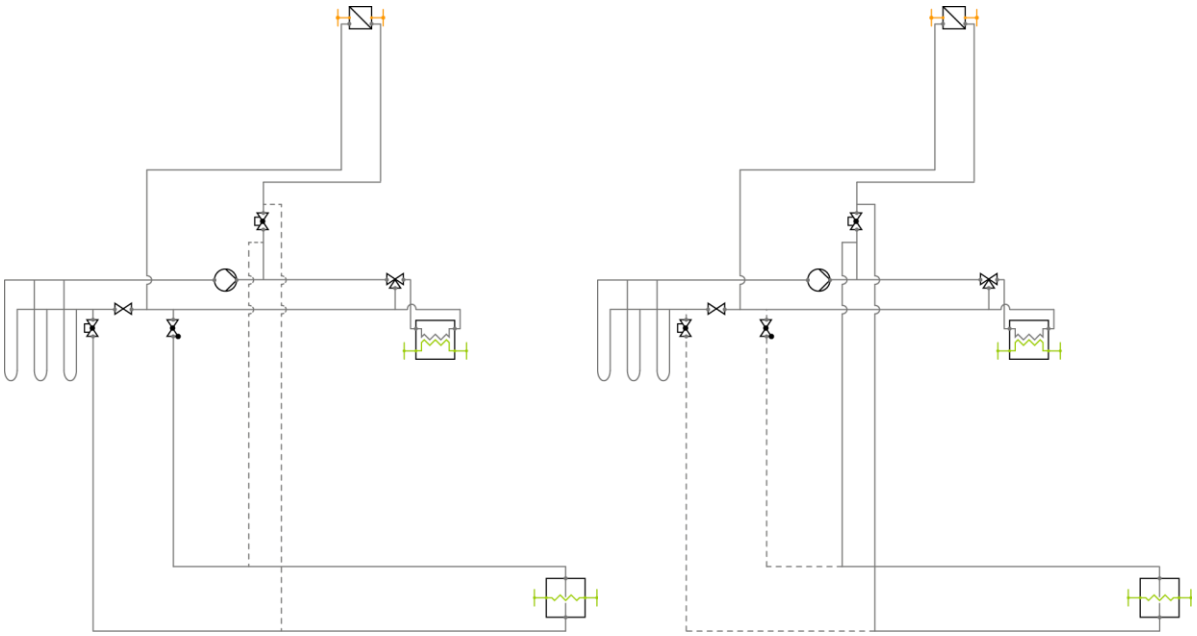

Figure 5-10: Winter mode (left) and summer mode (right)

Next, the actual GC BP mass flow could be determined by comparing the theoretical to the real BHX supply temperature:

$$\dot{m}_{GCIII,BP} = (\dot{m}_{GCIII} + \dot{m}_{AHXC}) * \frac{c_{p,BHX,sup} * T_{BHX,sup} - c_{p,BHX,sup,th} * T_{BHX,sup,th}}{c_{p,GCIII,ret} * T_{GCIII,ret} + c_{p,BHX,sup} * T_{BHX,sup}} \quad \textbf{(5.44)}$$

The GC III and GC III BP return temperature could be calculated using the mass flow $\dot{m}_{GCIII,BP}$.

$$T_{GCIII,ret,BP} = \frac{\dot{m}_{GCIII,BP} * c_{p,BHX,ret} * T_{BHX,ret} - \dot{m}_{GCIII} * c_{p,GCIII,ret} * T_{GCIII,ret}}{\dot{m}_{GCIII,BP} * c_{p,BHX,ret} + \dot{m}_{GCIII} * c_{p,GCIII,ret}} \quad \textbf{(5.45)}$$

The EE mass flow could be determined using the calculated mass flows. It is equal to the AHXC mass flow in summer mode

$$\dot{m}_{EE} = \dot{m}_{AHXC} \quad \textbf{(5.46)}$$

and equal to the GC III and GC III BP mass flow in winter mode.

$$\dot{m}_{EE} = \dot{m}_{GCIII} + \dot{m}_{GCIII,BP} \quad \textbf{(5.47)}$$

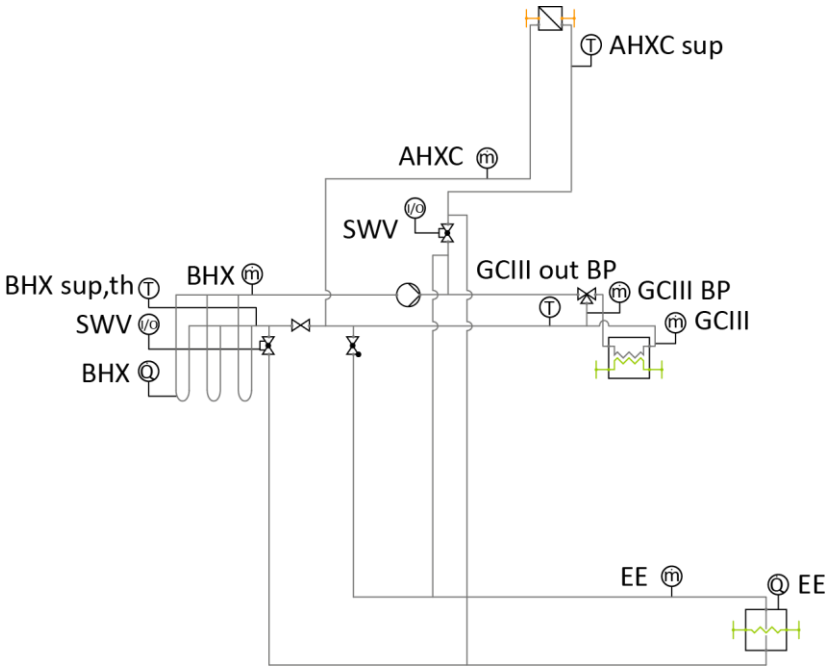

Figure 5-11: Calculated data in the BHX cycle

An overall mass balance led to the BHX mass flow.

$$\dot{m}_{BHX} = \dot{m}_{GCIII} + \dot{m}_{GCIII,BP} + \dot{m}_{AHXC} \quad \textbf{(5.48)}$$

Finally, it was possible to determine the EE and BHX heat flow by

$$\dot{Q}_{EE} = \dot{m}_{EE} * c_{p,EE} * \left(T_{EE,ret} - T_{EE,sup}\right) \quad \textbf{(5.49)}$$

and

$$\dot{Q}_{BHX} = \dot{m}_{BHX} * c_{p,BHX} * \left(T_{BHX,ret} - T_{BHX,sup}\right) \quad \textbf{(5.50)}$$

5.1.5. Air handling unit

The AHU can be considered a relatively relevant part of the supermarket, as it supplies the building's cooling demand and a considerable part of the heating demand. The AHU is shown in Figure 5-12. The measuring points in the AHU can be seen in Figure 5-13. Several temperatures, humidities, volume flows, heat flows and flap positions were measured. The ambient temperature and humidity were taken from the Norwegian meteorological institute [86]. The overall power consumption of the fans and the capacity of the individual fans were detected. Missing temperatures, humidities, mass flows and heat flows were calculated, as well as the enthalpies in all relevant points. The fans and various flaps influence the mass flow distribution in the system, which makes for a challenging calculation process. The calculated points

are drawn in Figure 5-14. The calculations were carried out using TILMedia fluid data for moist air. First, the absolute humidities of the supply, return and ambient air were determined as a function of the respective measured relative humidity and temperature.

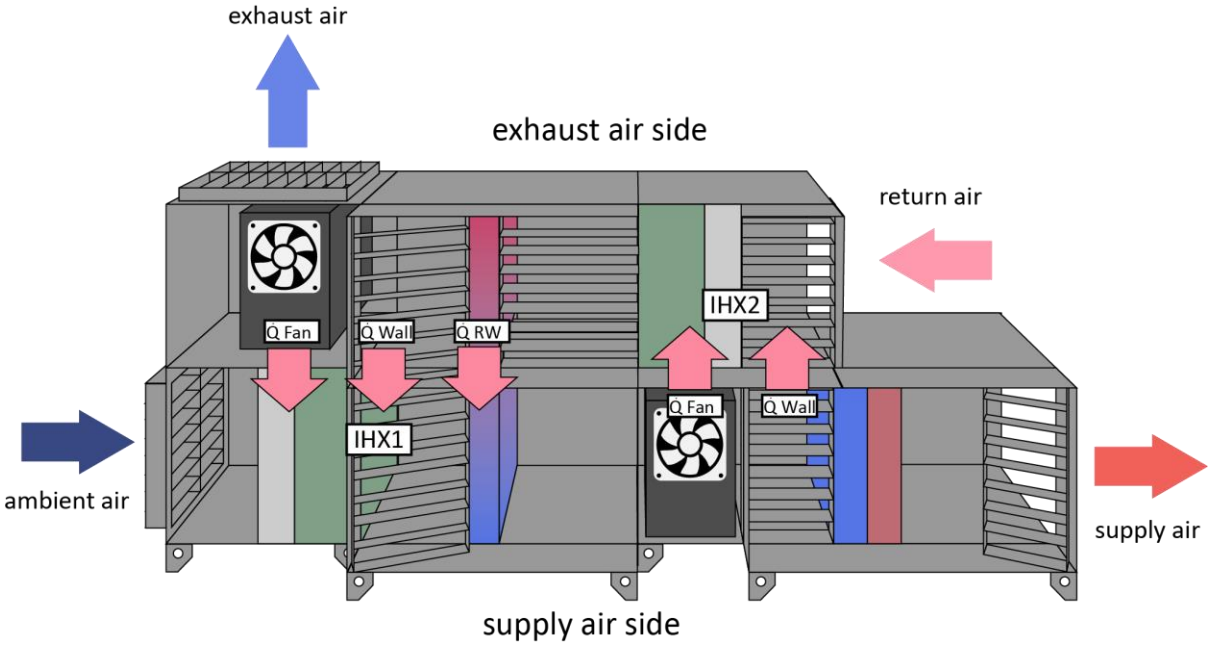

Figure 5-12: AHU including internal heat exchange

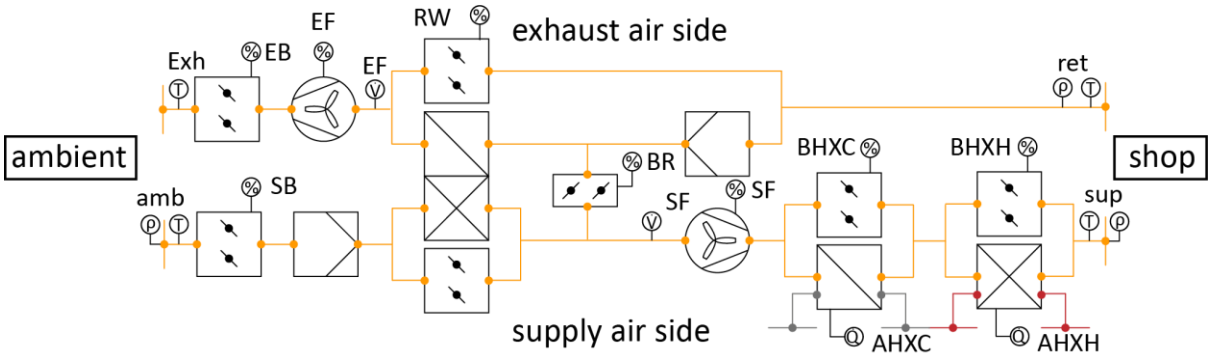

Figure 5-13: Measured data in the AHU

$$x_i = f(T_i, \varphi_i) \tag{5.51}$$

The corresponding enthalpies were calculated as a function of the respective pressure, temperature and humidity. The pressure was assumed to be 1.013 bar.

$$h_i = f(p_i, T_i, \varphi_i) \tag{5.52}$$

The relative exhaust humidity was determined as a function of the exhaust temperature, the exhaust pressure and the absolute return humidity, which is equal to the absolute exhaust humidity. The exhaust enthalpy was calculated as a function of the exhaust temperature, pres-

sure and humidity. The humidity in the shop was determined using the absolute return humidity x_{ret} and the shop temperature T_{Shop}. The shop enthalpy was determined using the shop temperature and humidity.

The total supply air mass flow was calculated using

$$\dot{m}_{sup} = \dot{V}_{sup} * \rho_{sup} \tag{5.53}$$

with

$$\rho_{sup} = f(p_{sup}, T_{sup}, \varphi_{sup}) \tag{5.54}$$

The exhaust air mass flow was calculated in an equivalent way.

The mass flow of the dry air $\dot{m}_{sup,dryair}$ could be calculated using

$$\dot{m}_{sup,dry} = \frac{\dot{m}_{sup}}{(x_{sup} + 1)} \tag{5.55}$$

which was derived from

$$x_{sup} = \frac{\dot{m}_{sup,water}}{\dot{m}_{sup,dry}} = \frac{\dot{m}_{sup} - \dot{m}_{sup,dry}}{\dot{m}_{sup,dry}} \tag{5.56}$$

The mass flow $\dot{m}_{exh,dry}$ was calculated in the same way.

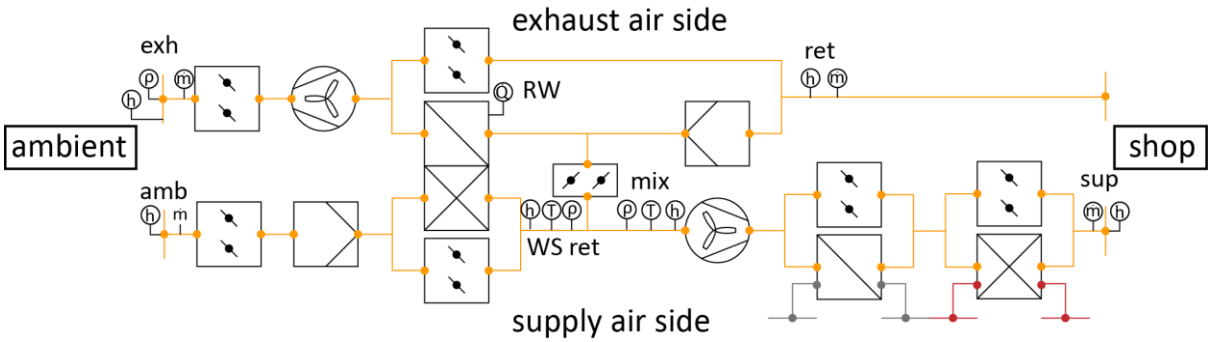

Figure 5-14: Calculated data in the AHU

The enthalpy of the mixed air h_{mix} was calculated using the supply air enthalpy and the heat flow of the AHXH and the AHXC.

$$h_{mix} = h_{sup} + \frac{\dot{Q}_{AHXH} + \dot{Q}_{AHXC}}{\dot{m}_{sup}} \tag{5.57}$$

Afterwards, the temperature T_{mix} was determined as a function of h_{mix} and x_{sup} and φ_{mix} as a function of T_{mix} and x_{sup}.

Internal heat transfer does not only occur in the rotary wheel, but also in the area between the ambient air inlet and the rotary wheel on the supply air side. Heat is transferred from the air on the warmer side to the air on the colder side through the walls. The overall internal heat flow (RW, fans, walls) is plotted in Figure 5-12.

$\dot{Q}_{IHX1}$ was calculated with the heat balance on the exhaust air side.

$$\dot{Q}_{IXH1} = \dot{m}_{sup} * (h_{ret} - h_{exh}) \quad \textbf{(5.58)}$$

The ambient dry air mass flow could be calculated using the heat and mass balance at the mixing point mix (Figure 5-14).

$$\dot{m}_{amb,dry} * h_{amb} + \dot{Q}_{IHX1} + \left(\dot{m}_{sup,dry} - \dot{m}_{amb}\right) * h_{ret} = \dot{m}_{sup,dry} * h_{mix} \quad \textbf{(5.59)}$$

Next, the ambient moist air mass flow was calculated.

$$\dot{m}_{amb} = \dot{m}_{amb,dry} * (x_{amb} - 1) \quad \textbf{(5.60)}$$

The return dry air mass flow was calculated using the overall mass balance of the AHU.

$$\dot{m}_{ret,dry} = \dot{m}_{amb,dry} + \dot{m}_{sup,dry} + \dot{m}_{exh,dry} \quad \textbf{(5.61)}$$

The return moist air mass flow was determined according to the ambient moist air mass flow.

$$\dot{m}_{ret} = \dot{m}_{ret,dry} * (x_{ret} - 1) \quad \textbf{(5.62)}$$

The specific enthalpy behind the rotary wheel on the supply air side was calculated using the internal heat flow and the enthalpy and mass flow of the ambient air.

$$h_{RWS,ret} = h_{amb} + \frac{\dot{Q}_{IHX1}}{\dot{m}_{amb}} \quad \textbf{(5.63)}$$

The respective humidity and temperature were calculated as a function of the pressure, enthalpy and the absolute humidity using fluid data. Mass transfer in the RW was neglected in the calculations, so it was assumed that the absolute humidity after the RW was equal to the ambient absolute humidity.

The shop temperature was compared to the return air temperature, with the conspicuous result that the return temperature was, depending on the operation point (low $\dot{m}_{sup}$ and T_{mix}), up to 2 K higher than the shop temperature, leading to the assumption that another internal heat flow occurred. It was assumed that some of the supply air fan waste heat or heat from the AHXH was transferred from the supply side to the exhaust side. The internal heat flow was calculated with the return mass flow, the return temperature and the shop temperature.

$$\dot{Q}_{IHX2} = \dot{m}_{ret} * \left(h_{ret} - h_{shop}\right) \quad \textbf{(5.64)}$$

The return air and ambient air volume flows were calculated using the mass flows and the density which was derived from fluid data as a function of the pressure, humidity and temperature.

Finally, the overall heat flow that was added or extracted from the building by the air handling unit could be calculated.

$$\dot{Q}_{AHU} = \dot{m}_{sup} * \left(h_{sup} - h_{shop}\right) \quad \textbf{(5.65)}$$

The heat load that was added by the ambient air flow was also calculated:

$$\dot{Q}_{amb} = \dot{m}_{amb} * (h_{amb} - h_{exh}) \quad \textbf{(5.66)}$$

5.1.6. Building

In addition to the technical plant, there are other heat sources and sinks, such as illumination, people, solar radiation or envelope losses, which influence the heat balance in the building. The power consumption for artificial lighting was measured and could be used directly in the heat balance. For the calculation of the heat from people, the exact number of people had to be known, which is a challenging task. The amount of door openings or receipts can be counted and used to deduce the number of people entering or leaving the shop. But they do not give any information about the time customers spent inside. There is no simple way to measure the number of people, so another way had to be found. The CO_2 content in the shop was measured and the AHU ambient air mass flow supplied to the shop was calculated in the AHU balance (5.1.5). These values were used to calculate the number of persons in the shop. A CO_2 balance was drawn for this purpose and the concentration in the shop was detected in parts per million (ppm). The temporal change of the CO_2 concentration in the shop times the volume in the shop V_{shop} is equivalent to the sum of CO_2 sources and sinks:

$$V_{shop} * \frac{dc_{CO2,shop}}{dt} = n_P * E_P + E_F - \left(c_{CO2,shop} - c_{CO2,amb}\right) * \left(\dot{V}_{amb} + \dot{V}_{DO} + \dot{V}_{NAE}\right)$$

(5.67)

There are several CO_2 sources in the system. The main source are the people in the shop. An emission rate E_P of 5 ml/s per person was calculated with the assumption that adults breathe 7.5 l/min and the CO_2 content in the exhaled air is 4 % [87]. The fruits located in the sales area also breathe and produce CO_2. Emission values for different fruits and berries were determined by Paech [88]. The amount of CO_2 produced by the fruits depends on the kind of fruit and its mass. It was assumed that on average 2,000 kg of mixed fruits with a CO_2 production

of 31.5 mg_{CO2}/(kg*h) were available in the supermarket sales area. An emission E_F value of 8.73 ml/s was calculated for the total amount of fruits. One CO_2 sink is the ambient air flow supplied by the AHU, which was calculated in the AHU balance (5.1.5). Additionally, the CO_2-content was reduced by the air flow caused by door openings and by natural air exchange in the building. The natural air exchange rate (NAER) is the air flow that is exchanged between a building and its environment if all windows and doors are closed. It is measured in air exchanges per hour (ACH or 1/h). The CO_2 content of the ambient air was assumed to be 375 ppm [89]. The volume flow caused by door openings and natural air exchange was not detected and had to be determined.

During night time, when no people are in the shop and consequently no door opening occurs, the CO_2 balance could be simplified:

$$V_{shop} * \frac{dc_{CO2,shop}}{dt} = E_F - \left(c_{CO2,shop} - c_{CO2,amb}\right) * \left(\dot{V}_{amb} + \dot{V}_{NAE}\right) \quad \textbf{(5.68)}$$

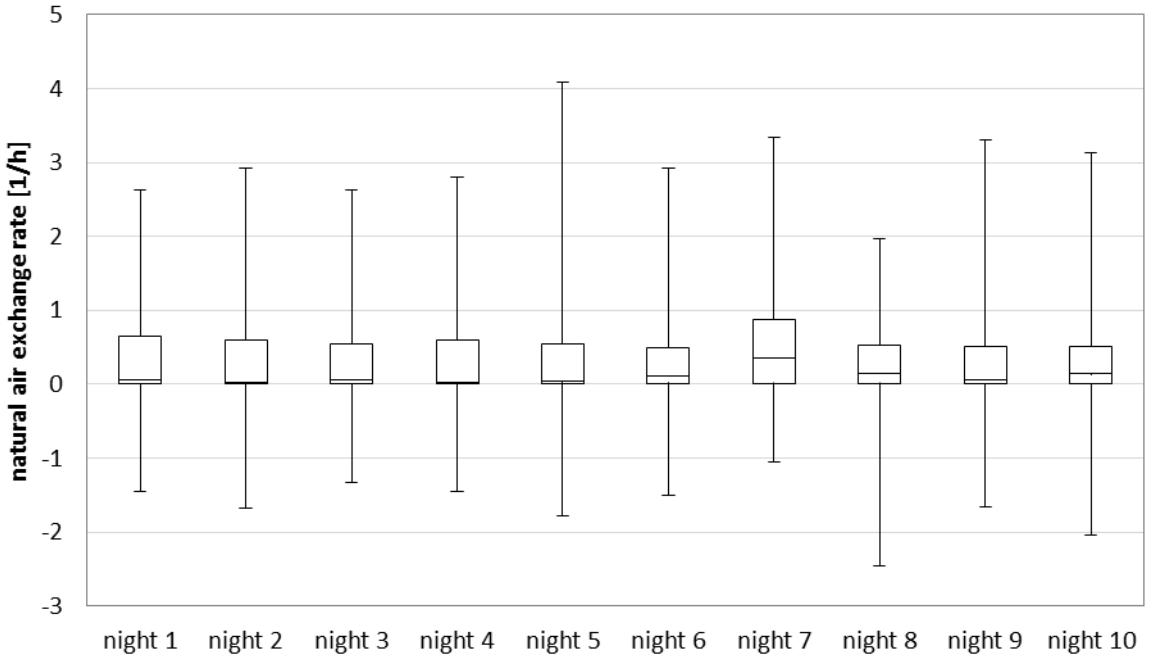

Figure 5-15: Natural air exchange rate for 10 example nights

The calculated values for ten example nights are represented in a box plot Figure 5-15. It can be seen that the values for the natural air exchange are low, but the plot also shows a high scattering. As there were no other data available, these values were used for further calculations. Though, investigated building is a modern building where the NAER is usually low. Moreover the influence of the NEAR to the supermarket's overall heating demand is relatively low. The determined average value for the natural air exchange was 0.18 1/h or 1.11 $m^3/h/m^2$. In a UK study, the influence of the air tightness on the energy efficiency was investigated. It could be shown that air tightness is crucial above a value of 3 $m^3/h/m^2$. The improvement of air

tightness below this value leads to diminishing results due to the fact that the cooling demand in winter is increased [68].

Subsequently, the volume flow caused by door openings could be determined:

$$\dot{V}_{DO} = \frac{n_P * 2 * V_{DO}}{t_s} \quad \textbf{(5.69)}$$

where V_{DO} is the total volume exchanged per door opening. It was multiplied twice by the number of persons, as the door opens twice per person and shopping event. Afterwards, it was divided by the average shopping time t_S. The average shopping time was assumed to be 30 minutes. The volume exchanged per door opening was calculated depending on the type and geometry of the door, as well as the temperature difference of the shop and ambient, according to Schälin [90]:

$$V_{DO} = 0.2 * \left(\frac{10}{273}\right)^{0.5} * w_D * {h_D}^{0.5} * \left(T_{shop} - T_{amb}\right)^{0.5} * t_{DO} * i_{AC} \quad \textbf{(5.70)}$$

with w_D being the width and h_D the height of the door. t_{DO} is the total time for one door opening process and i_{AirCu} a factor for the influence of the air curtain. As the entrance area was constructed as a sluice containing two doors in a row, a reduced value for the door opening time was used. It was assumed that the reduced time was 3 s and the influence of the air curtain 0.4.

The number of people could be detected by combining the equation for the overall CO_2 balance 5.68 and the equation for the volume flow of the doors 5.69. Dissolution for n_P resulted in:

$$n_P = \frac{V_{DO} * \left(\frac{dc_{shop}}{dt}\right) - E_F + \left(dc_{shop} - dc_{amb}\right) * \left(\dot{V}_{sup} - \dot{V}_{NAE}\right)}{\left(E_F - \left(dc_{shop} - dc_{amb}\right) * \frac{2 * V_{DO}}{t_s}\right)} \quad \textbf{(5.71)}$$

Finally, the total emitted heat by people was calculated

$$\dot{Q}_{P,tot} = n_P * \dot{Q}_P \quad \textbf{(5.72)}$$

$\dot{Q}_P$ is the heat of a person moving at moderate speed and was assumed to be 0.127 kW [91]. The heat from fruits was assumed to be 0.09 W/kg [88].

Solar radiation is another crucial heat load. Windows and aerogel windows were installed to reduce power consumption for electrical lighting. The exact determination of the solar heat flow into a building is complex. It depends on many factors, such as the transmission and absorption coefficient of the windows and the relation between diffuse and direct solar radiation, which are usually not measured. Nevertheless, the heat flow was estimated. The heat

flux caused by solar radiation was calculated in more detail through simulations (see 6.1). The simulation results were used to verify the assumptions and simplifications for the measurements.

The heat flux caused by solar radiation was calculated in a simplified way:

$$\dot{Q}_{solar} = R_S * f_s * (A_{WD} * \tau_{WD} + A_{AEW} * \tau_{AEW}) \quad \textbf{(5.73)}$$

where R_S is the solar radiation in W/m². The incidence angle of radiation, which depends on the position of the sun, is considered in the factor f_s. A_{WD} is the total window area (31.69 m²) and A_{AEW} the total aerogel window area (11.28 m²). τ_{AEW} and τ_{WD} are the transmission coefficients of the aerogel and the window. For the triple-glazed windows, a transmission coefficient of 0.74 was assumed [92].

The aerogel transmission and absorption coefficients for different wavelengths were measurements by Buratti for 14 mm aerogel plates with float glass coating [93]. To determine the average transmission coefficient, the transmission coefficient was integrated over the solar radiant intensity spectrum (see Figure 5-16).

$$\tau_{AEW,14mm} = \frac{\int_{\lambda=0nm}^{\lambda=2500nm} \left(\tau_{AEW,14mm}(\lambda) * I(\lambda)\right)}{\int_{0nm}^{2500nm} I(\lambda)} \quad \textbf{(5.74)}$$

.

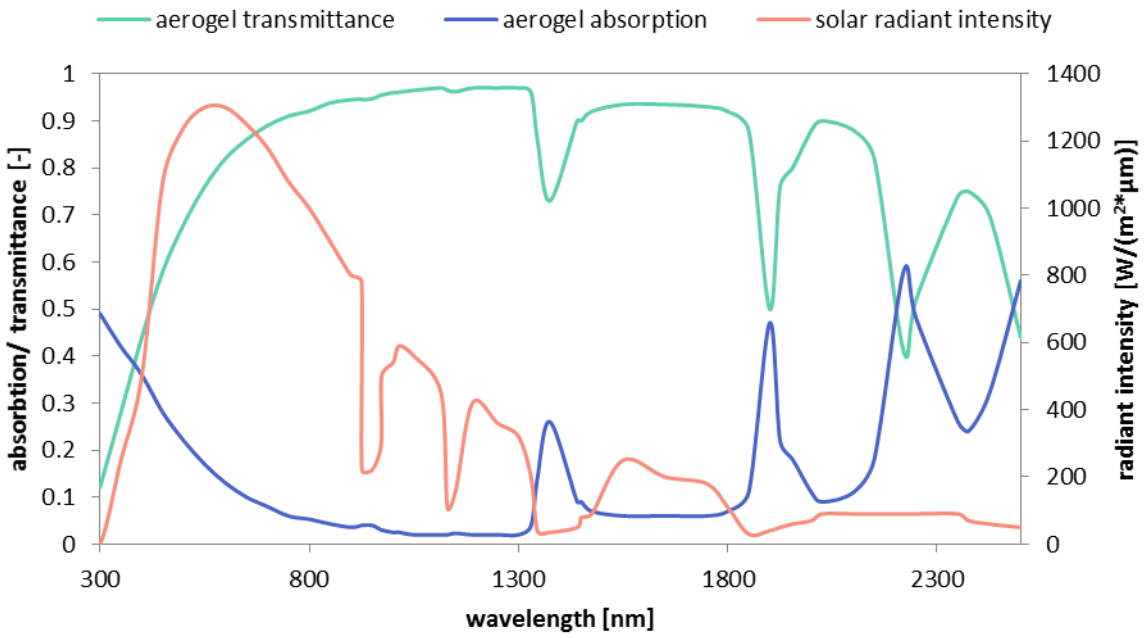

Figure 5-16: Solar radiant intensity **[94]** and optical properties of aerogel **[93]**

The calculated transmission coefficient was 0.83. In the test supermarket, aerogel with a thickness of 40 mm was installed. As measurement data for this thickness were not available, a transmission coefficient of 0.59 was assumed

The heat flow via the building's envelope is one of the main heat losses in the supermarket. The thermal mass of the walls was neglected in the calculations, as the overall heat flux was more interesting than the detailed course. The total thermal resistance was calculated using the individual parallel resistances.

$$\mathrm{R}_{total} = \left(\frac{1}{\sum \frac{1}{\mathrm{R}_{\lambda,i}}} \right) \tag{5.75}$$

where $R_{\lambda,i}$ is the resistance of the walls, windows and aerogel. The windows were triple-glazed windows with an argon filling, the aerogel windows were covered in layers of polyethylene.

The individual resistances were calculated using the resistance of the respective layers:

$$\mathrm{R}_{wall} = \left(\frac{1}{\alpha_{wall,inside}} + 2 * \frac{l_{wall}}{\lambda_{wall}} + \frac{l_{ins}}{\lambda_{ins}} + \frac{1}{\alpha_{wall,outside}} \right) * \frac{1}{\mathrm{A}_{wall}} \tag{5.76}$$

$$\mathrm{R}_{WD} = \left(\frac{1}{\alpha_{WD,inside}} + 3 * \frac{l_{glass}}{\lambda_{WD,1}} + 2 * \frac{l_{gas}}{\lambda_{WD,2}} + \frac{1}{\alpha_{WD,outside}} \right) * \frac{1}{\mathrm{A}_{WD}} \tag{5.77}$$

$$\mathrm{R}_{AEW} = \left(\frac{1}{\alpha_{PE,inside}} + 2 * \frac{l_{PE,1}}{\lambda_{PE,1}} + \frac{l_{AE}}{\lambda_{AE}} + \frac{1}{\alpha_{PE,outside}} \right) * \frac{1}{\mathrm{A}_{AEW}} \tag{5.78}$$

For all heat transfer coefficients, a value of 15 W/m^{2}K was assumed, which was validated using simulations. The resulting heat flows were compared to the simulation results.

Another relevant heat input into the building was the sum of all small electrical consumers in the supermarket. Even though the individual consumers are responsible for low power consumptions, in total they account for about 10-12 kW. The consumption was not measured for each consumer, but the overall consumption of the supermarket and the consumption of the main consumers were known. The power consumption of all smaller electrical devices could be determined by subtraction.

$$\mathrm{P}_{el.dev.} = \mathrm{P}_{total} - \left(\mathrm{P}_{comp.ref.} + \mathrm{P}_{AHU} + \mathrm{P}_{light} + \mathrm{P}_{plugin} \right) \tag{5.79}$$

Electrical devices include the ventilation, defrost and rail heating of the refrigeration plant and the pumps and fans of the secondary loops. In addition, consumers such as the cash desks, personal computers, dishwashers and controls contribute to this value. It was assumed that the power consumed by the electrical devices was released into the shop completely in the form of waste heat.

An overall heat balance was drawn where all calculated or measured heat gains and sinks of the building were added. Controlled heating via the FH tubes, AHU (AHXH and RW), AHUSR and the air curtain in the entrance area was considered in the balance. The rest was uncontrolled heating through the heat flow caused by solar radiation, people and fruits in the shop, plug-in cabinets, electrical lighting, AHU supply air fan, compressors of the refrigeration plant and other electrical devices. The heat sinks were fresh air flows into the building caused by the AHU, AHUSR, door openings and natural air exchange, the heat extraction by envelope losses, cooling and freezing cabinets and the AHU.

5.2. Results

An evaluation of the test supermarket's energy performance could be carried out for the main part of the year 2014. Even though data were not available for some periods, the results provided a large amount of information about the seasonal fluctuations of power consumption and heat flows. The results will be presented and discussed in the following chapter.

The annual power consumption in the supermarket in 2014 was 390.64 MWh. This corresponds to an energy intensity of 488.9 kWh/m² SFA and 390.64 kWh/m² total area. Tassou et al. measured the power consumption in 2,570 supermarkets in the UK [3] and showed that the average energy intensity drops with the size of the supermarket in the following way:

$$W_e = 3600 * A_S^{-0.18} \quad \textbf{(5.80)}$$

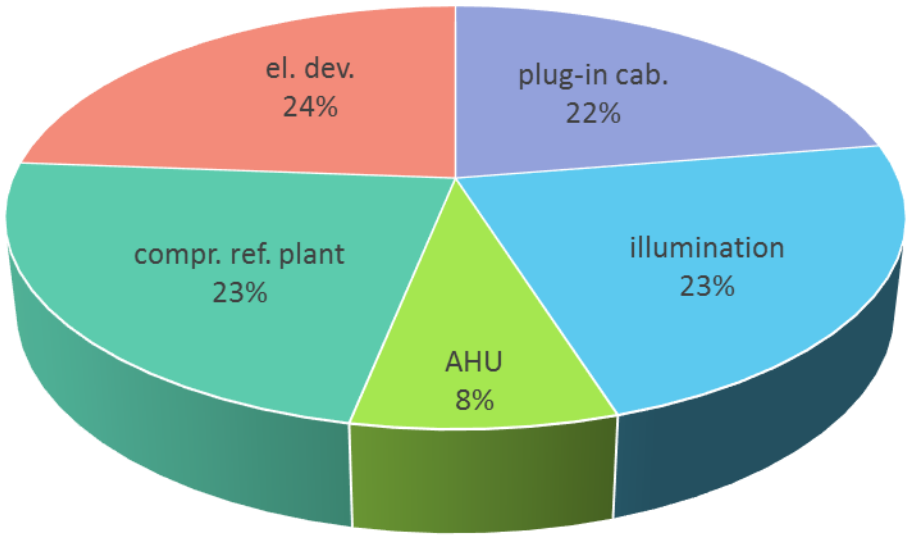

Figure 5-17: Disaggregation of the overall consumption for 2014

A_S is the sales area in m² and W_e is the energy intensity in kWh/m² SFA. For a sales area of 799 m², the average energy intensity accounts for 1081 kWh/m². The study showed that the

consumption for supermarkets of roughly that size varies from around 500 kWh/m^2 minimum to 1,700 kWh/m^2 maximum. The reference supermarket in Trondheim is in the top range of the energy performance. It has to be considered that the weather conditions and types of supermarkets in Norway differ from those in the UK. Moreover, different energy sources were compared in this study. For a detailed analysis, the thermal energy sources would have to be converted with a factor to be compared to the more expensive electrical energy used in the reference supermarket. Nevertheless, the study gives a reference point for the assessment of the test supermarket.

The disaggregation of the power consumption is shown in Figure 5-17. 45 %, which is equivalent to 178 MWh, was used for refrigeration including air conditioning. It can be seen that about 50 % of the refrigeration demand was met by plug-in cabinets. The energy for illumination accounted for around 23 % or 69 MWh. The power consumption of the AHU, including fans and rotary wheel, was 8 %, which is equivalent to around 24 MWh. The remaining 24 %, corresponding to 93 MWh, was consumed by other electrical devices.

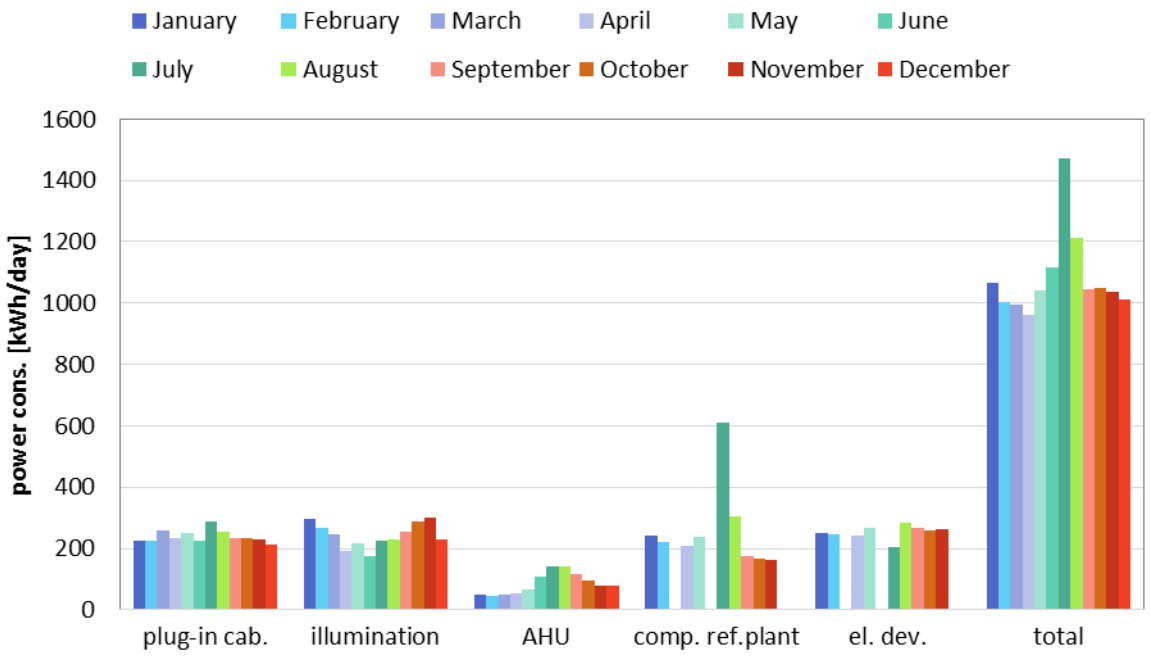

Figure 5-18: Monthly power consumption

Figure 5-18 demonstrates the measured monthly power consumption for the different consumers. It can be seen that the consumption for the plug-in cabinets and the compressors of the refrigeration plant increased during summertime. The high values for the compressors of the refrigeration plant in July and August can be explained by the fact that the refrigeration plant was also used for air conditioning in the sales area during this period. The consumption of the air handling unit was two to three times higher in summer than in winter. This was probably due to higher cooling demands requiring higher fan speed. Illumination was controlled according to the presence of natural light. This explains the drop in power consumption

during summer. The supermarket's overall power consumption was higher during the summer months. This indicates that the annual cooling demand was higher than the heating demand. Moreover, since the refrigeration plant was used for air conditioning, cooling was much more expensive than heating with waste heat in wintertime.

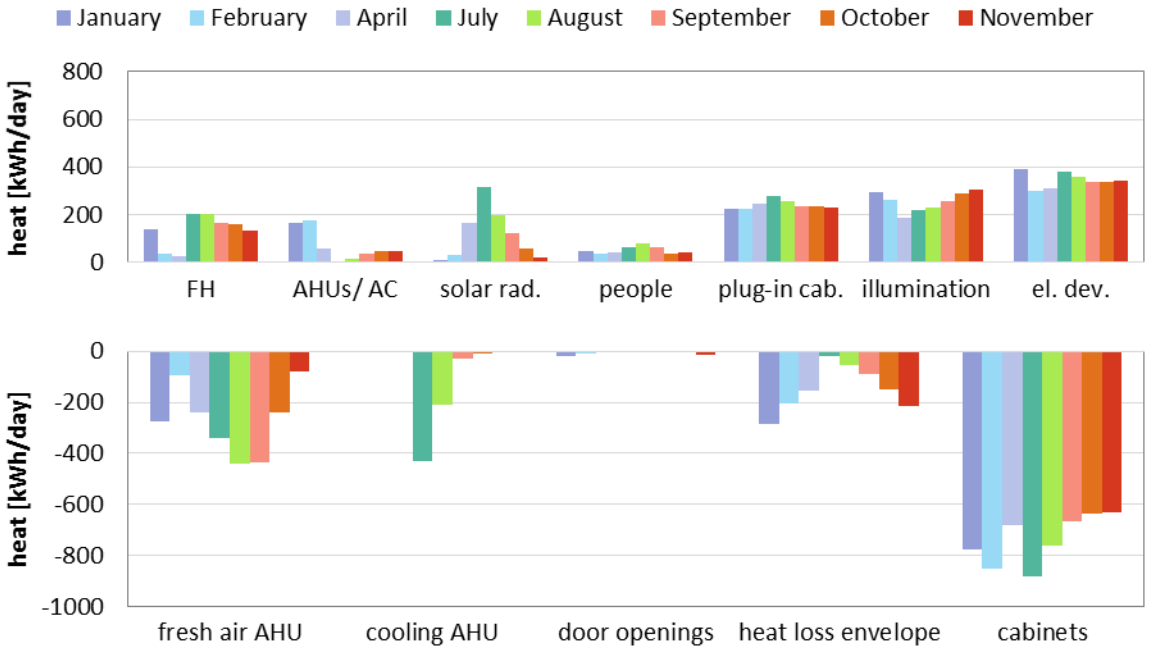

Figure 5-19: Annual heat gains and heat losses for the evaluated months

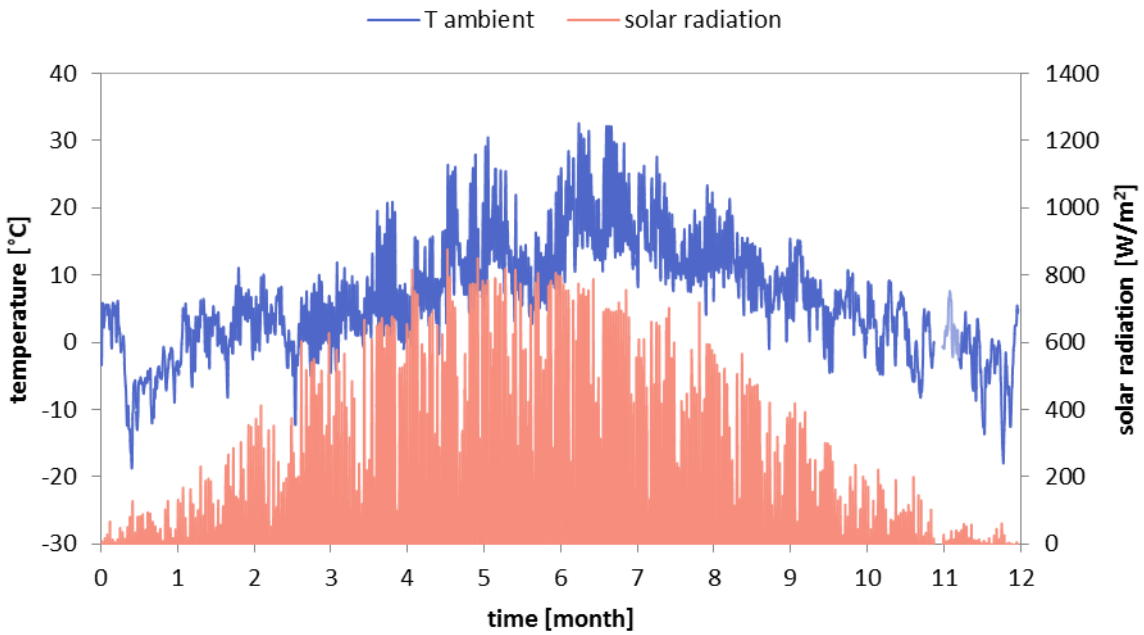

Figure 5-20: Ambient temperature and solar radiation **[86]**

A more detailed evaluation could be carried out for all months except March, May, June and December. The different heat losses and gains for the evaluated months in the building are shown in Figure 5-19. The measurements showed that the heating demand could be met by

heat recovery from the refrigeration plant throughout the year, as there was no additional electrical heating employed. Floor heating was used for almost the entire year for test purposes and to lower the gas cooler return temperature of the refrigeration plant. The average heat supply was about 150 kWh/day. Other forms of heating (AHU/ AHUSR/ AirCu) were mainly used in winter. In fact, additional electrical heating was not required at any time of the year. The values for the fresh air (FA) infiltrated by the AHU and AHU cooling prove that high cooling demands were caused by considerable heat loads during summer even when the ambient temperature was moderate (see Figure 5-20).

The main heat flows can be divided into those that were controllable, such as heating and cooling using the AHUs and FH system, and those that were not controllable, such as waste heat from electrical devices or solar radiation. Internal heat loads from illumination, plug-in cabinets, people, and other electrical devices remained more or less constant throughout the year.

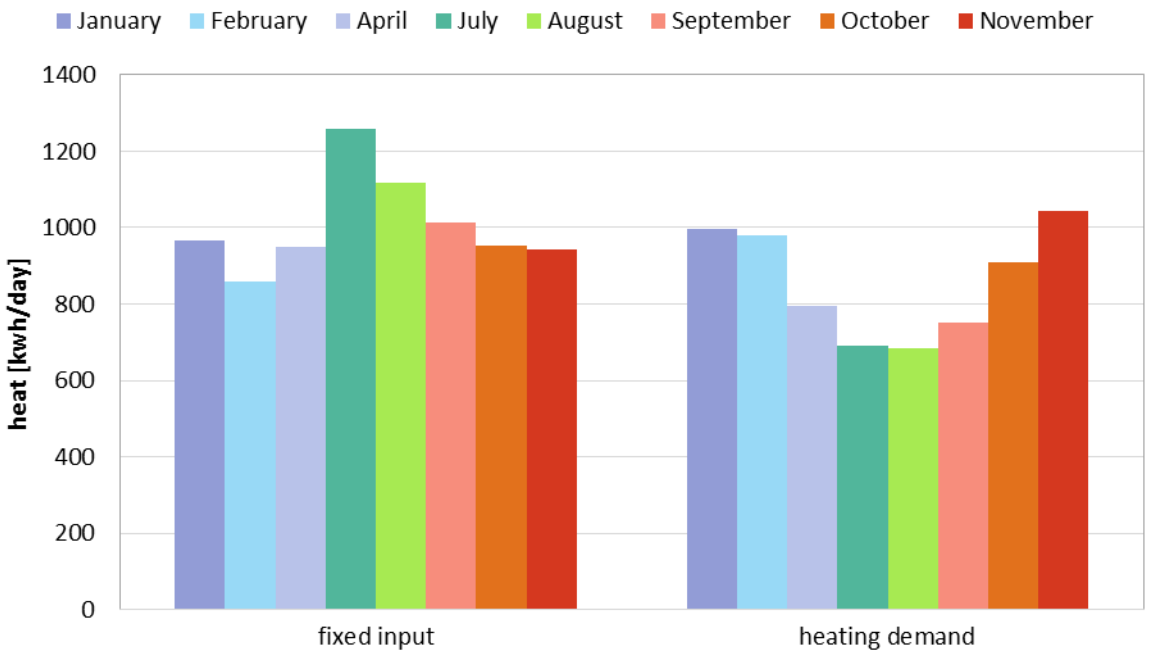

Figure 5-21: Uncontrollable heat load and heating demand for the evaluated months

It was defined as the sum of all heat loads that were not controllable:

$$\dot{Q}_{fixed\ input} = \dot{Q}_{people} + \dot{Q}_{solar\ rad.} + \dot{Q}_{el.dev.} + \dot{Q}_{illumination} + \dot{Q}_{plug-in} \quad \textbf{(5.81)}$$

The overall heating demand could be calculated according to:

$$\dot{Q}_{heating\ demand} = \dot{Q}_{in,fixed} + \dot{Q}_{AHU} + \dot{Q}_{FH} + \dot{Q}_{AirCu} + \dot{Q}_{AHUSR} \quad \textbf{(5.82)}$$

with:

$$\dot{Q}_{AHU} = \dot{Q}_{amb} + \dot{Q}_{AHXC} + \dot{Q}_{AHXH} + \dot{Q}_{IHX1} + \dot{Q}_{IHX2} \quad \textbf{(5.83)}$$

The fixed input and the overall heating demand are plotted in Figure 5-21. It is obvious that the uncontrollable part clearly exceeds the heating demand most of the time. Only in winter-time is it lower than the heating demand. This explains the high cooling demand throughout the year, especially in summertime.

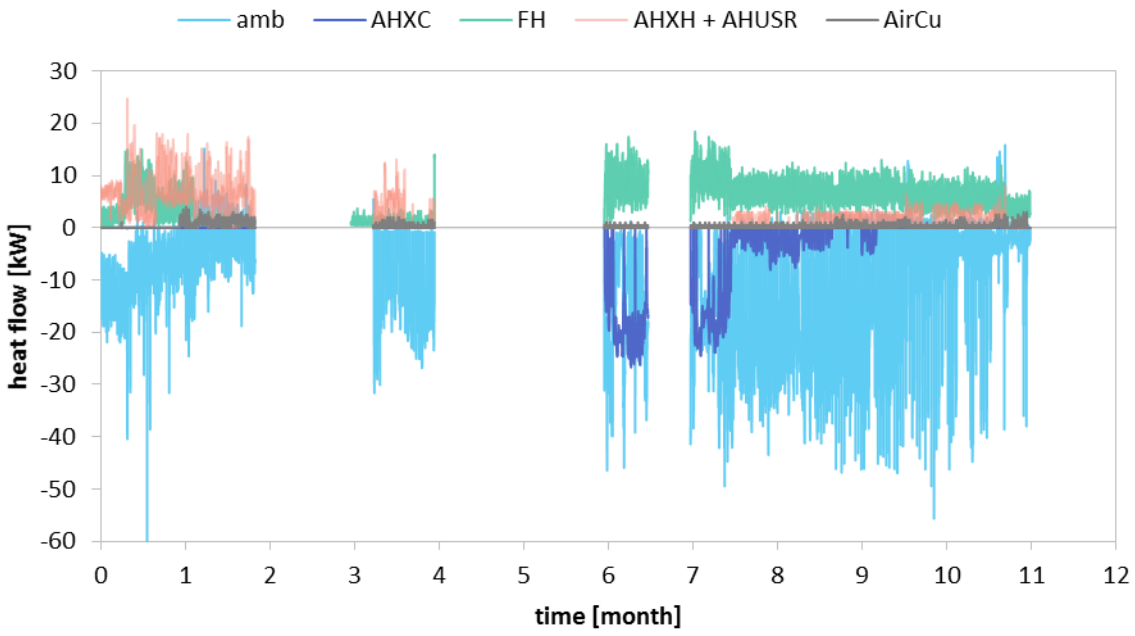

Figure 5-22: Annual heating and cooling for the evaluated months

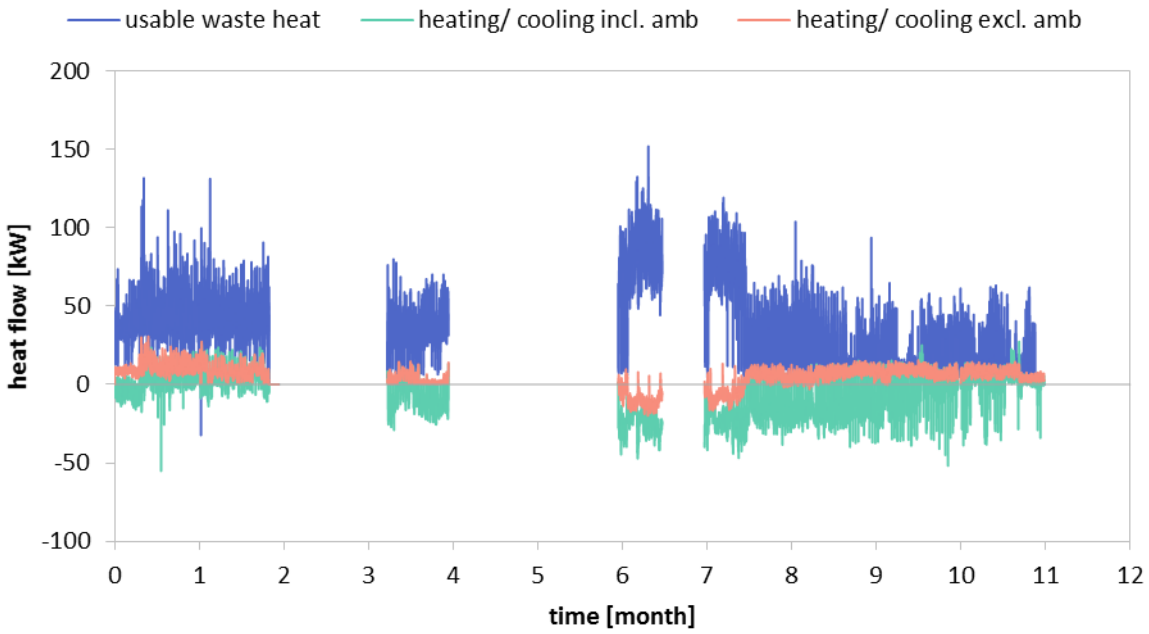

Figure 5-23: Heating/ cooling demand and recoverable heat for the evaluated months

The different controlled heating and cooling sources are plotted in Figure 5-22. It can be seen that heating and cooling were performed at the same time in some months. This was mainly because floor heating was also used to dispose of the waste heat from the refrigeration plant to lower the gas cooler return temperature and ensure a safe operation of the refrigeration plant. During the hot season, this caused an additional cooling demand.

Figure 5-23 illustrates the sum of all heating and cooling loads including ($\dot{Q}_{heating/cooling,\ incl\ amb}$) and excluding ($\dot{Q}_{heating/cooling,\ excl.\ amb}$) the heat losses or gains caused by AHU ambient air infiltration.

$$\dot{Q}_{heating/cooling,incl\ amb} = \dot{Q}_{AHU} + \dot{Q}_{FH} + \dot{Q}_{AirCu} + \dot{Q}_{AHUSR} + \dot{Q}_{amb} \quad \textbf{(5.84)}$$

$$\dot{Q}_{heating/cooling,excl\ amb} = \dot{Q}_{AHU} + \dot{Q}_{FH} + \dot{Q}_{AirCu} + \dot{Q}_{AHUSR} \quad \textbf{(5.85)}$$

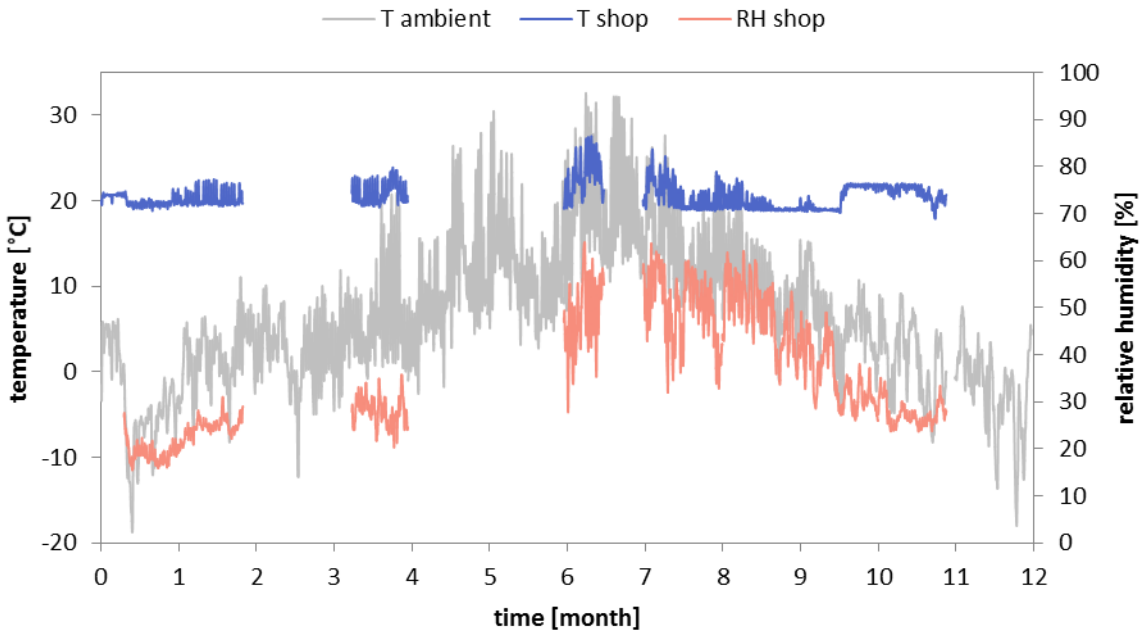

Figure 5-24: Shop temperature and relative humidity for the evaluated months

This differentiation was done because fresh air infiltration was not only used for space cooling but also to lower the CO_2 content in the shop. Considering the red line in Figure 5-23, it can be seen that there was a relatively low (average about 5 kW) heating demand almost all over the year. It has to be considered that ambient air infiltration is totally neglected in this curve. The green curve that includes the ambient air infiltration by the AHU shows much lower and mainly negative values the most part of the year. This indicates that internal loads were so high that heating was only required for a few months of the year, whereas cooling played a major role, especially in summertime. For comparison, the usable share of the total waste heat (see 5.1.1) is also plotted. The graphs show that the amount of usable waste heat from

the refrigeration plant was much higher than the heating demand of the supermarket. However, the heat extraction by the AHU ambient air has to be considered carefully. Ambient air was not only used for cooling, but also for reducing the CO_2 content in the sales area. The rotary wheel, however, was only used less than 1 % of the time, which indicates that ambient air infiltration was carried out largely for cooling purposes.

Figure 5-24 shows the shop temperature and humidity as well as the ambient temperature. Even though extensive cooling was applied in summertime, it was not possible to constantly keep the temperature around 20°C. In some cases in April and summer, the indoor air temperature exceeded the ambient temperature.

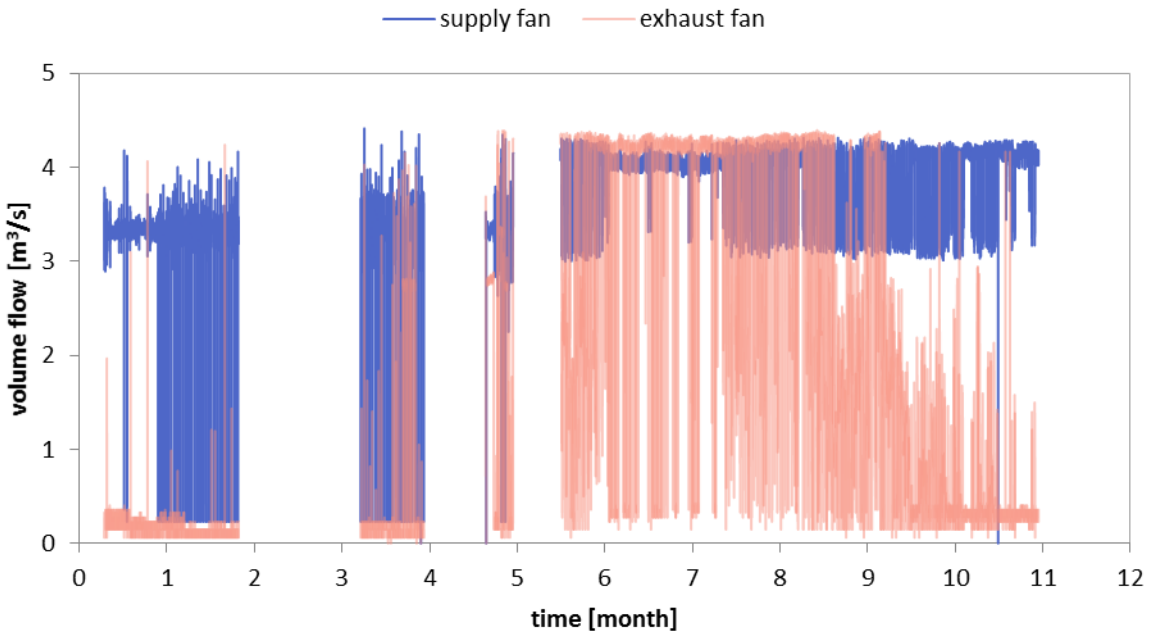

Figure 5-25: Volume flow of the AHU fans for the evaluated months

The capacity of the fans is shown in Figure 5-25. The graph illustrates that the supply air fan speed was more or less constant throughout the year, while the exhaust air fan speed increased along with cooling air demand in summertime. The exhaust air fan speed is high when ambient air infiltration is used and low if air recirculation is used. Comparing Figure 5-24 and Figure 5-25 shows that it was not able to keep the desired indoor air conditions during summer time even though the AHU fans were running on high speed. This is another indication for high internal heat loads that cause the high shop temperatures.

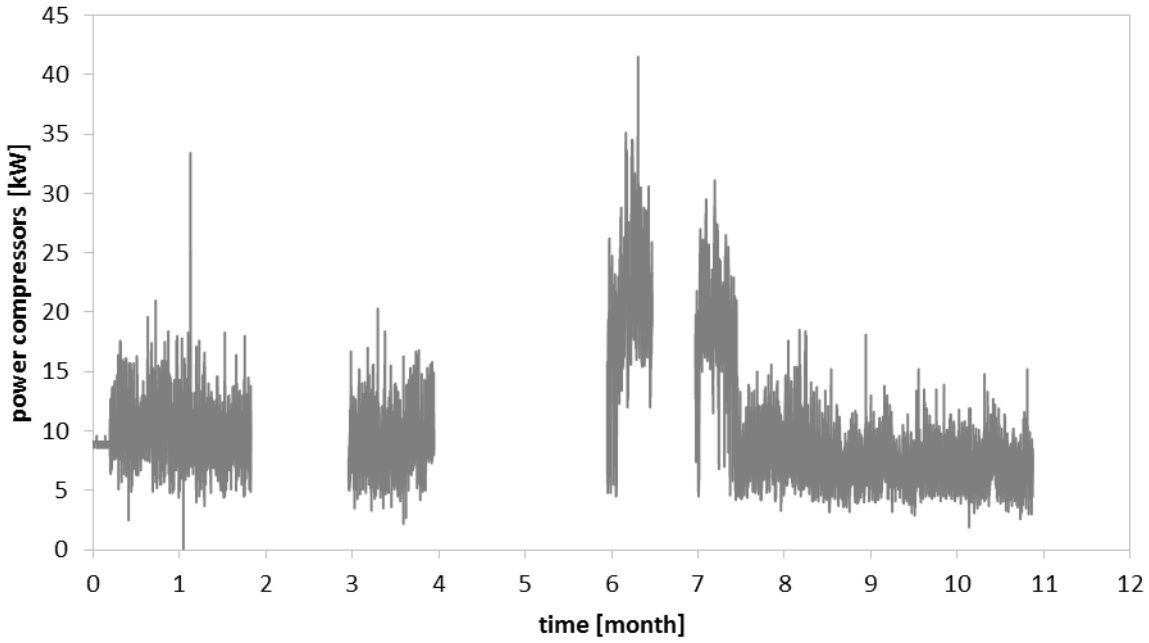

Figure 5-26: Power consumption of the compressors for the evaluated months

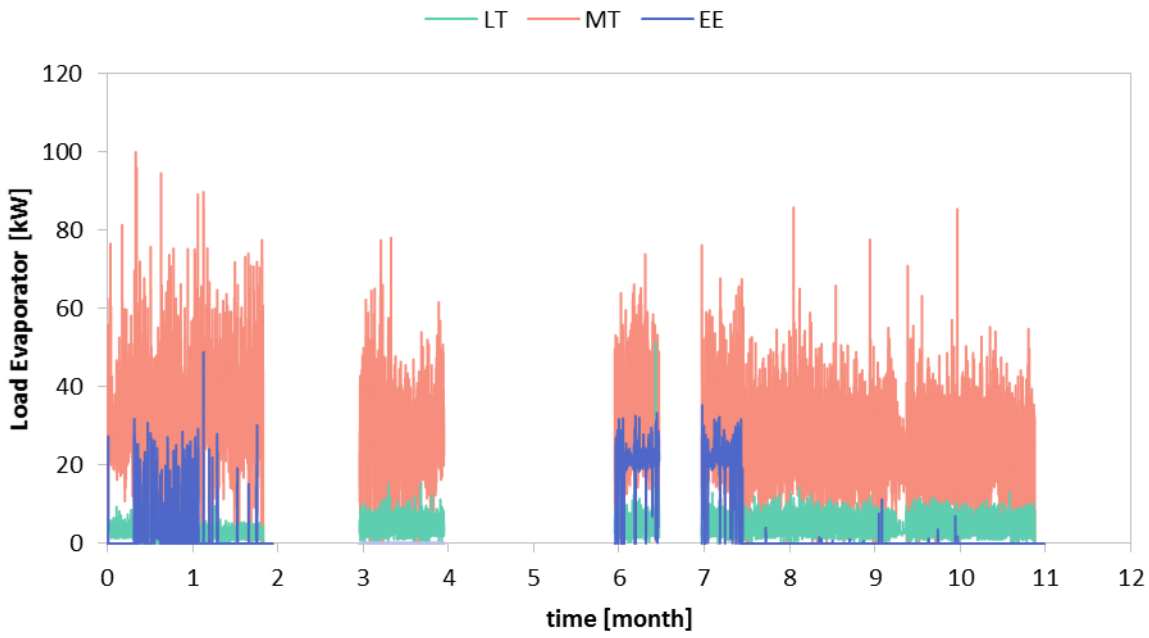

Figure 5-27: Daily heat load of the refrigeration plant for the evaluated months

The power consumption of the compressors of the refrigeration plant is plotted in Figure 5-26. The curve demonstrates that the context between the power consumption and the ambient conditions (Figure 5-20) is not too high. The consumption in six weeks in July and August was considerably higher than in the rest of the year. Figure 5-27 shows the freezing, cooling and extra evaporator load of the refrigeration plant. The load of the extra evaporator occurred mainly due to air conditioning purposes. It can be seen that the increase of the compressor's power consumption during summer is directly related to the extra evaporator's heat load.

Apart from the extreme rise due to the use of the extra evaporator, one reason for the higher consumption in summer was probably the higher heat load to the cabinets due to higher shop temperatures and humidity, ambient temperature and solar radiation.

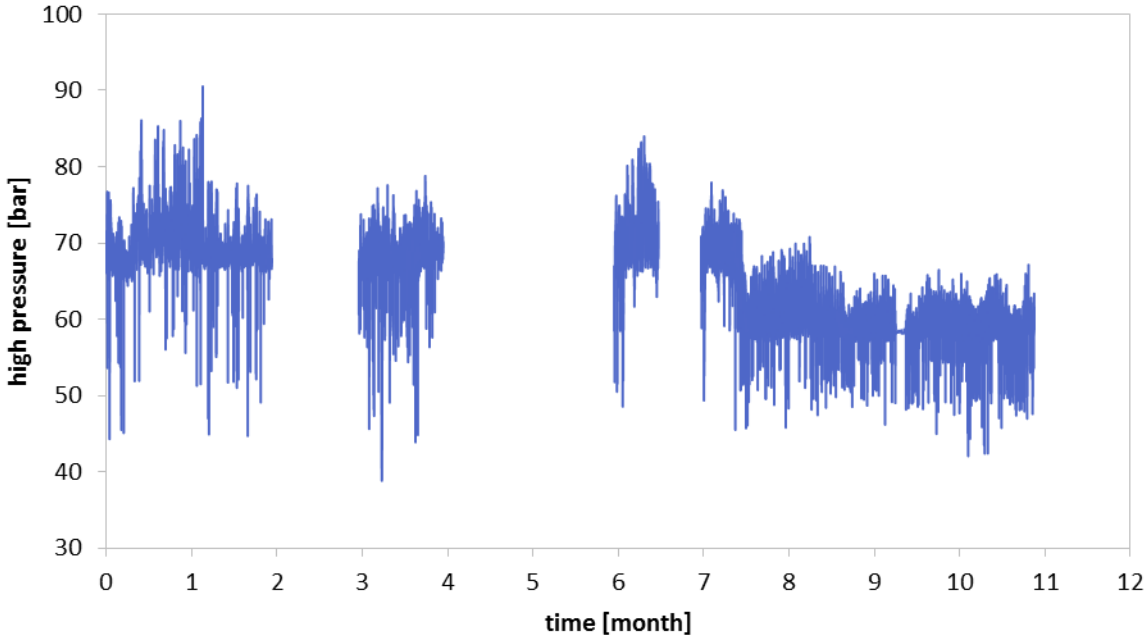

Figure 5-28: High pressure of the refrigeration plant for the evaluated months

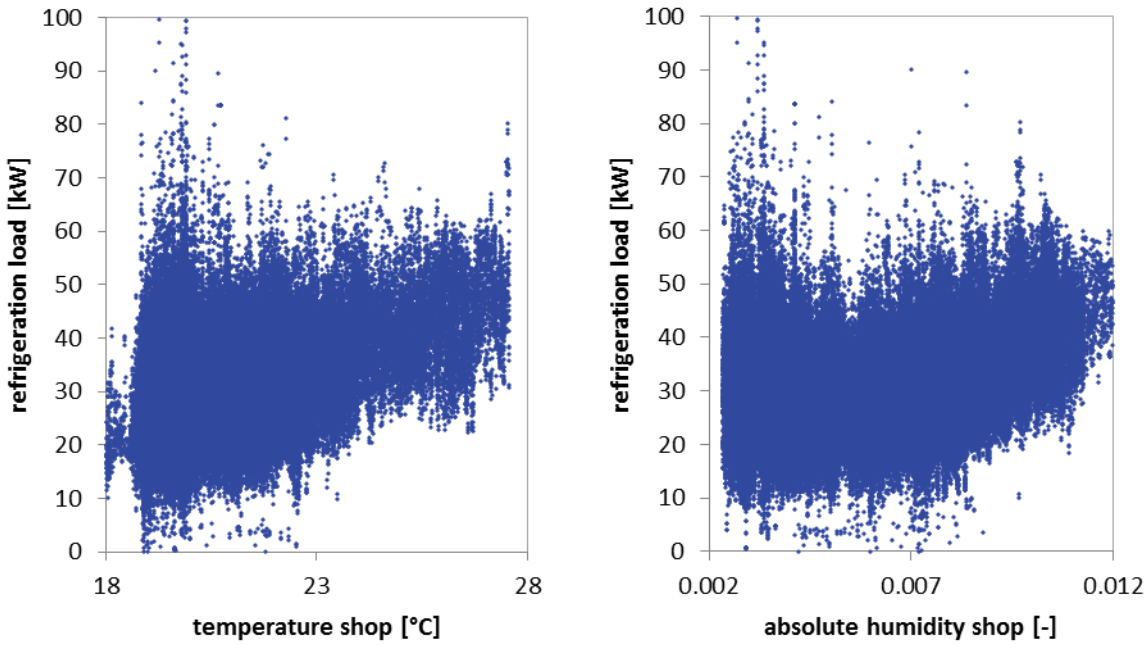

Figure 5-29: Dependence of heat load on the shop temperature and absolute humidity

The annual course of the shop temperature, shop humidity, ambient temperature and solar radiation in are plotted in Figure 5-20 and Figure 5-24. The variation of the refrigeration load in relation to the shop temperature and the absolute shop humidity are plotted in Figure 5-29.

Figure 5-30 shows the dependence of the refrigeration load on the ambient temperature. The plots show that the heat load is increases with high shop temperatures and absolute humidities but also with high ambient temperatures. Apart from this, the solar radiation, illumination and the number of customers all influence the heat load of the cabinets.

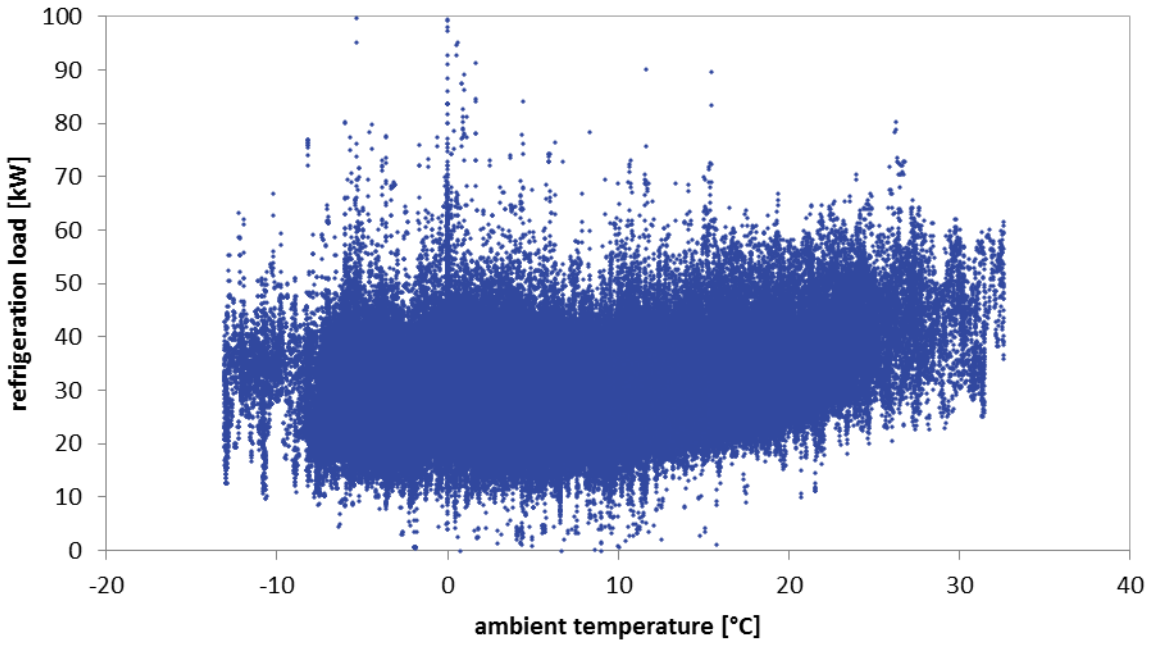

Figure 5-30: Dependence of heat load on the ambient temperature

Moreover, the performance of the refrigeration plant was poorer in summertime, probably due to the higher ambient temperature (see Figure 5-31).

The annual course of the refrigeration plant performance is represented in Figure 5-31, which plots the COP_{ref}, COP_{total} and COP_{max}, which were defined in 5.1.1. Once more, it should be noted that heat flows at different temperature levels are considered in the calculations for these COPs. Consequently, they can only be used for an internal analysis and should not be compared to other systems. For the considered supermarket, the COP_{ref} was between two and four most of the time. During summertime, especially when the extra evaporator was used, the COP_{ref} dropped to minimum values. As mentioned before, higher ambient temperatures led to a performance decrease and a lower heating demand of the building. Consequently, less heat was transferred to the AHUs and the FH cycles. The dry cooler was used, but the refrigerant could only be cooled down to the ambient temperature. The refrigerant temperature could be further decreased using the BHX, but its capacity is limited to approximately 30 kW.

The COP_{total} shows higher values, because it considers the used waste heat. Especially in wintertime, when heat recovery was realised, the COP_{total} reached values between four and six. The COP_{max} represents the highest COP that could theoretically be reached if all the available waste heat were used. Comparing the COP_{total} to the COP_{max} for January until April shows that

performance could be much better if more waste heat was used. The COP_{max} was almost twice as high in this period. In the second part of the year, the COP_{total} was much closer to the COP_{max}. One reason for this was probably the lower high pressure of the refrigeration plant, which led to reduced usable waste heat (see Figure 5-28).

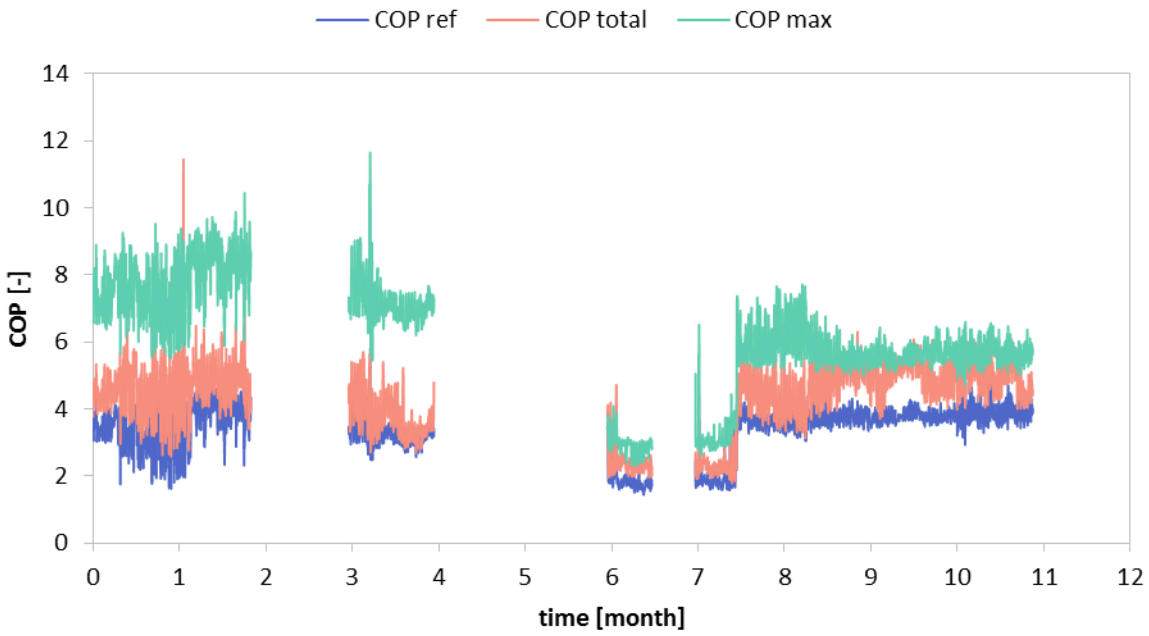

Figure 5-31: COPs of the refrigeration plant for the evaluated months

There are various parameters which influence the performance of the refrigeration plant, some of which are mutually dependent. This makes an analysis of the factors which influence the COP_{ref} challenging. The influence of the high pressure, refrigerant gas cooler return temperature and cooling load on the COP_{ref} are plotted in Figure 5-32, Figure 5-33 and Figure 5-34. As other influencing factors were not excluded in these plots, no concrete statements can be made, but a tendencies can be observed. The COP shows a decrease with the gas cooler return temperature. At low return temperatures, COP_{ref} values around 6 were reached. For high return temperatures, the COP_{ref} approximated a minimum value of around 2. However, the spreading in the low temperature region is much higher. This leads to the assumption that the influence of other parameters is higher in this area.

The COP_{ref} correlates with the cooling load in an almost linear way. One reason for the higher COP_{ref} at higher heat load could be the higher efficiency of the compressors at full load. The plot of the COP_{ref} over the high pressure shows scattering values, but there is a tendency. The graph shows that a lower high pressure leads to a higher performance of the refrigeration system. The annual course of the high pressure is plotted in Figure 5-28. Comparing this to the compressor's power consumption (Figure 5-26) shows that there is a context between COP and high pressure, keeping in mind that the high consumption in July and August were due to the use of the extra evaporator.

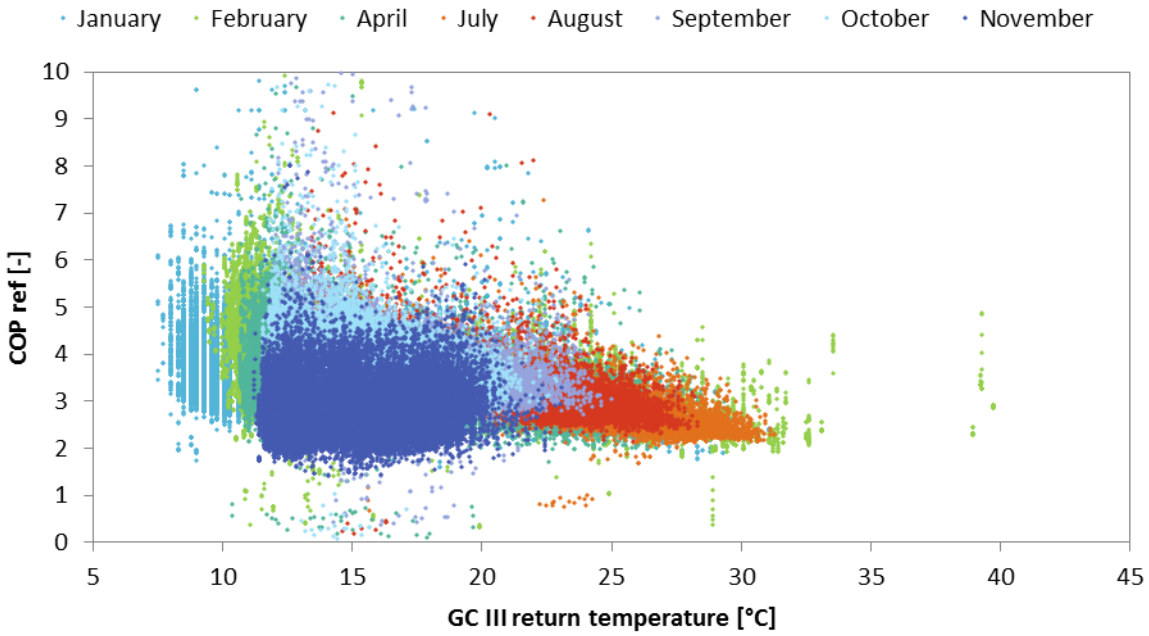

Figure 5-32: Dependence of the refrigeration COP on the gas cooler return temperature

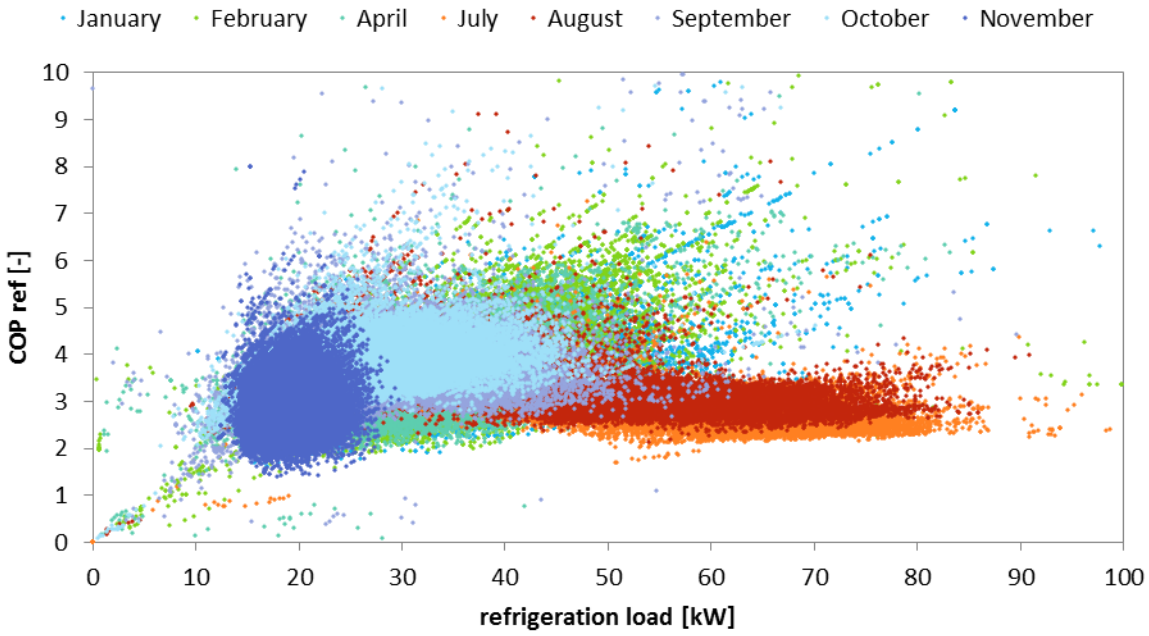

Figure 5-33: Dependence of the refrigeration COP on the refrigeration load

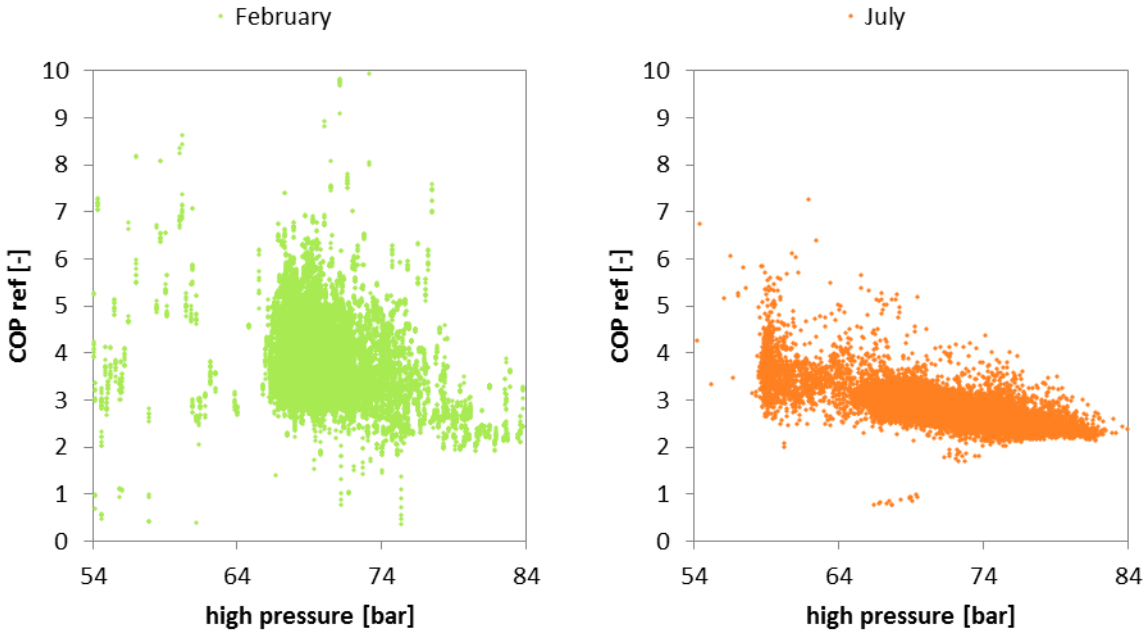

Figure 5-34: Dependence of the refrigeration COP on high pressure

Further measurement results can be found in Appendix A.

Conclusions and suggestions for optimisation

Some suggestions for improvements were developed using the conclusions that were drawn from the evaluated data. The efficiency of the plug-in cabinets is low compared to remote refrigeration. One reason for this can be that the condensing temperature of the plug-in cabinets is above the shop temperature of around 20°C, while the condensing temperature of the remote refrigeration corresponds to the ambient temperature. The ambient temperature is usually lower than the shop temperature, especially in wintertime. Savings could be achieved by replacing the integral cabinets by remote cabinets. Additionally, the fluorescent tubes could be replaced by LEDs. Illumination and plug-in cabinets have a high share in the uncontrollable internal heat loads. In summertime, this heat has to be rejected by the AHU or even by the refrigeration plant, which leads to a considerable increase of the power consumption of these systems. The AHU is the system with the highest seasonal variations in power consumption, which indicates a high savings potential. Savings could be achieved by employing a CO_2-based control strategy. These measures would reduce the power consumption for refrigeration, illumination and the air handling unit. However, replacing the illumination and plug-in cabinets could also cause some challenges. 100 % of their waste heat is released into the sales area. Without this waste heat, the heating demand in the building rises considerably in wintertime. The results showed that there was much more waste heat available than from the refrigeration plant, than required. Nevertheless, it has to be considered that the low heating demand was, to a large share, a consequence of the high amount of waste heat from illumination and plug-in cabinets. By reducing this waste heat, it can come to the situation where

the heating demand is higher than the refrigeration plant's waste heat. In this case, the waste heat of the refrigeration plant has to be raised, either by raising its high pressure or running it in heat pump mode, using the extra evaporator, which could lead to an increase of the compressor's power consumption. Usually, the efficiency of a heat pump is always higher than pure electrical heating, but in this case, it has to be considered that it is not possible to recover 100% of the refrigeration plant's waste heat. It can only be used until a certain temperature by the FH system.

Detecting all parameters that influence the refrigeration plant's performance was challenging. It was, however, possible to establish that the gas cooler return temperature and the high pressure should be kept low. For a low GC return temperature, as much heat as possible has to be extracted from the gas coolers, keeping in mind that the heat transferred in the dry cooler and the BHX cannot be used for heat recovery. This "lost" heat should be kept to a minimum. Moreover, the use of the dry cooler fans increases the total power consumption. Waste heat is valuable, particularly in winter. If it is not immediately required, is should be stored in the tanks. As shown in Figure 5-23, much of the waste heat from the refrigeration plant available in 2014 was not used. The amount of usable waste heat directly depends on the high pressure of the refrigeration plant. If the heating demand of the building is low, the high pressure of the refrigeration plant can be reduced. It should only be raised if heating is required.

Besides these conclusions and suggestions, the wealth of data and the detailed evaluations formed the base for the base for the simulations that were carried out in order to investigate different optimisation approaches. The data were used in order to develop, calibrate and validate a dynamic overall supermarket model. The models and the simulations will be described in the following chapter.

6. Simulations

Two optimisation strategies were derived from the improvement approaches suggested in 5.2. The strategies were developed and tested using a detailed and highly dynamic simulation model. The development of the model and the optimisation strategies will be presented in the following chapter. The simulation results will be presented and discussed.

6.1. Description of the models

The main task of the model was to analyse the benefit of different optimisation approaches in the test supermarket. In particular, the goal was to understand the impact of the developed control strategy on the energy performance. For this purpose, it was essential to consider the dynamic behaviour and different time constants of the system. Components and controllers were modelled in a detailed way. In order to map the feedback between the internal systems,

a model which describes the whole supermarket, including all subsystems, was developed. The refrigeration plant, AHU, building and secondary loops, including the tanks and borehole heat exchanger, were modelled in detail. The subsystems were modelled in such a way that several components, such as compressors, fans, tubes, valves and controllers, were considered. The mass flow distributions in the AHU, refrigeration plant and secondary loops were calculated based on pressure relations. Due to this high level of detail, long simulation times had to be accepted. Considerable effort was put into the validation and calibration of the system. Measurement data were used to calibrate the model in terms of pressure losses, thermal conductivities and efficiencies of the components and the building, among others.

The model was developed using the simulation tool TILSuite (Version 3.3.1) [95], which is based on the language Modelica [96]. It includes a large library for thermal components and various fluid data from the TILMedia library [97] can be used. For a more detailed description of TILSuite and Modelica, see 3.4.

The building model was derived by modifying the TILAddOn_Cabinet [98], [99] model with the help of a student [100]. For the storage tank, the TILAddOn_Heatstorage [101], [102] model was used. The model for the borehole heat exchanger was also developed based on the work of Averdam [103]. TILMedia fluid data for CO_2, a 30 % water-glycole mixture and moist air were used in the models for the refrigeration plant, secondary loops, AHU and building. TILMedia distinguishes between different fluids: liquids, in which no phase-change is considered, VLE fluids (VLE: vapour liquid equilibrium), in which phase-change is considered and gases.

Building

In the building model, heat flux by solar radiation, envelope losses, internal loads from electrical devices and people, and the extracted heat from the refrigeration cabinets were included. Thermal conductivities and capacities of the building's envelope and interiors were considered.

Three layer models were used for the walls and the roof and one layer models for the windows. The thermal and material properties of the walls and windows were fitted according to the manufacturer’s data. The alpha values on both sides of the walls were assumed to be constant. In the floor model, three layers were considered: one layer for the concrete, one for the insulation and one for the thermal-influenced ground. The thermal-influenced ground was defined as the ground layer that thermally interacts with the building. The thickness of the thermal- influenced ground was assumed to be 10 m and the temperature below the thermal influenced ground layer was assumed to be constant. The floor heating model was embedded into the floor model. TIL liquid tube models were used. The three parallel FH loops were modelled separately. Thermal contact between the tubes and the concrete layer was considered. The pressure loss in the tubes was calculated using the Konakov correlation [104] and the

internal heat transfer coefficient using the Gnielinski-Dittus-Boelter equation [105], [106], [94]. A horizontal temperature gradient in the floor was not considered.

The properties of air in the sales floor area were calculated in a moist air cell model, without considering temperature and moisture gradients in any direction. Thermal contacts between the moist air cell and the walls, floor, roof, windows, people and internals were modelled, internal heat sinks and sources treated as input values. The heat load to the cabinets was considered as an internal heat sink. The heat from the plug-in cabinets, illumination, other electrical devices, air curtain and AHURS was defined as internal heat loads. The input values were calculated using the measurement data (see 5.1.6). The heat and water production from people was included in the moist air balance. The number of people could be set as a parameter from the outside. It was assumed that the heat flux caused by solar radiation directly heats the interior, with the interior being in thermal contact with the air in the building. Thus, solar radiation was modelled as an indirect heat load to the indoor air. The moist air cell model was directly connected to the AHU model. Consequently, the temperature and humidity of the moist air cell were determined by the inflowing air of the AHU and building envelope losses, as well as internal and external heat losses and gains and moist air production by people in the shop. The CO_2 balance in the building was simulated dependent on the ambient air infiltration and the CO_2 production by people and fruits. The natural air exchange rate and the air exchanged by door openings were treated as input values. The door air flow was calculated as described in 5.1.6.

Properties such as the material and thickness of the walls and windows or the orientation of the building could be set according to the ground plan and manufacturer's data. Ambient conditions such as temperature, humidity, solar radiation intensity and sun position were set as input values. The weather data used were gained from measurements or the Norwegian meteorological institute [86]. The value for the number of people in the shop was calculated from measurement data (see 5.1.6).

The roof of the test supermarket was planted with sedum, which was neglected in the simulation model, even though the presence of humus and sedum probably have an influence on the building's heat balance. The plants and the humus have a thermal mass that is subject to considerable variations. When it rains, the humus gets wet and the water content in the plants rises. In addition, the colour of the plants changes with the seasons, meaning the amount of absorbed solar radiation also changes. Moreover, transpiration from the plants influences the infiltration of solar radiation. Photosynthesis phases change throughout the day and influence the overall heat balance of the plant. The influence of green roofs on heat transfer has been investigated in different papers [107], [108], with several experiments showing that it is complex and extremely dependent on height, colour, density and photosynthesis behaviour of the plant. The development of such a model would be extremely time-consuming and a validation

would not be possible with the measurement data Available. It was therefore decided to use a simplified roof model.

AHU

The AHU model (compare Figure 4-6 and Figure 5-13) was mainly built with the use of TIL models or modified TIL models. The calculation of the air flow distribution was based on pressure differences in the system and fan speed. The AHU model was directly connected to the building model.

TIL moist air-liquid fin and tube heat exchanger models were used for the AHU heat exchangers. A discretisation of 10 cells was set. The major part of the geometrical data was known from the manufacturer's data sheets. The remaining parameters were calibrated with simulations and measured or calculated heat and mass flows (see 5.1.5). Water condensation of the moist air was considered in the AHXH and AHXC models. The pressure drop on the liquid side was calculated using the correlation of Konakov and the heat transfer coefficient using Gnielinski-Dittus-Boelter. On the air side, fixed alpha values were assumed, which were calibrated with measurement data. The pressure drop correlation on the air side was adjusted to simulation data provided by the manufacturer.

The heat recovery wheel was modelled in a simplified way, assuming that it behaves like an air counter flow heat exchanger. Mass transfer between the fresh and exhaust air flow was neglected. The mass and the material properties, such as heat capacity and thermal transmittance values, were calibrated according to the evaluated data (see 5.1.5). Measurement data indicated that internal heat transfer occurred in the wall between the supply and exhaust air side. This internal heat transfer was considered in the AHU model. The thermal resistance and capacity of the wall were also considered.

The pressure losses caused by internal ducts and flaps in the AHU were modelled as quadratic pressure drops dependent on the hydraulic diameter, zeta values and mass flow. The hydraulic diameters were known from the manufacturer and the zeta values were calibrated according to the measured and calculated mass flow distribution in the AHU. The flap positions were treated as input values and the resulting pressure resistance was calculated. The pressure drop in the air distribution system was calculated as a quadratic pressure drop. The tube diameter and the coefficient of friction were calibrated. The pressure drops of the filters, rotary wheel and heating or cooling heat exchanger were calculated as exponential pressure drops dependent on mass flow, hydraulic diameter and zeta value and pressure drop correlations were also calibrated according to manufacturers’ data.

For the supply and exhaust air fan, TIL second order fan models were used. The characteristic lines of the fan models were calibrated according to manufacturer's data and measurement values.

A time-consuming calibration process had to be carried out for the AHU model. The power consumption of the fans is dependent on the internal pressure drops, fan speed and efficiencies, with internal pressure drops, in turn, depending on the geometry and flap positions. Measurement data were available, but partially missing or not reliable. Mass flow distribution inside the system was calculated as described in 5.1.5, but, due to complicated calculations, those values were not always reliable. Parameters such as fan efficiencies, different pressure losses and flap positions influenced each other and not all of them were determined by measurement or evaluation, which led to challenges in the development and calibration of the model. Very short time constants occurred in the AHU, causing numeric challenges for the simulations.

Refrigeration Plant

The refrigeration plant model (compare Figure 4-4) was mainly based on TIL components. The gas coolers and the internal heat exchanger of the refrigeration plant were modelled with TIL VLE-fluid-liquid or VLE-fluid-VLE-fluid plate heat exchanger models with a discretisation of 10 cells. Geometric data, such as the number of tubes, fin pitch or parallel flows, were available in part from the manufacturers. The remaining values were calibrated with the aid of simulations. For the refrigerant side heat transfer coefficients, fixed values were assumed, which were calibrated using simulations and measurement data. The pressure loss in the heat exchangers on the refrigerant side was neglected in the simulations. The pressure loss and alpha value on the liquid side were calculated according to the VDI directive for chevron plate heat exchangers [109].

The LT and MT evaporators of the refrigeration plant were not modelled individually, but were summarised into one large LT and MT evaporator respectively in the model. The same was done with the cabinet fan models. Moist air-VLE fluid fin and tube heat exchanger models and simple fan models were used. The extra evaporator was modelled separately from the LT and MT evaporators using a VLE fluid-liquid plate heat exchanger model. The refrigeration heat loads on the cabinets were treated as input values. The courses of the LT, MT and EE heat loads were derived from measurements, as described in 5.1.1.

The compressor models were taken from the TIL library. The volumetric, isentropic and effective isentropic efficiency were assumed to be independent of the compressor speed. The values for the efficiencies were calibrated according to measurement data. For numeric reasons, the parallel high pressure compressors were not modelled separately. The orifice valve models were adopted from TIL.

Secondary Loops

Liquid tube models were used in the secondary loops (compare Figure 5-3, Figure 5-5 and Figure 5-9). The exact geometries of the tubes were not known, so they were calibrated according to the calculated mass flow distribution (see 5.1.2, 0 and 0) in the systems and the power consumption of the pumps represented in manufacturers' data sheets. Heat losses via the tubes were not considered. Pressure losses in the tubes were calculated using the correlation of Konakov for smooth pipes. The models for valves and three way valves were also adopted from the TIL library. The pumps were modelled using the simple pump models from the TIL library and the mass flow was treated as an input value.

The geometry of the snow melting tubes and floor heating tubes in the freezing room (FH4, compare Figure 4-2) were calibrated according to measured and evaluated data (see 5.1.3). For the internal heat transfer coefficient, the correlation of Gnielinski-Dittus-Boelter was used. The thermal resistance of the floor areas above the SM and FH4 loops were calculated using simple resistance and heat capacity models that were also calibrated.

Dry cooler

The dry cooler was simulated with the TIL gas-liquid fin and tube model. The discretisation was set to 10. Some of the geometry data were known from manufacturers' data sheets. The alpha value on the liquid side was calculated using the correlation of Gnielinski-Dittus-Boelter and the pressure drop using the Konakov correlation for smooth pipes. The fin efficiency was calculated using the 1-D Schmidt approximation [110]. The fin side heat transfer coefficient was assumed to be a fixed value which could be calibrated using measurement data. The pressure drop was assumed to be linearly dependent on the air mass flow and was calibrated according to the values represented in the data sheet for the DC fans. The TIL simple fan model was used for the DC fans.

Tanks

The tank model was taken from the TILAddOn_Heatstorage library. The model describes a stratified storage tank. The discretisation was set to 65 cells in order to achieve reliable results in an acceptable simulation time. The modelled tank includes two direct liquid inlets, two direct liquid outlets and an internal tube heat exchanger. The geometry of the tank and insulation, as well as the position of the liquid inlets and outlets, were set according to the manufacturers' data. The thermal properties, such as conductivity and heat transfer coefficients, were calibrated according to measurement data.

Borehole heat exchangers

The BHX u-tube heat exchanger was modelled using one liquid tube model for the supply tube and one for the return tube. The pressure loss in the tubes was calculated using the correlation of Konakov and the alpha value inside the tube using Gnielinski-Dittus-Boelter. The borehole

ground or rainwater filling was considered. It was assumed that the ground is thermally influenced by the BHX up to a critical distance. The thermal influenced ground was modelled. The temperature beyond the critical distance was assumed to be constant. Information about the nature of the ground and ground water flow was not available, thus requiring extensive calibrations of the model. During the calibration process it was indicated that ground water flow occurred and the borehole was filled with water. A vertical discretisation of 10 cells was set for the BHX model.

Controllers

The controllers were modelled using TIL PI controller models. The controller set points and parameters and the control strategy were adjusted through extensive calibration.

6.2. Calibration and validation

As described in the previous chapter, the geometry and properties of the building, such as the wall materials and thickness, transmission coefficient of the windows or length of the floor heating tubes, were used on the model insofar as data were available. The same was done for the technical equipment, such as compressor sizes and efficiencies, tube lengths and pressure drops in the HVAC components. Nevertheless, many values were not available. Some of them could be calculated with the use of measurement data (see 5.1), while other data had to be adjusted with the help of calibration processes. These processes were challenging, due to the complex interactions in the supermarket.

Time-consuming calibration processes were used on the HVAC model. The consumption and volume flow of the fans were dependent on the pressure losses in the HVAC, fan speed and efficiency. For the efficiency, manufacturers' data were available, but those usually differ from measured data. The pressure losses were dependent on the pressure drops of single components such as internal ducts, distribution system, heat exchangers, filters and rotary wheel, but also on the mass flow distribution in the system, which is determined by the flap position. The volume flow of the fans was measured, but, in some cases, considerable measurement deviations occurred, especially for small volume flows. Due to missing data, the flap positions were only partially known. The pressure drops of the components were only known from manufacturers’ data and for certain volume flows. The capacities of the fans were not known and the fan speed could be extrapolated. The flap positions and fan speed determine the internal mass flow distribution and consequently the supply air temperature. At the same time, the temperatures, including the supply air temperature, depend on the mixture of ambient air and return air, but also on internal heat exchanges. The mass flow distribution and internal heat exchanges in the system were calculated as described in 5.1.5, but measurement errors had to be considered. The amount of ambient air does not only influence the supply air temperature, but also its quality, which is crucial for the indoor air CO_2 content. The CO_2 content

also depends on the number of people, which was also calculated (see 5.1.6). This example shows the complexity of supermarket systems and the challenges during the evaluation. Thus, extensive calibration and validation were required in order to verify both measured and simulated values.

Flap positions and pressure drops of the HVAC components were calibrated. Moreover, tubes, ducts, heat transfer coefficients, conductivities, geometry and thermal capacities for heat exchangers, walls and the floor had to be determined. The transmission, reflection and absorption coefficients of windows and aerogel were adopted from the values determined in the evaluations and were validated through simulations. For measured or calculated values, such as mass flows and volume flows and distributions, heat flows and temperatures were used to validate the simulation. A challenging process was the calibration and validation of complex systems such as the storage tanks, including the behaviour of the water inside the tanks (stratification or mixture) and consequently the temperature distribution and the quality of the insulation. Another time-consuming process was the calibration of the BHX model. Measurements, such as a thermal response test or the temperature course along the tubes, were not carried out.

The validation and calibration processes cannot strictly be separated. Validation always led to further calibration processes until reasonable results were obtained. Nevertheless, a final validation was carried out, the results of which are presented and discussed in the following. The calibrations were carried out for all simulated seasons in order to avoid a unilateral point of view. The simulated power consumption of compressors or fans, the heat flow in heat exchangers and the mass flow in different components were compared to the measured or evaluated values, among others.

In order to assess the quality of the models, the mean absolute error (MAE), as well as the mean absolute percentage error (MAPE) [111] were determined.

$$MAE_{sim} = \frac{1}{n} * \sum_{i=1}^{n} |\hat{y}_i - y_i| \quad \textbf{(6.1)}$$

$$MAPE_{sim} = 100 * \frac{1}{n} * \sum_{i=1}^{n} \left| \frac{\hat{y}_i - y_i}{y_i} \right| \quad \textbf{(6.2)}$$

y_i is the measured value and $\hat{y}_i$ is the simulated value.

Additionally, the measurement error was estimated using the manufacturer's data. An error propagation according to Gauß [112] was carried out for the evaluated data.

$$\Delta\overline{F} = \sqrt{\left(\frac{\partial F}{\partial x_1}\Delta\overline{x_1}\right)^2 + \left(\frac{\partial F}{\partial x_2}\Delta\overline{x_2}\right)^2 + \cdots} \quad \textbf{(6.3)}$$

wherein $\Delta\overline{F}$ is the mean error and, $\Delta\overline{x_1}$, $\Delta\overline{x_2}$ the error of the individual measured variable. $\partial F/\partial x_1$ and $\partial F/\partial x_2$ are the partial deviations of the function F= F(x_1,x_2,…).

The mean average error MAE

$$MAE_{meas} = \frac{1}{n} * \sum_{i=1}^{n} \left|\Delta\overline{F}_i\right| \tag{6.4}$$

and the mean average percentage error MAPE

$$MAPE_{meas} = 100 * \frac{1}{n} * \sum_{i=1}^{n} \left|\frac{\Delta\overline{F}}{y_i}\right| \tag{6.5}$$

with y_i as the measured value, were determined for n measured values for the January measurements.

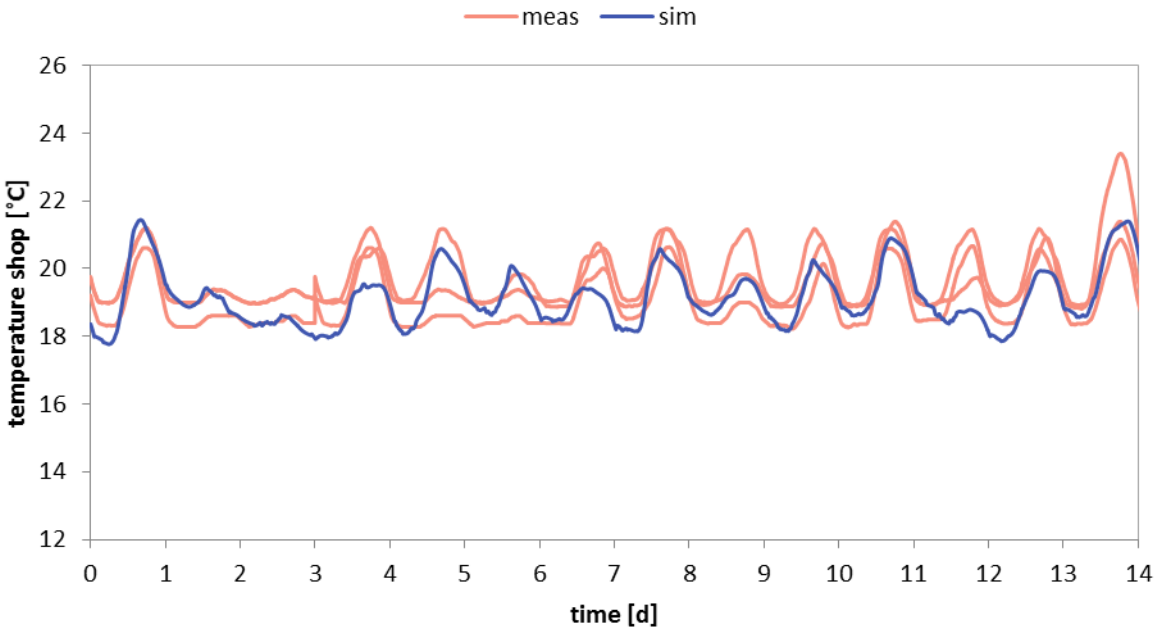

Figure 6-1: Simulated and measured temperature in the shop for two weeks in August

Some of the results will be presented and discussed in the following.

Figure 6-1 shows the simulated average shop temperature and the measured temperature at three different positions for two weeks in August. It has to be noted that in the model, the sales area was treated as one temperature zone, whereas in reality the temperature probably changed along horizontal and vertical directions. The vertical temperature stratification can be as much as 3.5-8 K/m [113]. Moreover, the sedum planting of the roof was neglected in the model. In the test supermarket, some thermocouples were located directly below the windows, where extremely high temperatures occurred in parts. Moreover, a measurement error of 1 K was assumed [114] for the thermocouples. Under these conditions it is difficult to

carry out a reliable validation. Despite those simplifications, the simulated temperature falls within the range of the measured temperatures. The mean average error of the simulations is shown in Table 6.1. It is below 1 K for all temperatures.

Table 6.1: MAE for the shop temperature for two weeks in August

	T Shop 1	T Shop 2	T Shop 3
MAE_{sim}	0.66	0.58	0.66

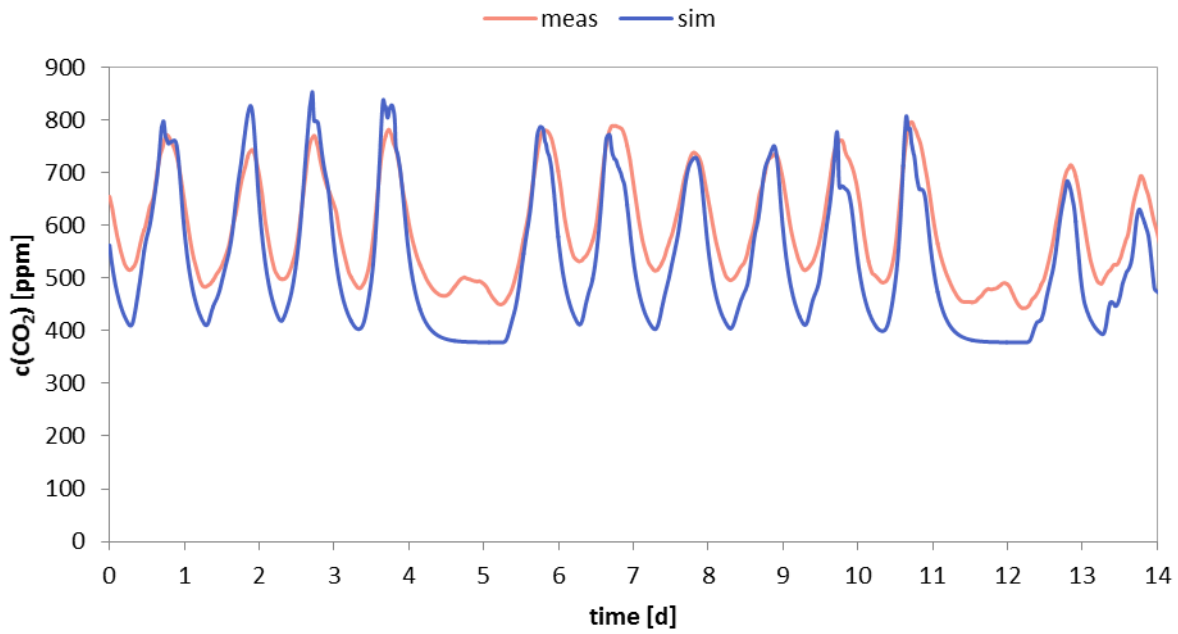

Figure 6-2: Simulated and measured CO_2 content in the shop for two weeks in January

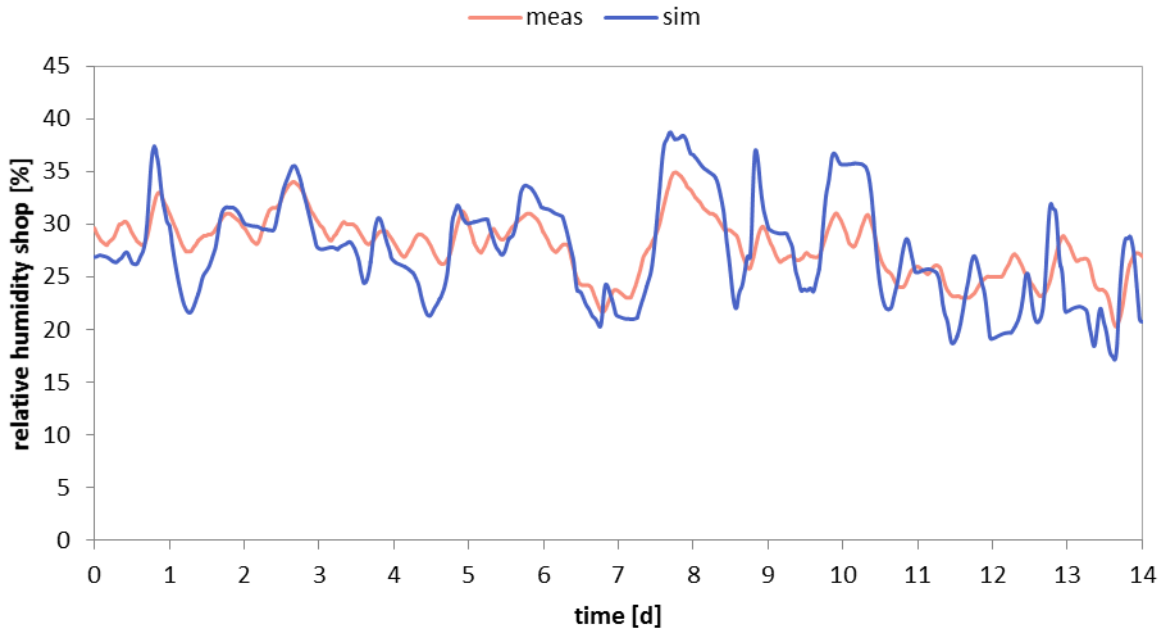

Figure 6-3: Simulated and measured relative humidity in the shop for two weeks in April

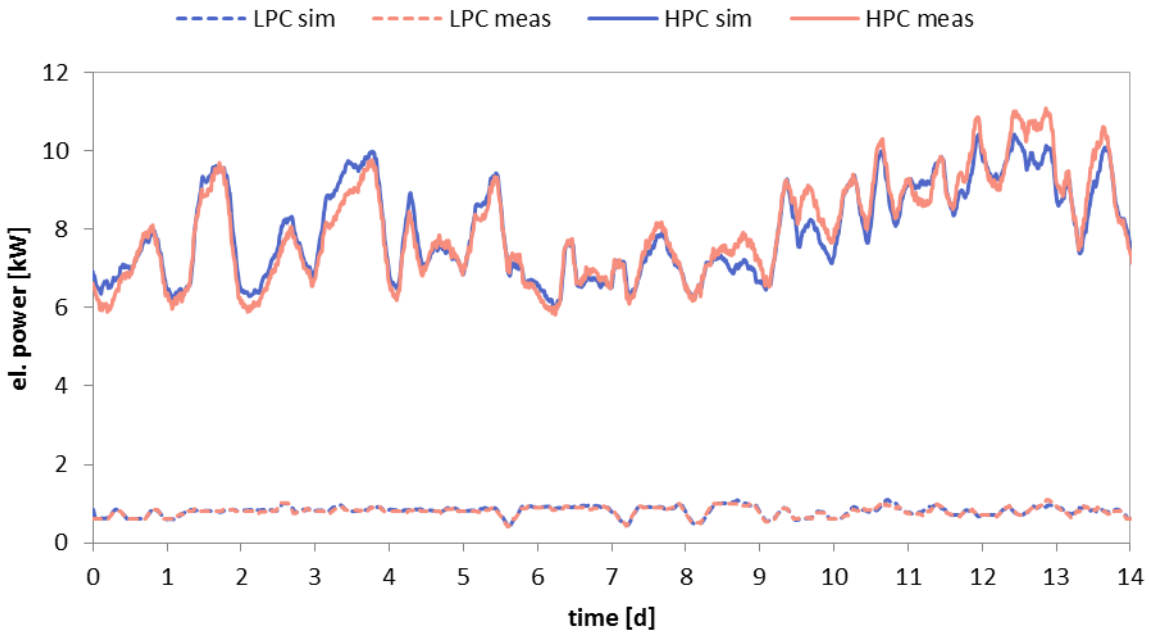

Figure 6-4: Simulated and measured compressor power cons. for two weeks in April

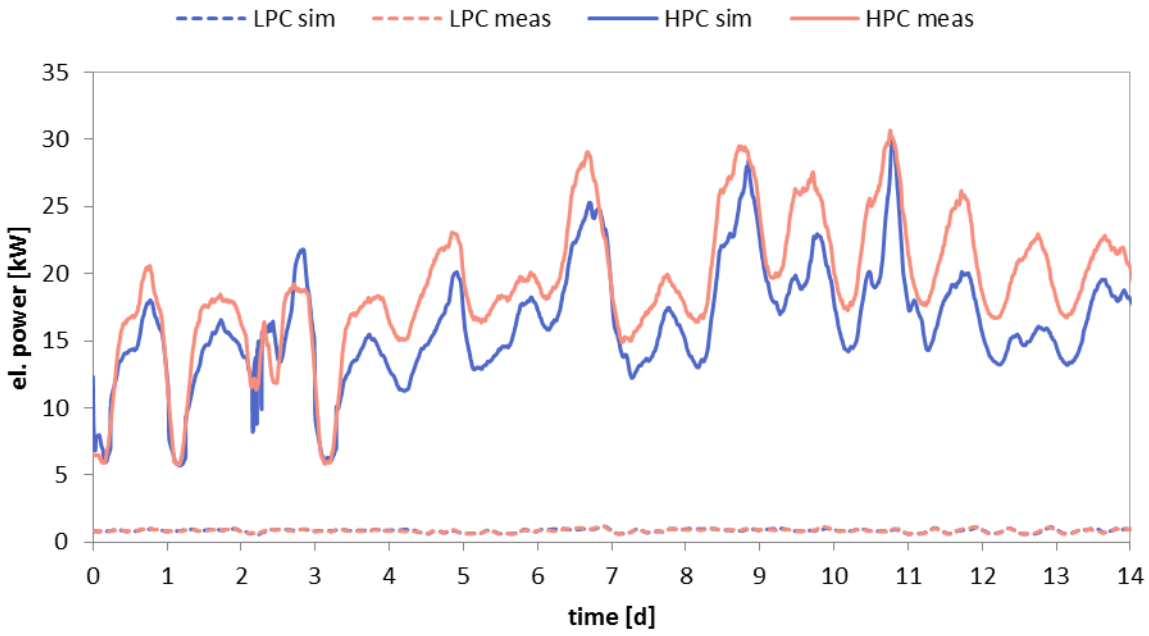

Figure 6-5: Simulated and measured compressor power cons. for two weeks in July

The CO_2 content in the sales area was a crucial factor for the control strategy. Figure 6-2 shows the measured and simulated values for the considered period in January. The course of the curves shows a good accordance. Certain deviations occurred when the CO_2 content was low. The simulated MAE is 66.71 ppm and the MAPE is 11.81 %. The CO_2 content of the ambient air was not measured and had to be assumed in the simulations. The real value was probably subject to seasonal fluctuations. This could be one reason for the deviating simulation values. Moreover, measurement errors of 2 - 3 % were assumed [115], which is equivalent to 40 - 80

ppm. Nevertheless, at high CO_2 levels the deviations are low. The dynamics of the simulated curve correspond to the measured curve.

The results for the relative humidity in the shop in April are shown in Figure 6-3. It can be seen that the values lie within the same range and the dynamic course of the curves is similar. The relative humidity probably varied in horizontal and vertical directions, dependent on the respective temperature. Moreover, the presence of moisture-increasing factors, such as people or fruits, or moisture-decreasing factors such as evaporators influenced the local values.

The measured humidity plotted was detected at the inlet of the AHU in the shop. It probably corresponds roughly to the medium shop humidity. The simulated MAE is 5.44 %, the MAPE is 11.11 %. However, the average simulated value is only 3.9 % below the measured one. The measured error was assumed to be around 2 % [116]. Another reason for the deviations could be that condensation in the AHU entrance area was neglected in the simulations.

In addition to the indoor air quality, power consumptions, mass flows and heat flows were considered to verify the assumed efficiencies and geometries in the different systems.

Table 6.2: MAE and MAPE for the compressor power consumption for two weeks in April

	el. power LP comp.	**el. power HP comp.**
MAE_{sim} [kW]	0.0322	0.2904
$MAPE_{sim}$ [%]	4.11	3.49

Table 6.3: MAE and MAPE for the compressor power consumption for two weeks in July

	el. power LP comp.	**el. power HP comp.**
MAE_{sim} [kW]	0.0397	3.0588
$MAPE_{sim}$ [%]	4.74	15.75

The curves for the power consumption of the refrigeration plant compressors are shown in Figure 6-4 for April and in Figure 6-5 for July.

MAE and MAPE of the simulations are listed in Table 6.2 and Table 6.3. The errors are within an acceptable range. The average simulated values are 2.4 % above the measured ones for the low pressure compressors and only 0.6 % for the high pressure compressors. The measurement error was assumed to be about 1 % [117].

The power consumption of the AHU fans is plotted in Figure 6-6. The simulated MAE is 2.24 kW, the MAPE is 13.78 %. It has to be repeated that the AHU is a very complex system and the power consumption is dependent on several factors, such as flap positions and fan speed. Moreover, the dynamics of the power consumptions were not measured in high resolution. The simulated total power consumption of the fans is 2.7 % above the measured power consumption for the time period in April, which is a satisfactory result.

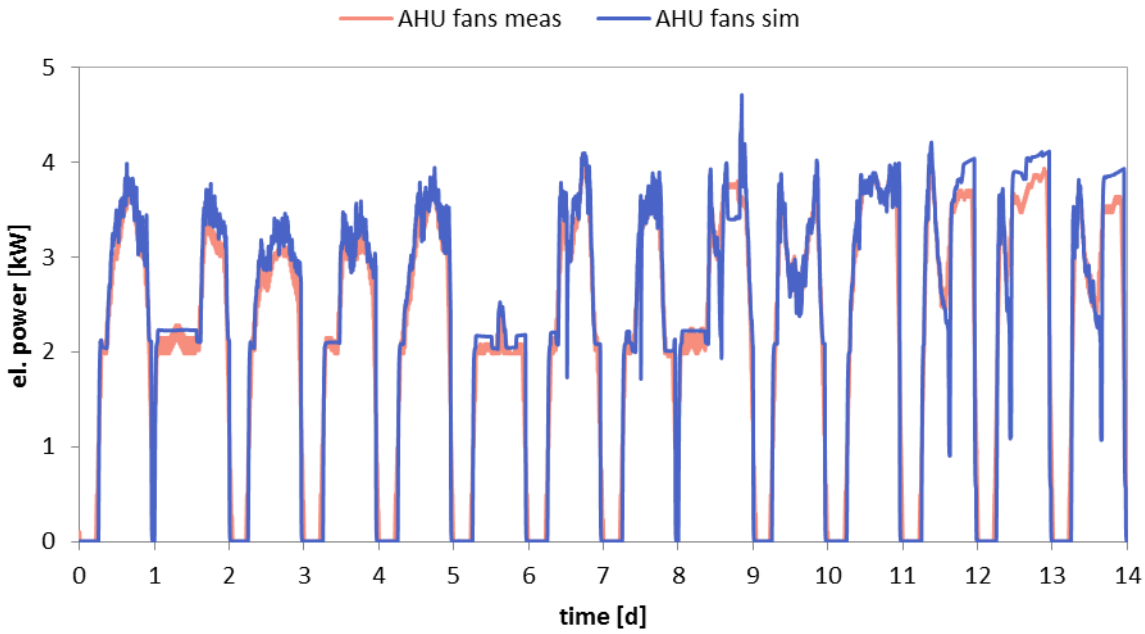

Figure 6-6: Simulated and measured AHU Fan Power Consumption for two weeks in April

Figure 6-7 shows the simulated and measured AHU exhaust air mass flow in July. The simulated MAE is 0.21 kg/s and the MAPE is 25.87 %. The high MAPE value was primarily caused by deviations in the range of very low mass flows. If the denominator of the equation converges to zero, the MAPE can easily reach extremely high values. The measurement error for the volume flow was assumed to be 2 - 3 % and was probably much higher for low volume flows. The average simulated value is only 4 % above the average measured value.

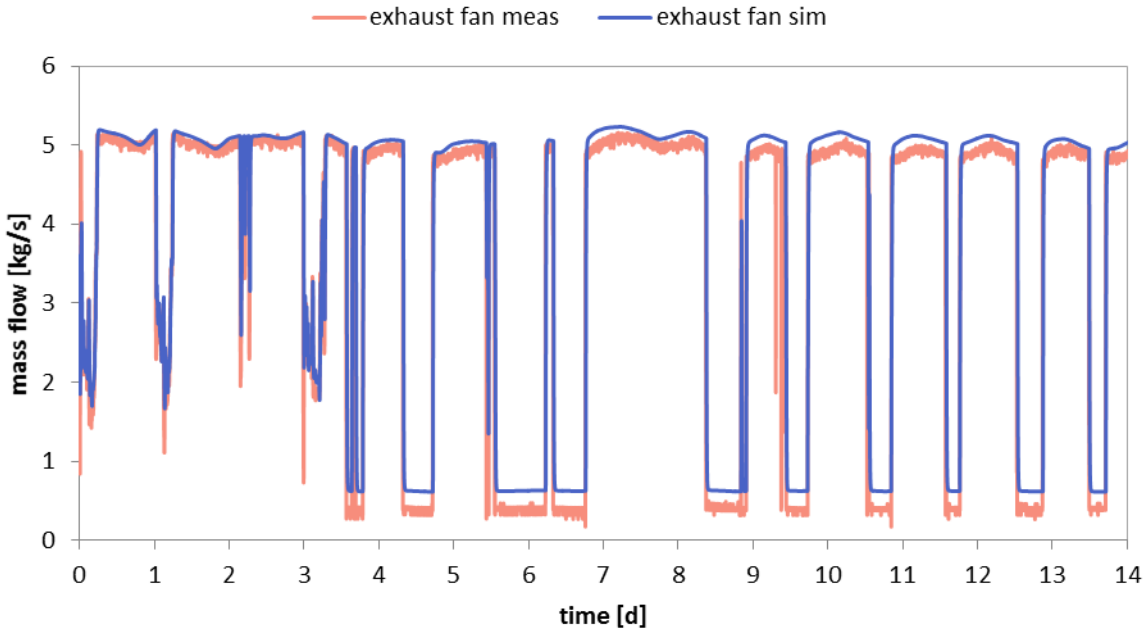

Figure 6-7: Simulated and measured AHU exhaust mass flow for two weeks in July

The results for the GC heat for April are presented in Figure 6-8 for April. The heat transferred in the gas coolers was a crucial factor as it directly influences the amount of recovered heat. The results depend on the quality of the refrigeration model and the secondary loop models, including tank, heat exchanger and floor models. MAE and MAPE for the simulations and the measurements are listed in Table 6.4. Even though the curves show a good dynamic accordance, the simulated errors are relatively high, especially for GC II. However, it has to be considered that the measurements show errors within the same range, apart from the heat flow in GC III, which is extremely high. This is due to the fact that the refrigerant return temperature of gas cooler GC I or GC II partially lays within the two-phase region. In this case, it is almost impossible to avoid high calculation errors. Nevertheless, the simulated values lie within the range of the measured ones, which suggests a well-designed model.

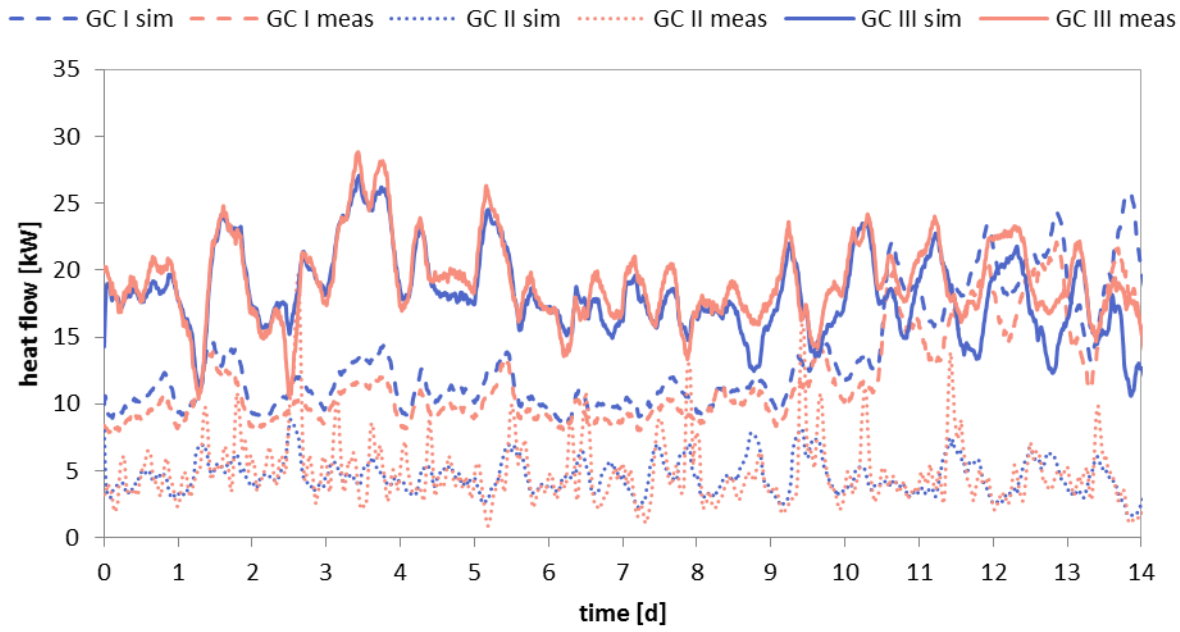

Figure 6-8: Simulated and measured gas cooler heat flow for two weeks in April

Table 6.4: MAE and MAPE for the gas cooler heat flow temperature for two weeks in April

	Heat Flow GC I	Heat Flow GC II	Heat Flow GC III
MAE_{sim} [kW]	2.0877	1.2502	1.7298
MAE_{meas} [%]	2.0437	3.0919	1.0842
$MAPE_{sim}$ [kW]	14.90	25.92	9.64
$MAPE_{meas}$ [%]	12.13	14.83	114.98

Further validation results can be found in the Appendix B.

6.3. Optimisation strategies

The heating or cooling demand in supermarkets on one hand depends on the geographical location and physical properties of the building and, on the other hand, to a large part on the type and control of the refrigeration plant and the AHU system. This influence was to be investigated in this work. The aim was to develop a smart control strategy considering the overall concept and communication between the different subsystems.

This was a challenging task, because the improvement of the control strategy for one subsystem was often accompanied by the deterioration of another system. For example, the power consumption of the HVAC system can be reduced by allowing higher shop temperatures in summer but this will also lead to higher loads to the refrigeration plant and thus to higher power consumptions of the fans. Insights from the measurements were applied and additional simulations were carried out in order to develop an optimisation strategy.

6.3.1. Investigation of heat recovery strategies

The heating demand of a building can differ considerably from the amount of available heat from the refrigeration plant. The heating demand of the supermarket depends on the ambient conditions, but also on internal loads from illumination and people. In addition, the AHU fresh air infiltration has an immense influence.

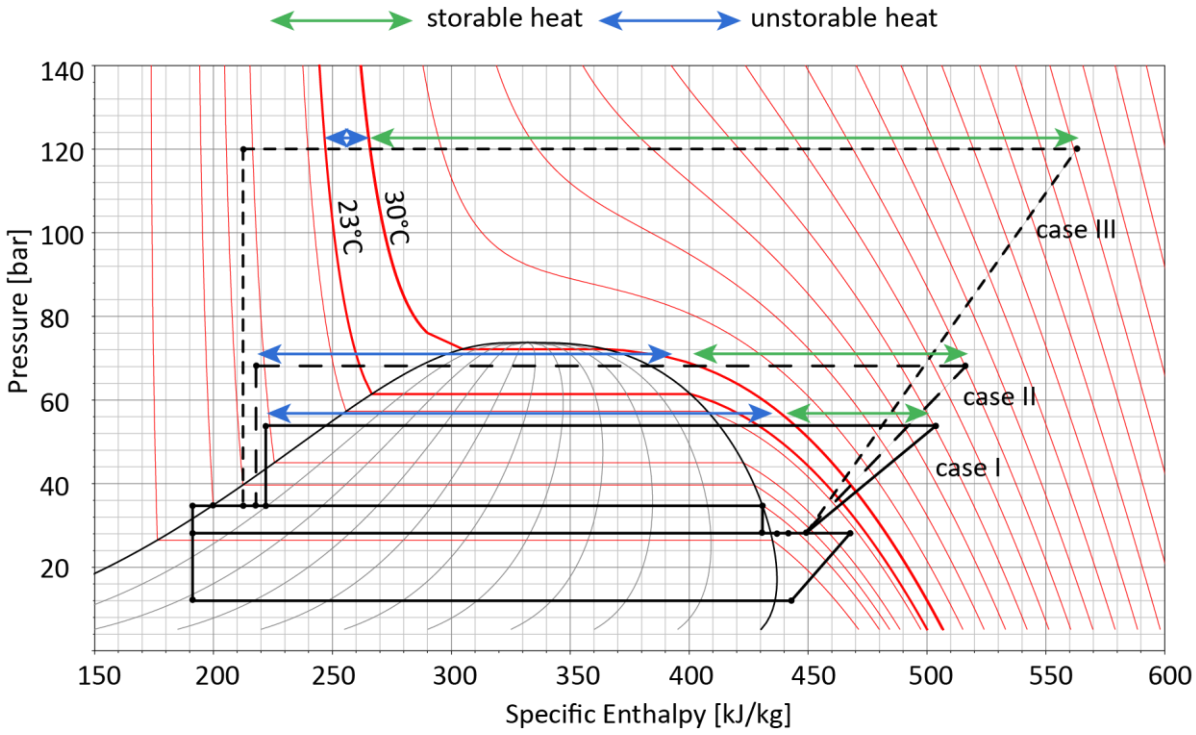

Figure 6-9: Storable and unstorable heat for different high pressure levels

The heat available from the refrigeration plant varies with the refrigeration load, which is subject to seasonal and daily fluctuations. The refrigeration load is influenced by the temperature and humidity in the sales area, as well as radiation from natural and artificial light and the air

infiltration of the cabinets. Besides this, only a part of the total waste heat can be used for heating. The amount of the usable waste heat depends on the GC II return temperature and the high pressure level of the refrigerant. The dependence of the usable waste heat on the high pressure is depicted in Figure 6-9.

Apart from the usable waste heat, the COP of the refrigeration plant varies with the high pressure. Simulations were carried out to determine the optimal refrigeration COP dependent on the refrigerant return temperature.

The following equation could be fitted for the optimum high pressure:

$$p_{COPopt} = a * T_{GCIII,ret}^{5} - b * T_{GCIII,ret}^{4} + c * T_{GCIII,ret}^{3} - d * T_{GCIII,ret}^{2} + e * T_{GCIII,ret} + f$$

(6.6)

where p is the high pressure in Pa, T is the temperature in K and a-f are parameters which are listed in Table 6.5. The pressure p_{COPopt} ensures the optimal COP if only refrigeration is considered. This pressure is not the optimal solution, if heat recovery is required.

Table 6.5: Parameters for the high pressure function

Parameter	a	b	c	d	e	f
Value	0.2513	376.77	225711.47	67534698.12	10092418238.25	602622154228.91

Different functions have been developed for the optimal refrigeration high pressure in transcritical CO_2 systems [69], [75], [118], [119], [120], [121] , [122]. The deviations of the different investigations might be attributed to differences in size and construction of the refrigeration plants. In many cases, the high pressure was calculated as a function of the ambient air temperature. In the test supermarket, the ambient temperature has a limited influence on the performance of the refrigeration plant, due to the complexity of the heat recovery system. Thus, the GC III refrigerant return temperature was chosen as a reference value.

Figure 6-9 shows the log p, H-Diagram of the refrigeration plant for three different high pressures. For initial considerations, it was assumed that, in the case of full heat recovery, the GC I refrigerant return temperature is around 30 °C and the GC II refrigerant return temperature is around 23°C. The intersection with the high pressure isobaric indicates the amount of usable waste heat. If the high pressure is low (case I), the refrigeration COP of the system is high, but only around 10 % of the waste heat can be used. Around 70 % of the usable waste heat is transferred to GC I and can consequently be stored in the tanks. This case is useful if the heating demand is low and the tank temperatures are high. Raising the high pressure up to 68 % (case II) leads to a considerable increase of the usable waste heat because the condensing pressure is above the GC II return temperature. Consequently, the entire condensing heat can

be transferred to GC II and used in the floor heating cycle. This case is the preferred case if heating is required. The increase of compressor power compared to case I is extremely low compared to the increase of the usable waste heat. Nevertheless, it has to be noted that only around 40 % of the usable heat can be stored in the tanks. The remaining 60 % have to be used immediately, otherwise they are lost. In case III, the high pressure is 120 bar and around 90 % of available waste heat can then be stored in the tanks. This case should be applied if the heating demand of the building varies quickly and the tank temperatures are low.

Additionally, there is the opportunity to increase the refrigeration load by using the extra evaporator (see Figure 4-2).

In order to compare different high pressure cases, the COP of the additional usable waste heat was defined as the extra usable heat gained by raising the high pressure divided by the extra power consumption of the fans compared to the base case. The base case was defined as the case with the optimal refrigeration COP [123].

$$COP_{AUWH} = \frac{\dot{Q}_{usable} - \dot{Q}_{usable,BC}}{P_{comp.ref.} - P_{comp.ref.,BC}} \quad \textbf{(6.7)}$$

Simulations were carried out during one winter day as an example scenario. The COP_{AUWH} was determined for five cases that differ in high pressure, the use of the extra evaporator and the use of GC III. The cases are listed in Table 6.6.

Table 6.6: Different refrigeration plant control cases

case	a	b	c	d	e	f
high pressure [bar]	P_{COPopt}	68	68	120	120	120
extra evaporator	bypassed	bypassed	used	bypassed	used	used
GC III	used	used	used	used	used	bypassed

Case a was the base case where the high pressure was controlled in order to gain the optimal COP. In case f, GC III was bypassed in order to avoid heat losses to the borehole heat exchanger cycle.

Figure 6-10 shows the average COP_{AUWH} for the different cases. The amount of usable waste heat is plotted in Figure 6-12. The highest COP_{AUWH} was achieved in case b, where the high pressure was raised slightly above the GC II return temperature. The low pressure increase of about 18 bar led to a multiplication of the usable waste heat by the factor 5 approximately. Further pressure increase caused a lower increase of the usable waste heat, as the 23°C isotherm runs very steep in the area to the left of the two-phase region (see Figure 6-11). In comparison, the increase of the power consumption was relatively high. The use of the extra evaporator led to a considerable increase of the COP_{AUWH}, especially at 68 bar high pressure.

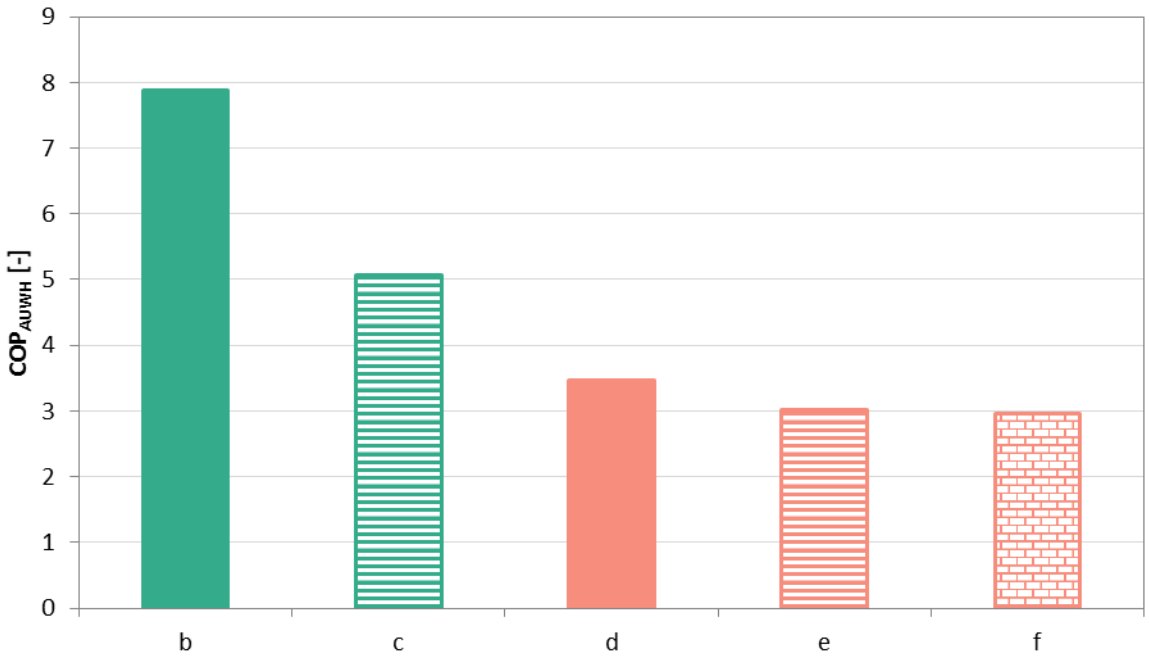

Figure 6-10: COP additional heat **[124]**

Consequently, in the case of heating demand, the pressure should be raised above the condensing pressure of the GC II return temperature. If this heat is not sufficient, the extra evaporator should be used. Extremely high pressures should be avoided.

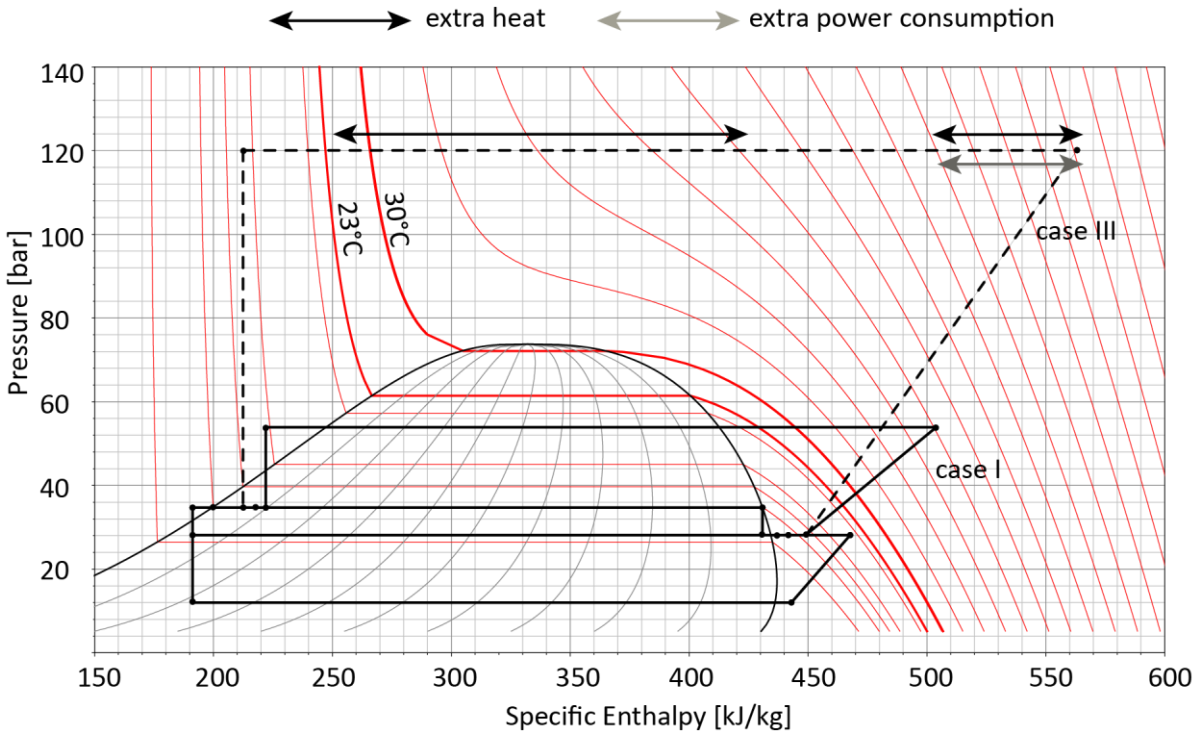

Figure 6-11: Additional heat/ power consumption for high pressure variation **[124]**

For the development of a control strategy, the relation between the available heat and the heating demand of the building has to be considered. The heating demand is depicted in Figure 6-12 for the example day. The COP_{AUWH} can only be used as a benchmark if all the available

waste heat is recovered. In case c, for example, the COP_{AUWH} is high, but the available heat exceeds the heating demand.

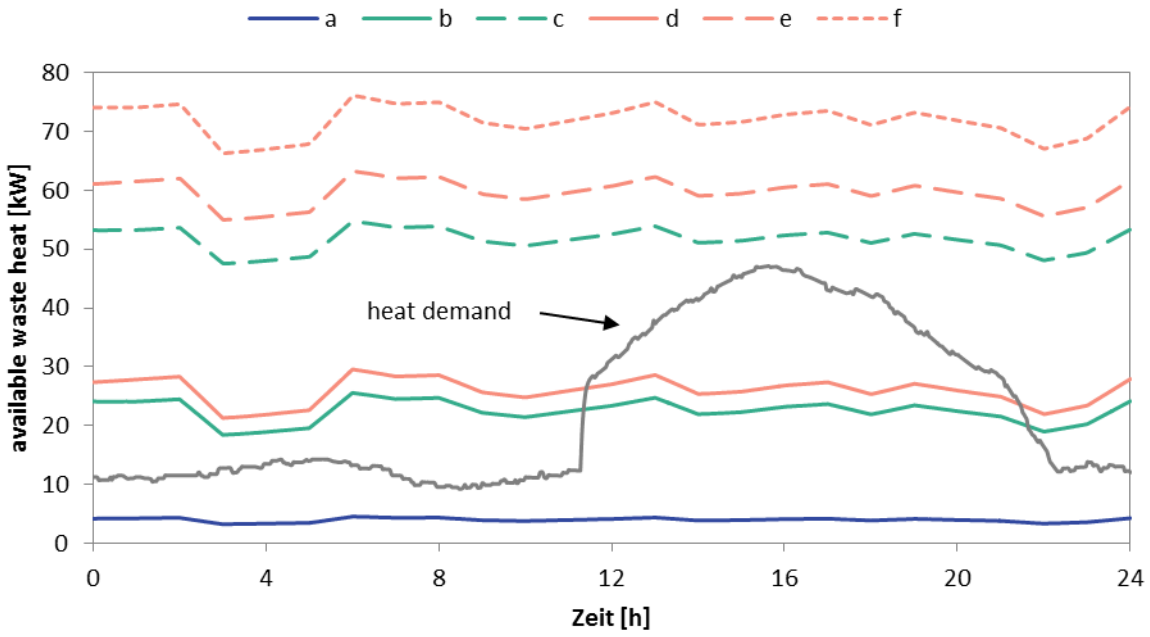

Figure 6-12: Available waste heat

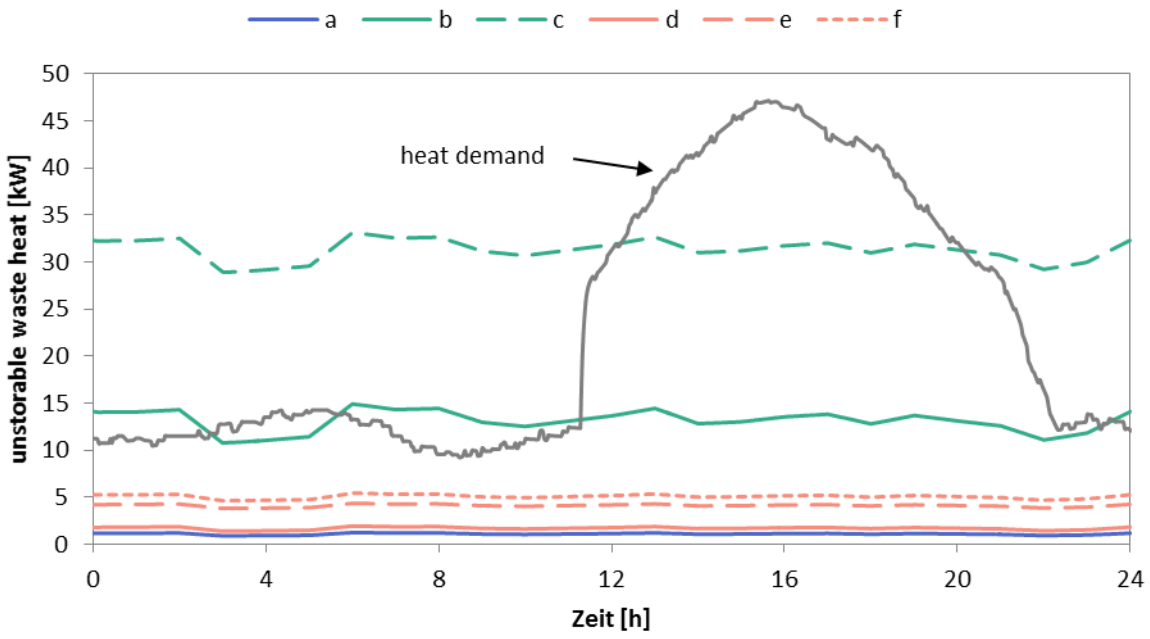

Figure 6-13: "Unstorable" waste heat

A high heat supply can be advantageous if the tanks are empty and can be filled with the surplus heat. One possibility is to run this mode until the tanks are filled and return to the optimal COP mode afterwards. The prerequisite for making this strategy suitable is that the surplus heat is storable, which means that it can be extracted in GC I. As mentioned above, the share of the available heat that cannot be stored has to be used immediately in the floor

heating loops, otherwise it is lost. The amount of “unstorable” heat is shown in Figure 6-13. Further on, the building's heating demand is plotted. It can be seen that in case c, the amount of “unstorable” heat is two to three times higher than the heating demand for about 80 % of the time. This indicates that the extra evaporator should only be used when the actual heating demand is high. If the aim is to fill up the storage tanks, a high pressure increase should be favoured.

In case b, the section of “unstorable” heat primarily lies within the range of the heating demand, with the exception of the period between 12:00 and 23:00. Between 23:00 and 12:00, the tanks can be filled with the surplus heat (see Figure 6-12). The stored heat can be used between 12:00 and 23:00, where the overall available waste heat is below the heating demand.

This example scenario illustrates the importance of an adjusted control strategy to cover the heating demand with minimal effort. The course of the heating demand is subject to daily fluctuations. The heating demand and the available waste heat are highly dynamic values which depend on a plurality of factors that are hard to predict. An overall control strategy was developed, considering the interfaces between the different subsystems.

6.3.2. Control strategy

Based on the insights from the evaluation of the measurement data and the accomplished simulations, a control strategy was developed. The control strategy was tested in simulations. The simulation results are presented and discussed in 6.4.

As described in the previous chapter, heat storage is crucial in the development of a heat recovery strategy. In the test supermarket, heat storage in three stratified storage tanks is possible. In addition, the thermal capacity of the floor has to be taken into account, as it leads to a notable delay in the floor heating system. The floor heating loops make it possible to use a high share of waste heat. Liquid return temperatures of 22°C or less can be reached in the floor heating loops, while the return temperature of the AHU unit is usually around 30 - 35°C.

The heating demand of the building was defined as a central value for the control strategy. The main goal of the investigations was to satisfy the heating demand with minimum overall power consumption.

It was assumed that the heating demand directly correlates with the temperature level in the storage tanks. The tank temperatures are dependent on the available heat from the refrigeration system and the heating demand of the building. The refrigeration system was controlled in order to reach the optimal COP if the average temperature in the tanks exceeded a limit temperature. This means that the high pressure is kept as low as possible depending on the GC III return temperature, meaning this temperature has to be kept as low as possible. In the test supermarket, the gas cooler return temperature depends on the heat flow of all three gas

coolers. The first gas cooler is connected to the storage tanks and gas cooler. The position of the gas cooler poses a challenge (see Figure 4-2): on the one hand, as much heat as possible should be rejected from the refrigeration plant in order to achieve low refrigerant return temperatures; on the other hand, if the available waste heat is rejected by the DC, it is not available in the floor heating loops. Consequently, the dry cooler was controlled dependent on the floor heating cycle. A variable DC liquid return temperature was set. When the floor heating loops were on, the return temperature was set to a higher value, whereas the return temperature was lowered when the floor heating was off. With this control strategy, heat was only rejected by the DC if it was not used in the FH loops. To reduce the power consumption of the pumps in the tank cycle, the mass flow was controlled according to the GC liquid return temperature.

The refrigeration waste heat at a lower temperature level can be used in the floor heating cycle. There is no possibility of storing this heat, which means that it is lost when the floor heating loops are off. Thus, floor heating was preferred over AHU heating. The AHU was used when floor heating was not sufficient. Moreover, it was used to compensate the large time constants of the floor heating system. Due to the high thermal mass of the floor, it was not possible to avoid simultaneous heating by the FH and cooling by the AHU during some periods. The snow melt loops were used to reject as much heat as possible. The mass flow in the SM loops was controlled according to the liquid return temperature.

A similar control strategy was chosen for the pumps in the BHX cycle. The mass flow was controlled according to the liquid return temperature of the gas cooler after mixing with the fluid returning from the AHU coil. Thus, the maximum heat could be extracted or supplied by the BHX while the mass flow was kept low. The mass flow into the cool coil was controlled by the preceding valve.

Giving preference to the FH loops over the AHU has the additional advantage that the AHU fan speed can be reduced. The aim of the AHU control strategy was to supply the required heating or cooling at minimum power consumption of the fans. Another goal was to reduce the heating demand in the AHXH to avoid the emptying of the storage tanks. This can be achieved by using the rotary wheel, which has an efficiency of about 70 %. Using it leads to an immense reduction of the heating demand, but causes high pressure drops in the wheel. Moreover, the exhaust air has to be filtered before entering the wheel. If the wheel is off, the filter can be bypassed. The use of the filter causes an additional pressure drop. If the wheel is avoided, the power consumption of the fans is low, but high heating demands can occur. This can be advantageous if much waste heat is available. In this case, a high heating demand leads to an improvement of the refrigeration COP. However, if not enough waste heat is available, the refrigeration plant is forced to run in a less efficient mode in order to supply the required heat. It is obvious that both objectives, low fan speed and low heating demand, are contra-

dictory. A compromise had to be found: the rotary wheel was only used if the tank temperature was below a limit value and the rotary wheel capacity was controlled according to the AHU supply temperature set point in order to avoid that the wheel return temperature on the supply air side exceeds the supply air temperature set point. The AHU supply air temperature was controlled by a cascade control system and the set point for the supply air temperature was determined dependent on the shop temperature.

Furthermore, the overall pressure drop in the AHU was reduced. The main pressure drops occur in the filters, the rotary wheel and the heating and cooling heat exchangers. These components were bypassed whenever they were not needed. The supply air fan was controlled according to the shop temperature. When the heating or cooling demand was high, the supply fan flow was increased. The amount of ambient air supply was determined by the exhaust air fan and controlled through the CO_2 content in the sales area air. The maximum CO_2 content was set to 800 ppm, which provides a good indoor air quality [26], [125]. When cooling was required in the shop, ambient air cooling was preferred, which has the advantage of lowering the CO_2 content in the shop. If ambient air cooling was not sufficient, the AHXC was used. Two modifications were investigated: summer mode and winter mode (see Figure 5-10). In winter mode, the AHXC was directly connected to the BHX and the evaporator could not be used. In summer mode, the AHXC was connected to the EE. This led to a lower AHXC supply temperature, but also to a lower mass flow due to a higher pressure drop caused by the evaporator. In this case, the evaporator was controlled from the refrigeration plant side. At moderate shop temperatures, the orifice valve in front of the evaporator in the refrigeration plant was closed. Despite this, the liquid in the BHX cycle had to pass the EE before entering the AHXC. This leads to a lower cooling capacity of the AHXC compared to the winter mode, due to lower mass flow and equal supply temperatures on the liquid side. The evaporator was only used if the shop temperature exceeded a limit temperature.

The control of the refrigeration plant was realised in a way to efficiently provide or reject the required amount of heat for space heating or cooling. As mentioned above, the storage tanks were used as an indicator for the heating demand of the building. If the average temperature in the tanks was above a limit value, the high pressure was controlled in a way to achieve the optimal refrigeration COP (see 6.3.1). Below this tank limit temperature, measures had to be taken to fill the tanks. The first measure was a high pressure increase. The high pressure was set to two bars above the GC II return temperature condensing pressure. Consequently, the entire condensing heat could be recovered. The extra evaporator was used when this heat was not sufficient.

In the test supermarket, about 50 % of the refrigeration load was provided by plug-in cabinets. Plug-in cabinets are usually less efficient than remote refrigeration and their entire waste heat is rejected into the sales area at all times. Consequently, the heat loads to the building are high and the application of a control strategy is likely to have a limited effect. Moreover, this

leads to a high cooling demand in summer, which is why the replacement of the plug-in cabinets by remote refrigeration was investigated. The performance of the plug-in cabinets could not be determined through measurement data. A COP of 2.6 was assumed for the medium temperature integrals and a COP of 1.4 for the low temperature integrals. Additionally, the effect of more efficient illumination on the overall power consumption was investigated. It was assumed that the replacement of fluorescent tubes with LEDs would lead to power savings of 30 % for illumination.

6.3.3. Tested strategies

The control and rebuilding strategies described in the previous chapter were investigated with simulations of the validated models. Two cases and the base case were simulated. The base case was according to the test supermarket in terms of the technical equipment and the control strategy. In case a, the technical equipment was equivalent to the base case, but the adjusted control strategy described in 6.3.2 was applied. During very hot summer time, it was distinguished between case a WM and case a SM. In case a WM, the refrigeration plant was never used for air conditioning purposes. In case a SM, the refrigeration plant was used for air conditioning, if the temperature in the sales area was above 24°C. In case b, the control strategy described in 6.3.2 was applied. Additionally, the plug-in cabinets where replaced by the remote refrigeration system and it was assumed that the illumination costs could be decreased by 30 % by using more efficient illumination (LEDs). The investigated cases are summarised in Table 6.7.

Table 6.7: Description of the optimisation cases

case	Description
Base case	Application of the original control strategy; partly usage of refrigeration plant for air conditioning; no structural measures
Case a/ case a WM	Application of the adjusted control strategy (for a detailed description see 6.3.2); no usage of refrigeration plant for air conditioning; no structural measures
Case a SM	Application of the adjusted control strategy (for a detailed description see 6.3.2); usage of refrigeration plant for air conditioning; no structural measures
Case b	Application of the adjusted control strategy (for a detailed description see 6.3.2); no usage of refrigeration plant for air conditioning; Replacement of plug-in cabinets by refrigeration plant; reduction of electrical consumption for illumination by 30 %

6.4. Results

The overall supermarket was modelled in a very detailed model, which led to long simulation times (see 6.1). Thus, only crucial seasons were simulated and assumptions for the missing

periods were extrapolated. One winter period (January), one transition time period (April) and two summer periods (June/ August) were simulated. The June period was a very hot period, whereas the August period was a moderate summer month. The developed control strategy was tested for all periods with and without modifications of the system.

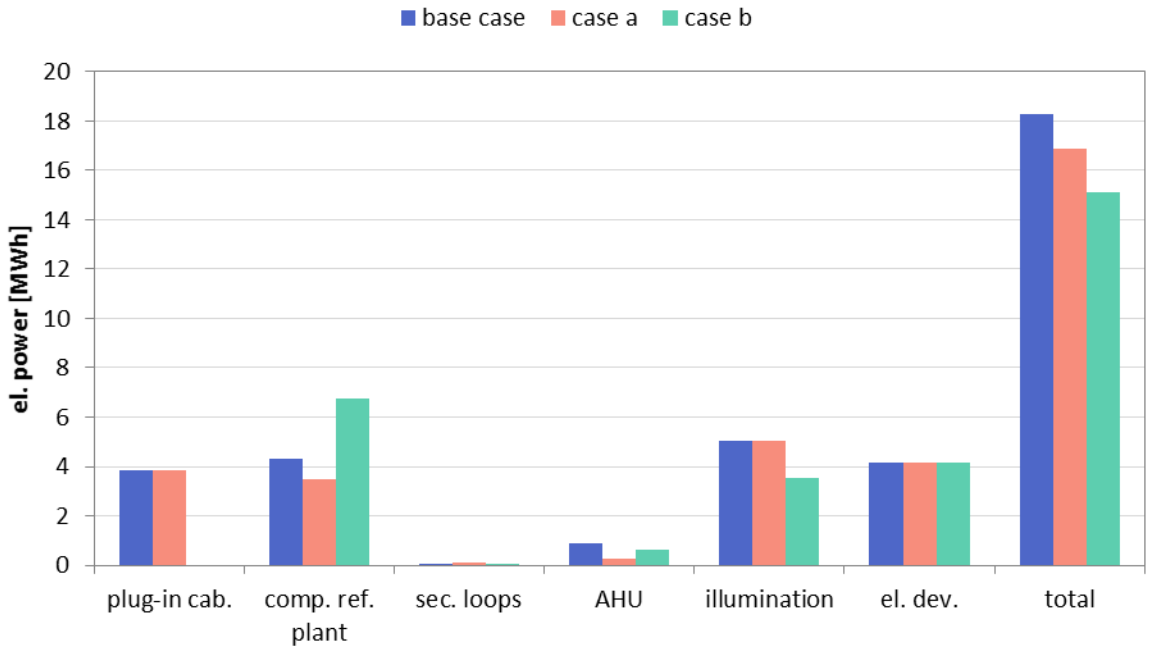

Figure 6-14: Simulation results for different control strategies in January (cases: see 6.3.3)

The main task of the simulations was to analyse the saving potential of the developed strategies. The saving potential of the subsystems and the overall system was determined. The savings were correlated with the overall power consumption of the base case. The validated simulations of the original case from 2014 were defined as the base case:

$$S_{subs.} = \frac{P_{subs.,BC} - P_{subs.}}{P_{total,BC}} \quad \textbf{(6.8)}$$

Whereas $S_{subs.}$ is the saving for each subsystem in %, $P_{subs.}$ is the power consumption of the subsystem in the respective case and $P_{subs.}$ in the base case. $P_{total,BC}$ is the power consumption of the whole supermarket. This evaluation was used in order to assess the impact of the applied measure on the overall system.

The simulation power consumptions for the January period are shown in Figure 6-14. The savings are listed in Table 6.8. According to the results, the application of the developed control strategy (case a) led to a total energy reduction of 7.55 % in January. The savings were mainly achieved due to the refrigeration plant, with 4.48 %, and the AHU unit, with 3.32 %. The total saving potential would be more than twice as high if additional modifications were undertaken. As can be seen in Table 6.8, the main savings in this case could be achieved by improving the illumination. Moreover, the replacement of the plug-in cabinets led to savings

of 7.77 %. These measures caused a considerable reduction of the heat load. This heat had to be replaced by heat recovery.

Table 6.8: Savings* for the optimisation strategies for January (cases: see 6.3.3)

		plug-in cab.	comp. ref. plant	ref. total	sec. loops	AHU	illuminat-ion	total
case a	%	0.00	-4.48	-4.48	0.25	-3.32	0.00	-7.55
	kWh/day	0.00	-48.11	-48.11	2.70	-35.72	0.00	-81.13
case b	%	-21.00	13.23	-7.77	0.06	-1.25	-8.24	-17.19
	kWh/day	-225.66	142.17	-83.48	0.67	-13.42	-88.56	-184.79

Consequently, the high pressure in the refrigeration plant had to be raised during some periods. Despite the higher heating demand, using the extra evaporator was not necessary. The course and the average values of the total power savings are represented in Figure 6-15, which shows that in certain periods the savings were around zero, but clearly positive for most of the time. The average values are 3.4 kW for case a and 7.7 kW for case b.

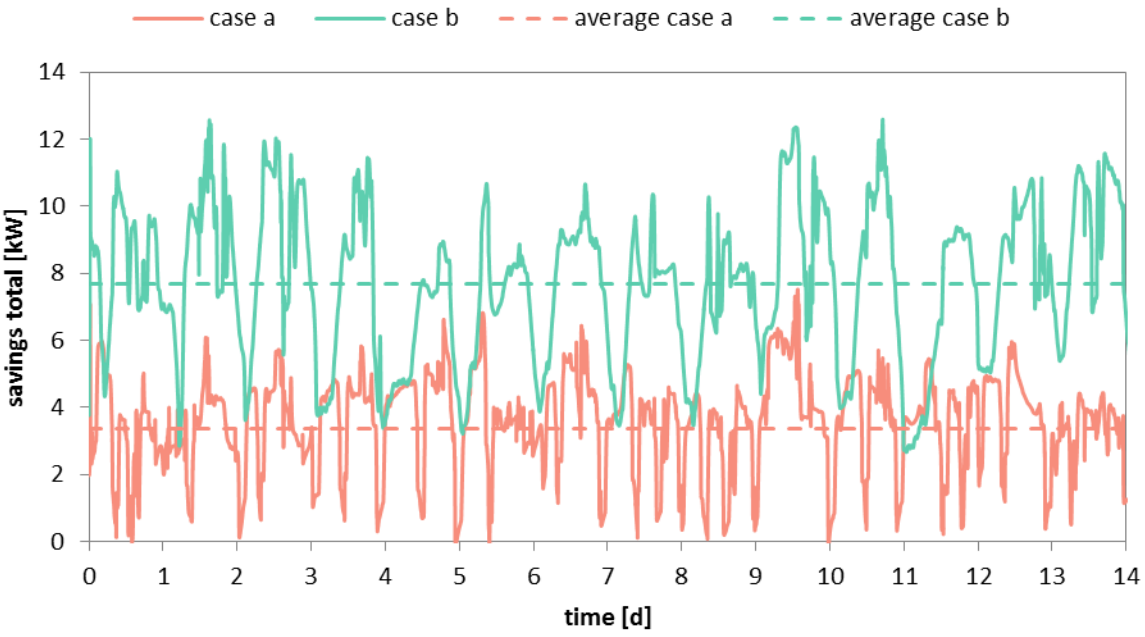

Figure 6-15: Total power savings in January (cases: see 6.3.3)

The main savings were achieved during daytime. It is likely that the saving potential was to a large part determined by the power consumption of the AHU. During cold periods, the heat delivered by the FH loops was not sufficient, so the AHU fans ran on high speed to meet the heating demand and the recovery wheel was used in some cases, which led to an increase in

* referred to the overall energy consumption in the base case

power consumption. Furthermore, as described above, floor heating was preferred over AHU heating. Due to the slow reaction time of the FH, AHU cooling was sometimes required in order to compensate for the FH surplus heat, in particular in case a.

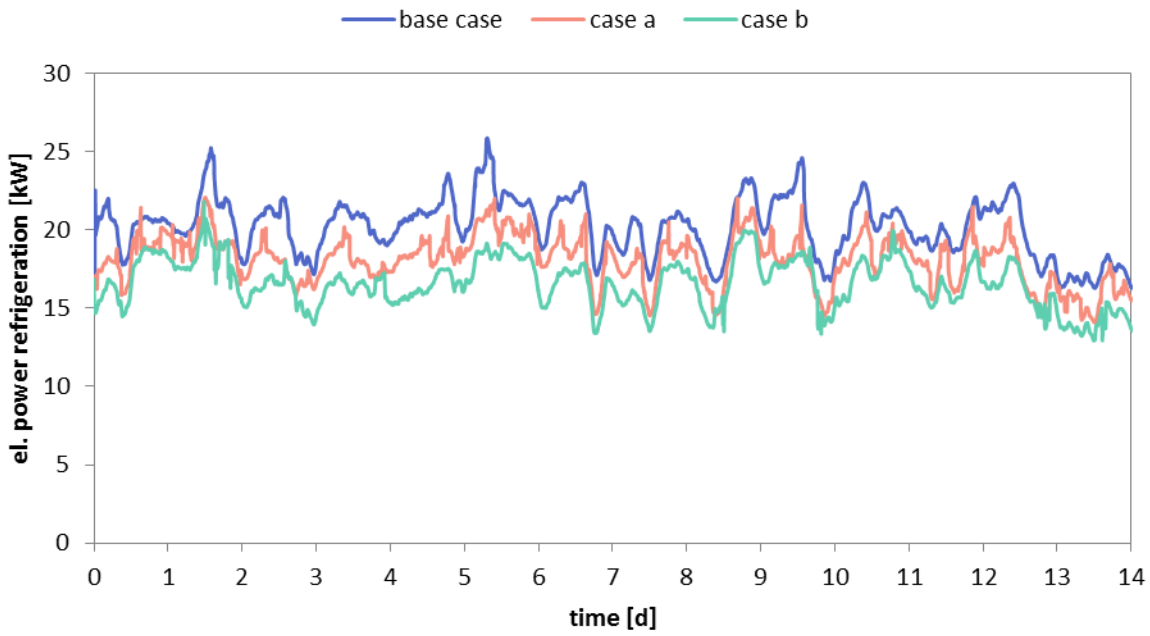

Figure 6-16: Power consumption for refrigeration in January (cases: see 6.3.3)

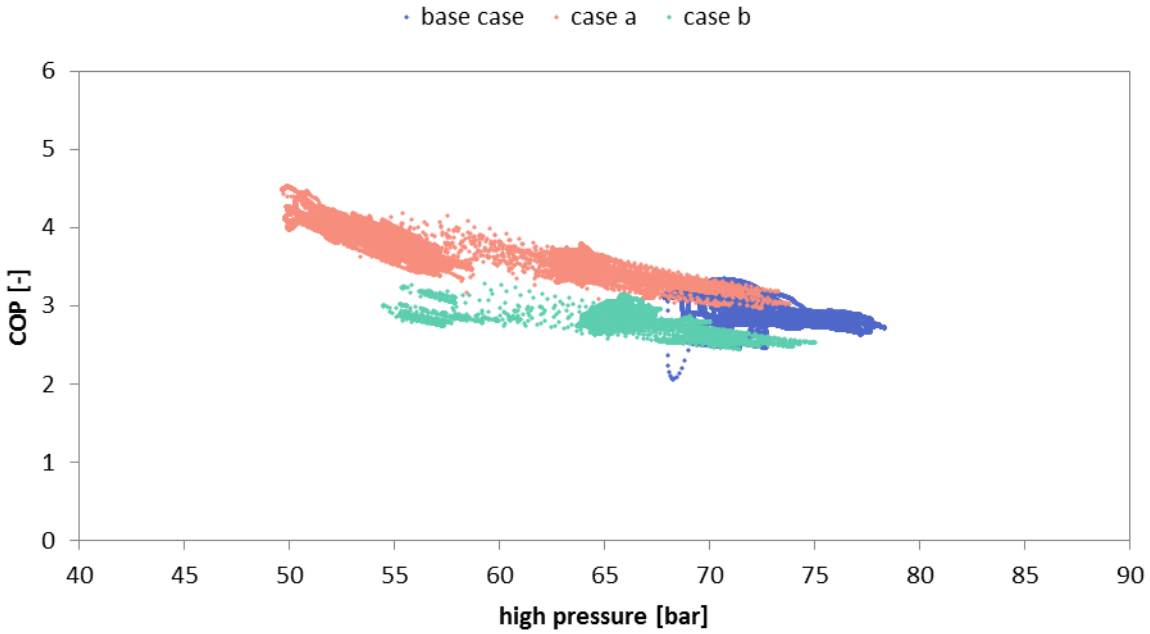

Figure 6-17: COP_{ref} for the simulated cases in January (cases: see 6.3.3)

Figure 6-16 shows the power consumption for refrigeration in all three cases. The values for case a are below the base case most of the time, although in some periods the curves converge. This was probably due to high pressure increasing to cover the building's heating de-

mand. In case b, the overall power consumption was clearly lower than in the base case. However, the average high pressure could be reduced in both cases compared to the base case. Figure 6-17 shows the COP_{ref} for the three simulated cases. Obviously, the COP_{ref} increased with decreasing high pressure. Comparing case a to the base case, it is evident that a much higher COP_{ref} could be reached by applying the control concept compared to the base case. The COP_{ref} in case b is slightly lower than in the base case. It has to be noted that the heat load to the refrigeration plant is much higher in case b compared to the other cases. the plug-in cabinets of the base case and case a were not considered in this plot. Consequently, this graph is not suitable for a comparison of case b to the other cases.

The high pressure was varied, according to the requirements, from 50 - 75 bar in case a and about 55 - 75 bar in case b, whereas in the base case the high pressure only moved within the range of 65 - 80 bar. The high pressure control in case a and b was directly dependent on the GC II return temperature. Floor heating was often used and low GC II return temperatures could be achieved. The COP in case b was below the COP in case a at the same high pressure level, which was probably due to the fact that the refrigeration load of the remote refrigeration system in case b was much higher than in case a and the base case. Additionally, the relation of freezing load to total refrigeration load was much higher in case b. It has to be noted that the plug-in cabinets, with assumed COPs of 1.4 for LT and 2.8 MT cooling, were not considered in Figure 6-17.

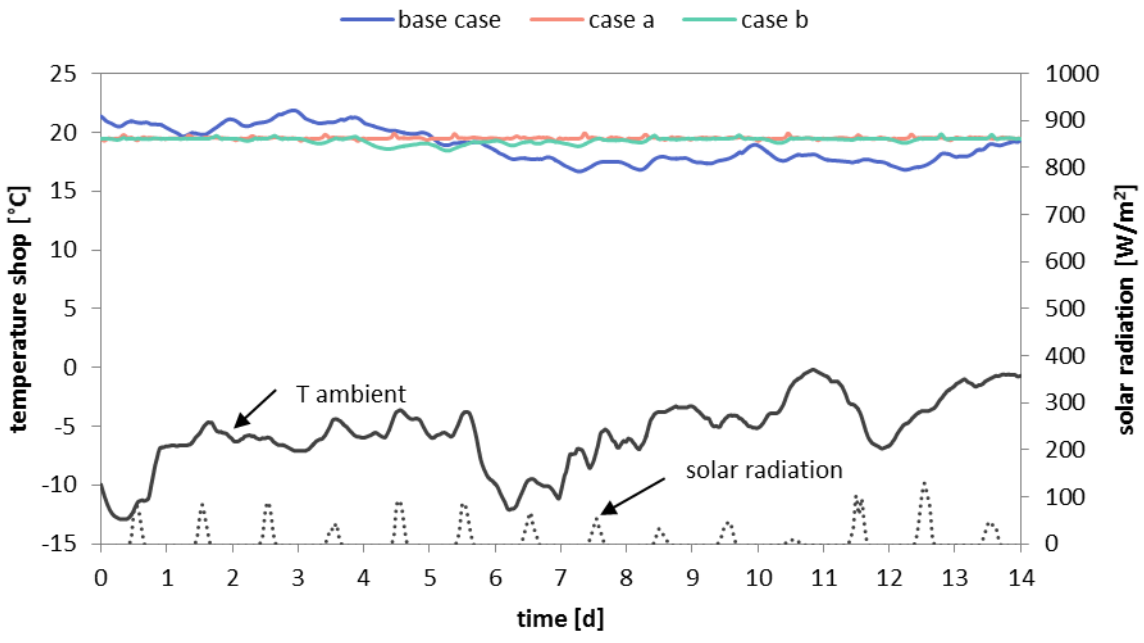

Figure 6-18: Simulation results for the shop temperature in January (cases: see 6.3.3)

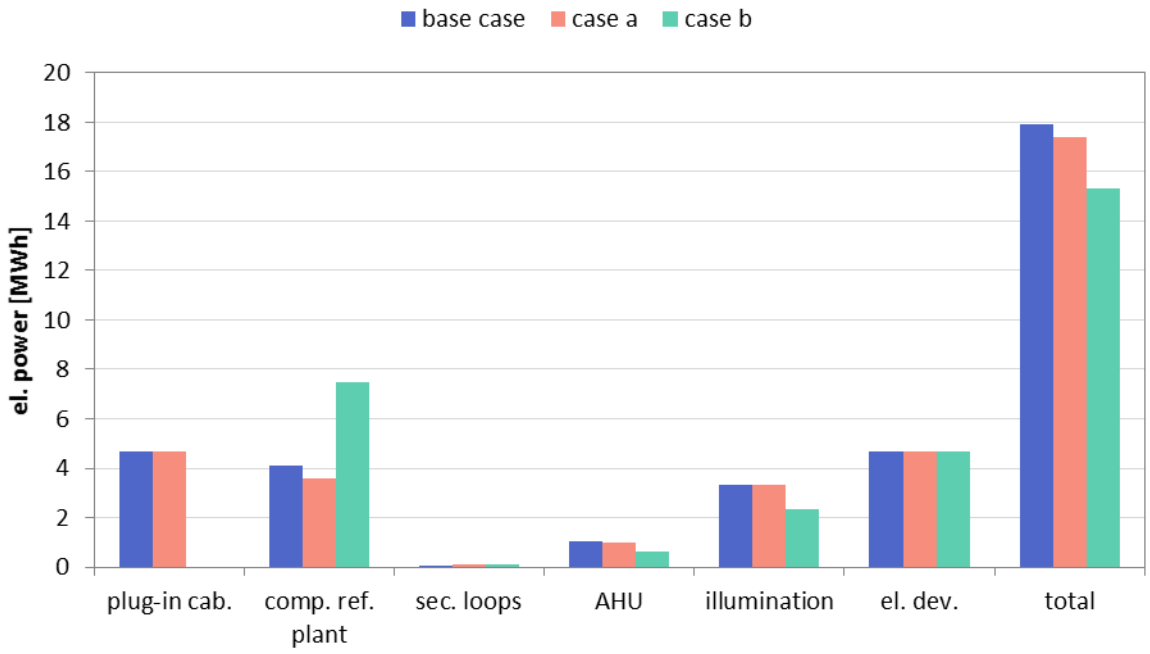

Figure 6-19: Simulation results for different control strategies in April (cases: see 6.3.3)

Figure 6-18 shows the simulated shop temperatures for the different cases in January. The ambient temperature and the solar radiation are also plotted. The shop temperature was within an acceptable range in all cases, but in cases a and b, a more exact temperature control could be achieved, mainly due to an adjusted AHU control. Nevertheless, it has to be noted that the control strategy in the test supermarket could not be transferred exactly to the simulations of the base case. The measurements showed a better shop temperature control than the simulations.

A period in April was simulated as an example of a transition month. The simulations show less saving potential than in wintertime (see Figure 6-19).

Table 6.9: Savings* for the optimisation strategies for April (cases: see 6.3.3)

		plug-in cab.	comp. ref. plant	ref. total	sec. loops	AHU	illumination	total
case a	%	0.00	-3.04	-3.04	0.59	-0.40	0.00	-2.84
	kWh/day	0.00	-28.65	-28.65	5.59	-3.73	0.00	-26.79
case b	%	-26.11	18.77	-7.34	0.62	-2.24	-5.62	-14.57
	kWh/day	-246.14	176.94	-69.20	5.86	-21.08	-52.94	-137.36

* referred to the overall energy consumption in the base case

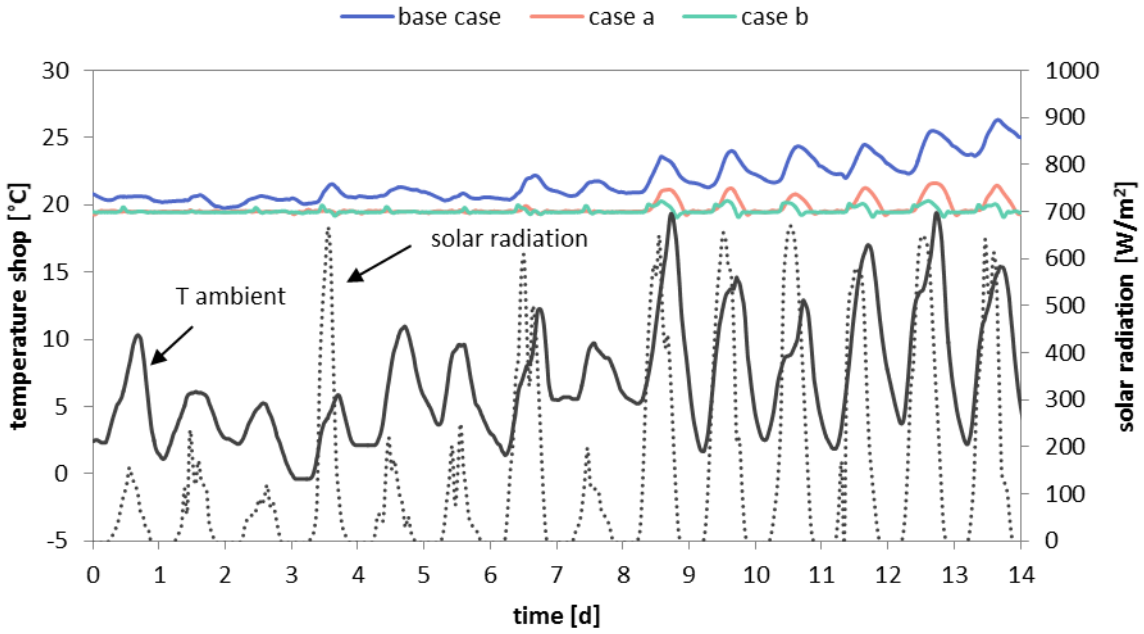

Figure 6-20: Simulation results for the shop temperature in April (cases: see 6.3.3)

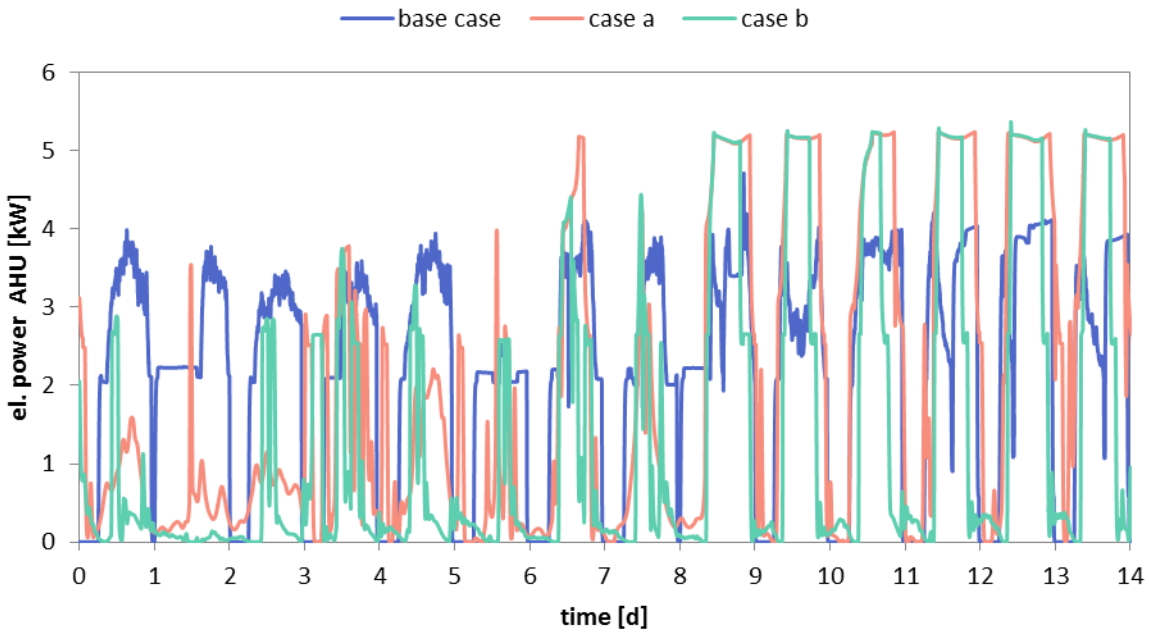

Figure 6-21: AHU power consumption for the simulated cases in April (cases: see 6.3.3)

For the application of the control system only, an improvement of 2.84 % in energy performance was predicted. By contrast, the simulations of case b gave more promising results. The overall power consumption was considerably lower than in the base case for almost all of the time. The simulations predicted power savings of 15.19 %. The savings were predominantly achieved in the refrigeration system, the illumination and the AHU. The simulated power savings are listed in Table 6.9. The saving potential of the refrigeration plant was within the same

range as in January. Figure 6-20 shows that a much better shop temperature control could be achieved in cases a and b. This was probably due to the adjusted AHU control in both cases and the reduction of the internal loads in case b. Figure 6-21 shows the power consumption of the AHU in all three cases. Even though the fan power in case a and b considerably exceeded that of the base case between days 6 and 16, the overall consumption was slightly lower compared to the base case (see Table 6.9).

However, it has to be noted that the higher fan power consumption had a direct influence on the indoor air quality. The shop temperature is plotted in Figure 6-20. In the base case, it exceeded the set point temperature of 19.5°C throughout the simulated period. Maximum deviations occurred in the second week, when the ambient temperature approached 20°C during daytime and the solar radiation achieved values above 500 W/m^2. The shop temperature in case a and especially in case b could be controlled much closer to the set point even in the second week. It is important to keep the shop temperature within the controlled range for comfort reasons. Moreover, high shop temperatures lead to a considerable increase in refrigeration load to the cabinets. The influence of the indoor air conditions on the refrigeration load was not considered in the simulations. Considering them would probably lead to the result that a further reduction of the power consumption of the refrigeration plant could be achieved. The influence of the indoor air conditions on the refrigerant load was investigated both in chapter 5.2 and in a publication by Orphelin et al. [126]. Additionally, at lower indoor air temperatures, the power consumption for the anti-sweat heater and defrost can be reduced if an adjusted control is applied [47], [127].

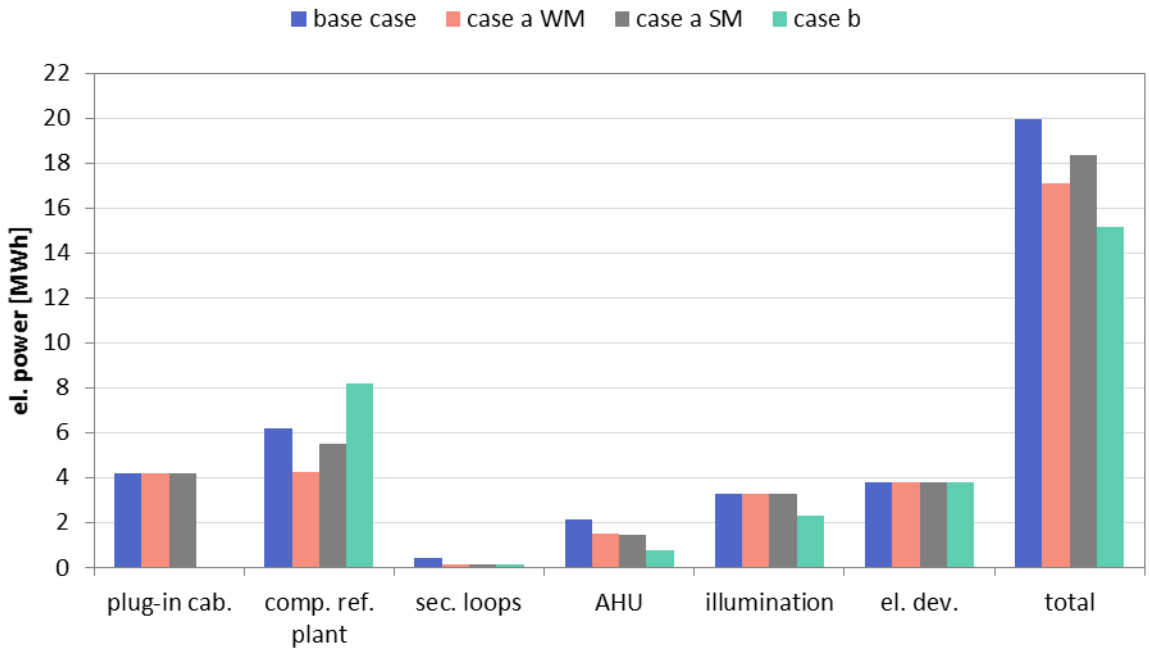

Figure 6-22: Simulation results for different control strategies in July (cases: see 6.3.3)

Table 6.10: Savings* for the optimisation strategies for July (cases: see 6.3.3)

		plug-in cab.	comp. ref. plant	ref. total	sec. loops	AHU	illumina-tion	total
case a WM	%	0.00	-9.70	-9.70	-1.37	-3.11	0.00	-14.18
	kWh/day	0.00	-128.93	-128.93	-18.24	-41.33	0.00	-188.49
case a SM	%	0.00	-3.42	-3.42	-1.24	-3.22	0.00	-7.88
	kWh/day	0.00	-45.53	-45.53	-16.42	-42.85	0.00	-104.80
case b	%	-20.98	10.02	-10.96	-1.33	-6.71	-4.94	-23.93
	kWh/day	-278.97	133.21	-145.76	-17.64	-89.15	-65.63	-318.17

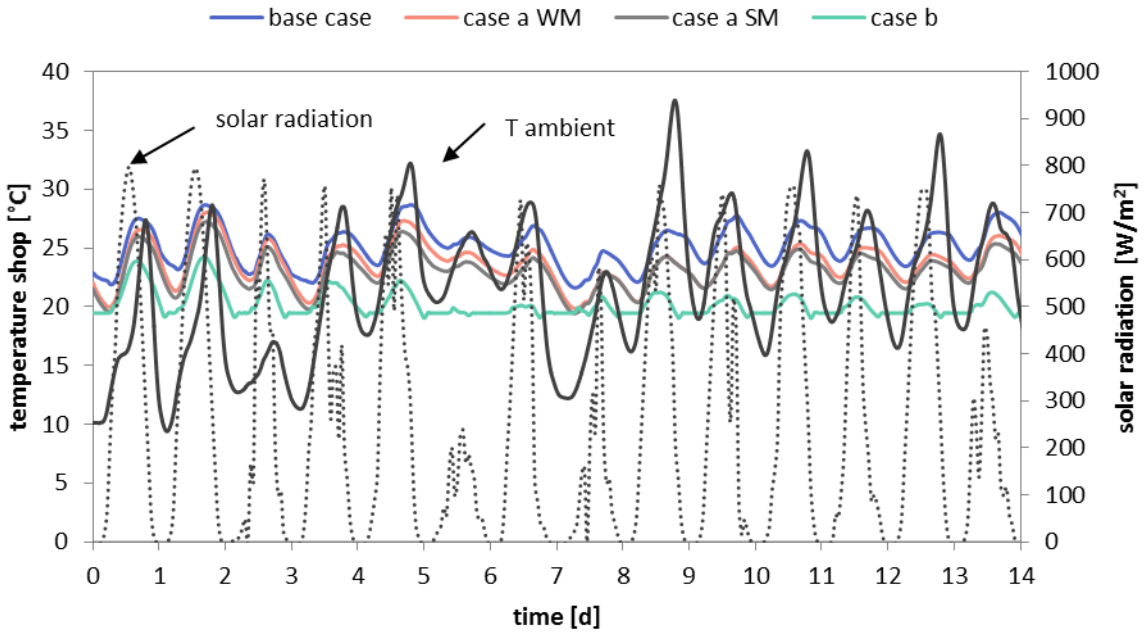

Figure 6-23: Simulation results for the shop temperature in July (cases: see 6.3.3)

The simulated power consumption in July is represented in Figure 6-22. The unique feature in this period was that the BHX cycle was set to summer mode (see Figure 5-10), which means that the liquid was cooled in the EE before entering the AHXC. The simulated cases distinguished between three cases. In case a WM and case a SM, the control system was applied. In case a WM, the BHX cycle was set to winter mode, in case a SM to summer mode. In case a SM, the evaporator was only used when the indoor air temperature exceeded a limit value of 24°C. In order to evaluate the benefits of the summer mode compared to the winter mode,

* referred to the overall energy consumption in the base case

both power consumption and room temperature were compared. Case b corresponds to case a in the other months, when the BXH cycle was set to winter mode.

The simulated saving potential (see Table 6.10) in July was 14.18 % in winter mode and only 7.88 % in summer mode. Figure 6-22 indicates that this difference in power consumption was caused by the refrigeration plant only. The benefits in case b were considerable: savings of 23.93 % could be achieved. This was mainly due to savings of the refrigeration systems, but high savings were also possible in the AHU.

Table 6.11: Savings* for the optimisation strategies for August (cases: see 6.3.3)

		plug-in cab.	comp. ref. plant	ref. total	sec. loops	AHU	illumina-tion	total
case a	%	0.00	-0.30	-0.30	0.56	-6.29	0.00	-6.03
	kWh/day	0.00	-3.27	-3.27	6.07	-67.62	0.00	-64.82
case b	%	-22.57	18.76	-3.80	0.57	-10.24	-6.30	-19.77
	kWh/day	-242.51	201.65	-40.87	6.09	-110.06	-67.65	-212.49

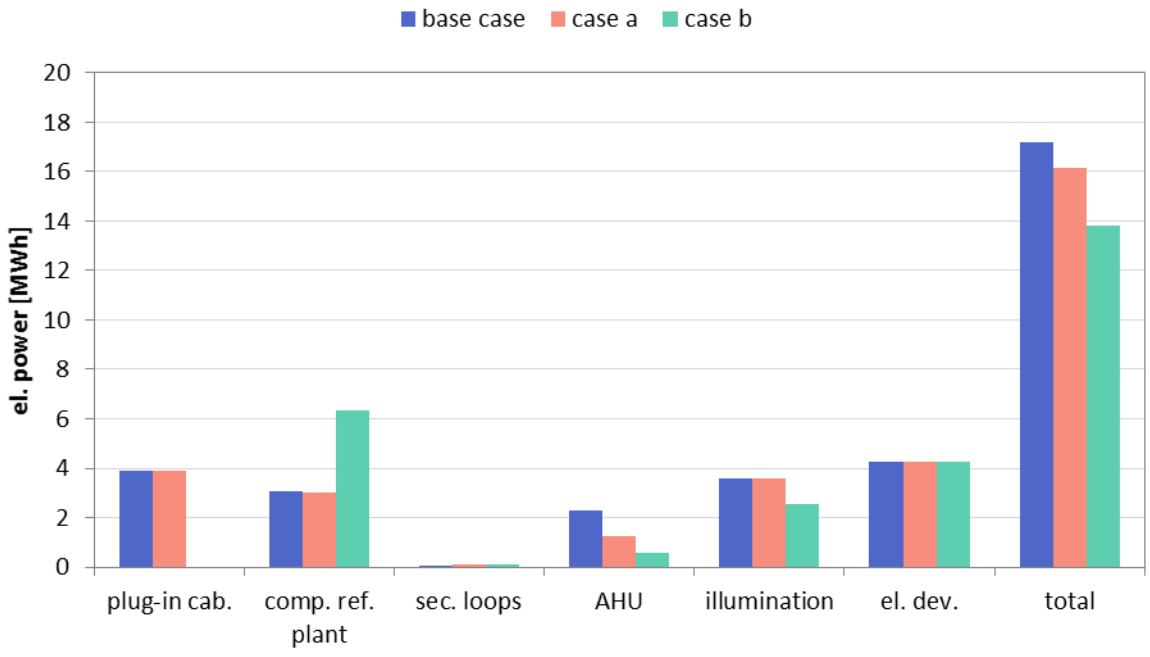

Figure 6-24: Simulation results for different control strategies in August (cases: see 6.3.3)

* referred to the overall energy consumption in the base case

The indoor air temperature, ambient temperature and solar radiation are plotted in Figure 6-23. In all three cases, an improvement of the shop temperature could be achieved. On average, the shop temperature could be reduced by 1.52°C in case a WM and by 2.07°C in case a SM. The advantage of SM over WM was only 0.55°C and hardly compensates for the extra energy consumed in case a SM. A significant improvement of the indoor air temperature could be achieved in case b: the temperature was reduced by 4.99°C compared to the base case and an average temperature of 20.19°C could be achieved. This is a satisfactory result, considering that the ambient temperature occasionally reached values clearly exceeding 30°C and the solar radiation showed maximum values of up to 800 W/m^2 on most days. As mentioned above, the indoor air quality has a direct influence on the performance of the refrigeration plant. These simulations show that there are considerable benefits to remote refrigeration compared to plug-in cabinets in hot regions. High savings can be achieved in southern European countries, such as Spain or Italy, by replacing plug-in cabinets in combination with an adjusted control concept.

In 2014, the BHX cycle was set to summer mode for six weeks in total. Another summer period in August was investigated, where the BHX cycle was set to winter mode and the ambient temperature was more moderate. The simulated power consumptions are plotted in Figure 6-24. The results indicated that power savings of 6.03 % were possible in case a (see Table 6.11). Almost all the saving potential was based on better AHU performance. The adjusted control of the floor heating system led to less cooling demand. As a result, the amount of ambient air and air supplied by the AHU could be reduced.

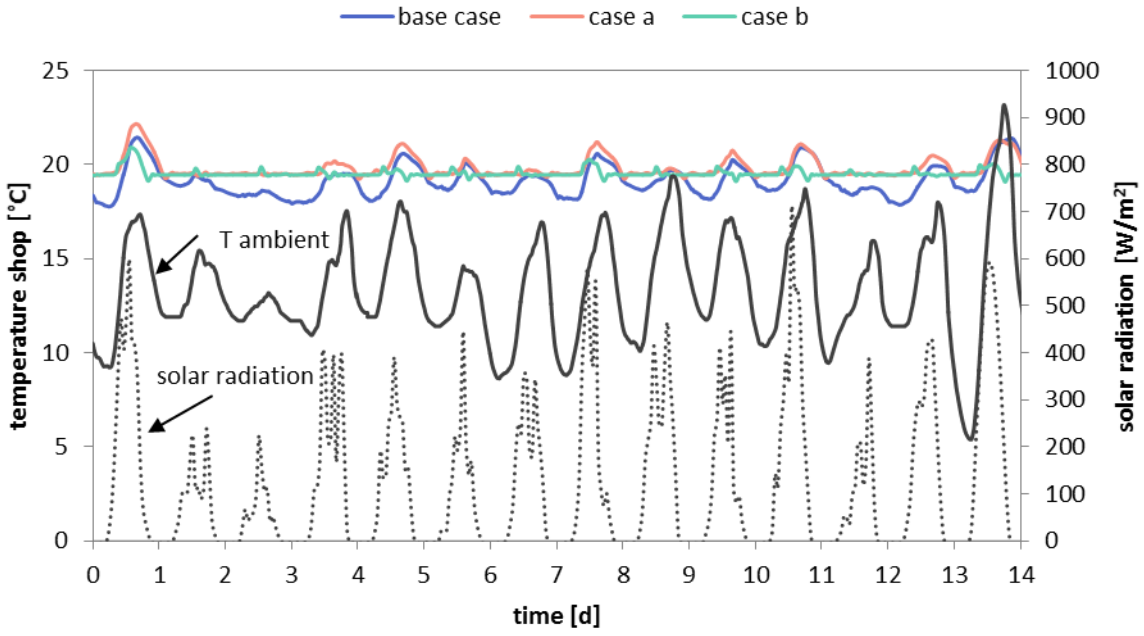

Figure 6-25: Simulation results for the shop temperature in August (cases: see 6.3.3)

This effect became even more dominant in case b: 10.24 % of the total power consumed could be saved by the AHU alone. Roughly the same amount of power reduction could be achieved through illumination and refrigeration. In total, savings of 19.77 % were predicted for case b. Figure 6-25 shows the average shop temperature in the simulated cases in August. The temperature could be kept within an acceptable range in all three cases. The shop temperature in the base case in August was closer to the desired value compared to the base case in the last April week. One reason could be a more adjusted AHU control in August. Moreover, the solar radiation in the last April week was higher compared to August. However, better temperature control was achieved in cases a and b compared to the base case for August as well.

Further simulation results can be found in Appendix C.

Generally, it can be concluded that one significant benefit in case b is the high flexibility of the system. To assess its flexibility, the heat load to the building can be subdivided into a part that is fixed or not controllable and a part that is flexible or controllable. An example for the fixed heat load is the waste heat from the plug-in cabinets, whereas the FH heat belongs to the controllable heat loads. The sum of fixed and flexible loads has to be high enough to cover the heating demand of the supermarket throughout the year. This could be proven. The fixed heat load plays a major role, especially in relation to the total heating demand of the building. The fixed heat load was calculated according to equation 5.81, and the heating demand according to equations 5.82 and 5.83.

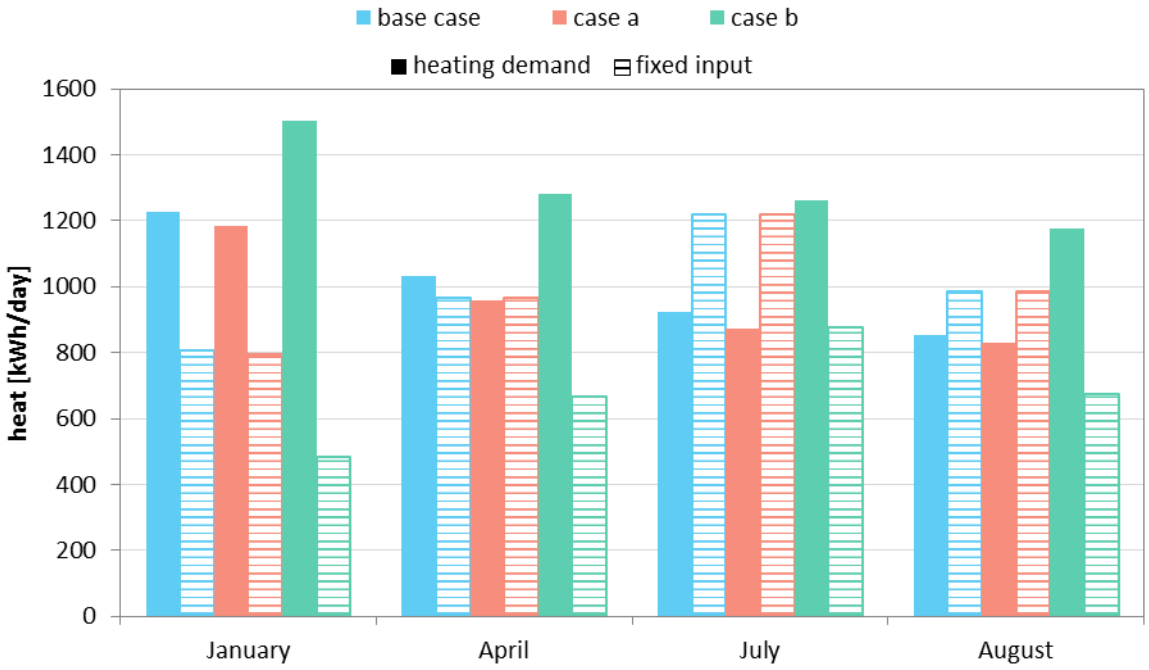

Figure 6-26: Total heat load and fixed heat load to the building (cases: see 6.3.3)

For reliable indoor temperature control it is important that the fixed heat load is significantly below the total heat load to avoid a high cooling demand and power consumption of the AHU. If the fixed heat load considerably exceeds the heating demand, the indoor air temperature

cannot be kept within the desired range. The calculated values for the considered periods are presented in Figure 6-26. The results for the base case and case a show that in April, the fixed heat load lays within the range of the heating demand, whereas in July and August, it was considerably above the heating demand. In April and July, the indoor air temperature partly showed high deviation from the set point in the base case. In August, the ambient temperature was moderate, so the high cooling demand could be covered by free cooling of the AHU. Nevertheless, a high power consumption of the AHU was the consequence. It was only in January that the fixed heat load was significantly lower than the heating demand.

Table 6.12: Assumed average and limit temperatures for the different seasons

season	winter	transition	summer	summer (hot)
average temperature [°C]	-5.42	6.39	13.38	19.26
lower limit [°C]	-	0.48	9.88	16.32
upper limit [°C]	0.48	9.88	16.32	-

The plotted values represent the average values over the simulated periods, which means that daily fluctuations were not considered. The difference between the fixed heat load and total heating demand occasionally was much higher during daytime. The simulation results for case b show that the fixed heat load stayed below 70 % of the overall heating demand for all months. This made an optimal temperature control in the sales area possible. As discussed above, the temperature could be kept close to the set point in all considered periods.

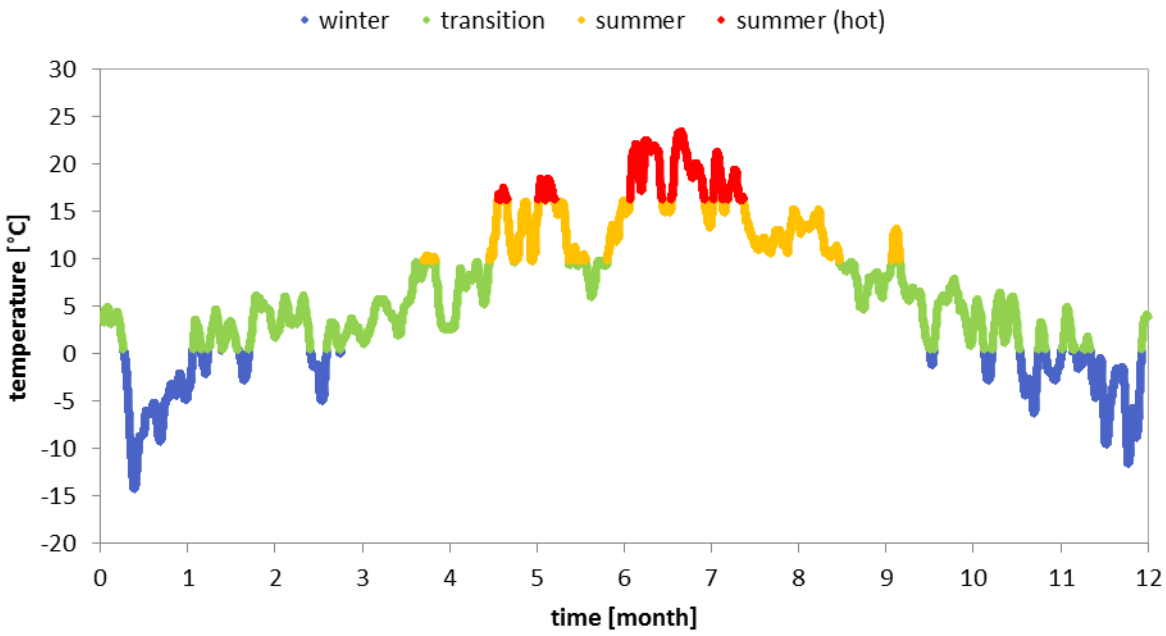

Figure 6-27: Classification into temperature ranges

Simulations were carried out for the most important ambient conditions: winter, transient, summer and hot summer. The annual power savings were extrapolated from these results. Two approaches were chosen. In both approaches, the whole year 2014 was disaggregated into days which can be assigned to one of the simulated periods. In approach I, the disaggregation was executed in a way that the annual power consumption of the base case simulations corresponds to the measured annual power consumption. Several combinations were possible. A solution with an appropriate distribution of the seasons was chosen, although other combinations led to similar results.

Another approach was the disaggregation of the year 2014 according to temperature ranges. The average temperature of each season was calculated and the mean value between the temperatures of two seasons was set as the limit value. The mean values and the limits are represented in Table 6.12. Each day of the year 2014 was assigned to one of the temperature ranges. The resulting distribution is visualised in Figure 6-27.

The resulting power consumptions and savings are presented in Table 6.14. The annual power consumption resulting from assumption II was 2.7 % below the measured value. Savings of 6 - 6.5 % could be determined for both assumptions in case a WM. If the summer mode was used during the very hot seasons, the saving potential would be between 5 and 5.5 %. In case a SM and case a WM, both assumptions led to similar results. In case b, the predicted savings account for 17.6 % for assumption I and 15.4 % for assumption II. The number of months that were assigned to each season are listed in Table 6.13 for both approaches.

Table 6.13: Assumed distribution of seasons

	winter	**transition**	**summer**	**summer (hot)**
number of months (I)	3.31	5.27	2.31	1.38
number of months (II)	2.49	5.73	2.54	1.27

Table 6.14: Predicted savings for the optimisation strategies for one year (cases: Table 6.7)

	assumption I			**assumption II**		
	en. intensity [kWh/m²/a]	**savings [MWh/a]**	**savings [%]**	**en. Intensity [kWh/m²/a]**	**savings [MWh/a]**	**savings [%]**
base case	476			489		
case a WM	447	31.2	6.4	458	28.9	6.1
case a SM	451	26.8	5.5	462	24.9	5.2
case b	403	86.3	17.6	403	73.1	15.4

An economic analysis was carried out with the predicted results. Energy prices in Norway are relatively low, with 16.53 €-Cent/ kWh in 2014 [128]. Additionally, a discount was usually given to bulk purchasers, which was assumed to be 50 % in these calculations [129].

Table 6.15: Predicted economic savings for the optimisation strategies for one year (cases: Table 6.7)

	assumption I		**assumption II**	
	energy cost [€/a]	**savings [€/a]**	**energy cost [€/a]**	**savings [€/a]**
base case	31408		32286	
case a WM	29499	1909	30225	2061
case a SM	29766	1642	30516	1770
case b	26582	4826	26591	5696

Table 6.15 shows the cost savings for both approaches and all simulated cases. It should be repeated in this context that the relation between energy costs and profit is between 1:4 and 1:1, depending on the supermarket [56], [60]. US Energy Star predicted an increase of sales of $59 for a $1 reduction in energy cost [61]. Furthermore, the environmental impact of the measures was estimated. In the base case, all refrigeration systems mainly used natural refrigerants, so the savings of direct CO_2 emissions were negligible. The reduction of indirect CO_2 emissions due to power savings was also investigated. The electricity mix for Norway, Germany and the UK [130], [131], [132] and typical values for the CO_2 emission of different power plant types [130] were used for the calculations. The predicted CO_2 savings are listed in Table 6.16.

In fact, the calculated reduction of CO_2 emissions is negligible, since 98.5 % of the electricity in Norway is obtained from hydropower, the ecological impact of which is almost zero. In this respect, Norway holds a unique position in Europe and globally. However, it could also be argued that, if power savings were achieved in Norway, the saved electricity could be exported to other European countries with fewer regenerative energy sources. The potential CO_2 emission savings for a German and British electricity mix were also calculated: in both countries, over 10,000 kg of CO_2 savings were predicted for case a WM and about 10,000 kg of CO_2 for case a WM for both assumptions. In case b, about 30,000 kg of CO_2 savings were calculated for the two countries. In general, the test supermarket showed a relatively good performance with 488.9 kWh/m^2 SFA and the optimisation strategies provided promising results. Nevertheless, some other measures could also be adopted in order to lower the energy costs. The defrost control, for example, could be controlled in a demand-driven way instead of a time con-

trol. Moreover, there is also the possibility of optimising the dry cooler position. Other simulations are necessary to investigate if placing the dry cooler in the BHX loop would be a reasonable option.

Table 6.16: Predicted economic savings for the optimisation strategies for one year (cases: Table 6.7)

	savings Norway [kg_{CO2}/a]		**savings Germany [kg_{CO2}/a]**		**savings Great Britain [kg_{CO2}/a]**	
	assumption I	**assumption II**	**assumption I**	**assumption II**	**assumption I**	**assumption II**
case a WM	31	29	11409	10568	12413	11498
case a SM	27	25	9799	9089	10661	9889
case b	87	73	31527	26711	34301	29062

The discussed investigations were carried out for one specific supermarket in Norway. It is not possible to simply apply the conclusions drawn here to other supermarkets, due to different framework conditions, such as weather, size and food:non-food ratio. Nevertheless, some of the results can also be useful for other supermarkets. One crucial point is that, when a supermarket is built, the overall heating demand, fixed heat load and heat recovery potential for different control strategies should be estimated for summer, winter and transition seasons. The fixed heat load should be adjusted, as far as possible, in a way that it remains below the heating demand during all seasons and allows flexible heating by heat recovery. The fixed heat load consists of all heat loads that cannot be controlled, such as solar radiation and waste heat from electrical devices and plug-in cabinets. The heating demand depends on the weather conditions but also, for example, on the size of the building, window area and quality of the insulation. Both the heating demand and the fixed heat load can be influenced at least partially. To lower the fixed heat load, plug-in cabinets should be avoided and glazed facades can be covered with window insulation films or flexible blinds can be installed. In warm countries where heating is hardly required, these measures are extremely important to lower the cooling demand. It could be seen that, even in a cold country like Norway, space cooling can become a challenge if the internal loads are too high. In warm regions, the highest savings can be achieved by reducing the cooling demand and thus the power consumption of the HVAC. In addition to the diminishing of internal loads, an advanced HVAC control is indispensable. If a supermarket is built from scratch in southern countries, borehole heat exchangers with a sufficient capacity can be installed if possible. Small windows are also an option to reduce the solar radiation. Avoiding plug-in cabinets is also recommendable in colder climates. It could be shown that in Norway, even in wintertime, the rejected heat from the refrigeration plant was sufficient to satisfy the heating requirements. This shows that, in many cases, a high per-

centage of the heating demand can be covered with an advanced heat recovery strategy. However, this presupposes an adjusted structure of the secondary/heat recovery loops and an adjusted heat recovery control strategy, as well as the presence of floor heating loops and well-designed storage tanks. If the available heat is not sufficient, the refrigeration system can be equipped with an extra evaporator.

7. Summary

The aim of this thesis was the analysis of the power consumption in supermarkets and the investigation of saving potentials. For this purpose, field measurements were carried out in a Norwegian test supermarket. The test supermarket was a discount supermarket located in a stand-alone building in Trondheim with a total area of 1,000 m^2. Detailed evaluations of the measurement data of one year were carried out in order to gain all relevant information. The measurement data were used to derive approaches for the optimisation of the supermarket's energy efficiency, with a special focus on the control strategy. Furthermore, a dynamic model of the supermarket was developed. The model was used for the development investigation of optimisation strategies. A highly dynamic model was developed which includes all subsystems, such as the refrigeration system, HVAC, secondary loops, storage tanks, borehole heat exchanger and building. The interaction between the different subsystems plays an important role in the overall power consumption. The subsystems were modelled in a detailed way. Pressure losses, heat transfer and thermal capacities were considered. The controllers were modelled in order to analyse the influence of the control strategy on the power consumption. Furthermore, the different time constants and the highly dynamic behaviour of the components and resulting heat and mass flows were considered. The model was validated using measurement data.

The measurement results indicated a good performance with an average energy intensity of 488.9 kWh/m^2 sales floor area in 2014. It could be shown that throughout the year, cooling was needed much more than heating. During summertime, the set point shop temperature was occasionally exceeded considerably. Only a small part of the available waste heat from the refrigeration plant was used for heating. The main saving potentials were assigned to the refrigeration plant and the AHU. The influence on the refrigeration plant performance was investigated. It became clear that the gas cooler return temperature and the high pressure should be kept as low as possible, ideally by extracting as much heat as possible through the gas coolers. At the same time, this heat should be used for heating or saved in the storage tanks for heating purposes later on. To reduce the power consumption of the AHU, the fans should be controlled dependent on the heating demand and the CO_2 content in the sales area. The high power consumption of the AHU was mainly due to high cooling demand in summertime, so the cooling demand should be reduced by reducing the heat load to the building. An

alternative approach was developed, recommending that all plug-in cabinets be replaced with remote refrigeration cabinets and that more efficient illumination be used.

Based on this knowledge, an overall control concept was developed, considering the refrigeration plant, AHU, heat recovery and secondary loops. Simulations were carried out in order to investigate two approaches: case a, where only the control concept was applied, and case b, where the control concept was applied and the plug-in cabinets and illumination were replaced. The base case was simulated and compared to the optimisation approaches. Simulations were carried out for the relevant seasons and the annual power consumption was determined post-processing. The simulation results indicated that a power reduction of about 6 % would be possible in case a. In case b, savings of around 15 - 18 % were predicted. Furthermore, a much better indoor temperature control would be possible in both cases, but especially in case b. These results showed that even in a cold country like Norway, internal heat loads can be high enough that the high cooling demands can partly not be satisfied. Consequently, one of the most crucial points during the design of a supermarket is the investigation of heating and cooling demands. The heat loads that are not controllable, such as waste heat from plug-in cabinets, illumination and other electrical devices, as well as solar heat flux, should be kept considerably below the overall heating demand. Otherwise, high fan speed and air conditioning are required and keeping the indoor air conditions in the desired range becomes a challenge.

One drawback of these investigations is that only one specific supermarket was investigated. The developed optimisation strategies and the control concept cannot easily be adopted by any other supermarket. Supermarkets differ considerably, for example in size, food:non food ratio and technical equipment. The ambient conditions differ significantly, depending on the geographical location. Moreover, the implementation of a borehole heat exchanger is not always possible, for example in urban regions. On the other hand, a very detailed analysis has been carried out, investigating the interactions of refrigeration plant, HVAC, heat recovery and building. Some of the general conclusions can be helpful for the development of supermarket concepts.

References

[1] SKM Enviros, “Phase down of HFC consumption in the EU-assessment of implications for the RAC sector,” Executive summary, 2012.

[2] M. Kolokotroni, S. A. Tassou and B. L. Gowreesunker, “Energy aspects and ventilation of food retail buildings,” *Advances in building energy research,* pp. 1 - 19, April 2014.

[3] S. A. Tassou, Y. T. Ge, A. Hadawey and D. Marriott, “Energy consumption and conservation in food retailing,” *Applied thermal engineering,* p. 147– 156, August 2010.

[4] European Parliament and the Council of the EU, Directive 2009/29/EC of 23 April 2009 amending directive 2003/87/EC so as to improve and extend the greenhouse gas emission allowance trading scheme of the community, 2009.

[5] Nielsen, “results of the 15th inventory of retail grocery in Belgium,” Grocery Universe, 2013.

[6] “CREATIV,” Sintef, [Online]. Available: https://www.sintef.no/projectweb/creativ. [Accessed 04 02 2016].

[7] J. Arias, “Energy Usage in Supermarkets - Modelling and Field Measurements,” Doctoral thesis, Royal Institute of Technology - Department of Energy Technology, Stockholm, 2005.

[8] v. D. Baxter, “IEA annex 26: advanced supermarket refrigeration / heat recovery systems,” Final report volume 1 – executive summary, International Energy Agency, Oak Ridge, 2003.

[9] Y. You, “Investigation of Deep-freeze Refrigeration Systems in Supermarket Application,” Master thesis, Stockholm, 2001.

[10] D. Clodic, C. Le Pellec and I. Darbord, “Comparison of Energy Efficiencies of Commercial Refrigeration Direct and Indirect Systems,” in *International Refrigeration and Air Conditioning Conference*, Purdue, West Lafayette, USA, 1998.

[11] G. Cortella, P. D’Agaro and O. Saro, “Prediction of the energy consumption of a supermarket refrigeration system (Presentation),” in *International Conference of Refrigeration*, Prague, 2011.

[12] D. Cowan, J. Gartshore, I. Chaer, C. Francis and G. Maidment, “REAL Zero – Reducing refrigerant emissions & leakage- feedback from the IOR Project,” The Insitute of Refrigeration, 2010.

[13] "The Montreal protocol on substances that deplete the ozone layer," United Nations Environment Programme, 2015. [Online]. Available: http://ozone.unep.org/en/treaties-and-decisions/montreal-protocol-substances-deplete-ozone-layer. [Accessed 23 03 2016].

[14] J. A. Evans, G. G. Maidment and A. M. Foster, "A Retail Road Map for Supermarkets," in *International Conference of Refrigeration*, Prague, 2011.

[15] European Parliament and the Council of the EU, Regulation (EC) No 842/2006 of 17 May 2006 on certain fluorinated greenhouse gases, 2006.

[16] European Parliament and the Council of the EU, Regulation (EU) No 517/2014 of 16 April 2014 on fluorinated greenhouse gases and repealing Regulation (EC) No 842/2006 Text with EEA relevance, 2014.

[17] S. Sawalha and M. Karampour, "Supermarket refrigeration and heat recovery using CO2 as refrigerant - a comprehensive evaluation based on field measurements and modelling," Royal Institute of Technology (KTH), 2014.

[18] Shecco, "Guide 2014: natural refrigerants continued growth and innovation in Europe," Brussels, Belgium, 2014.

[19] D. Hinde, S. Zha and L. Lan, "Carbon dioxide in north American supermarket," *ASHRAE Journal,* pp. 18-24, February 2009.

[20] M. Likitthammanit, "Experimental investigations of NH3/CO2 cascade and transcritical CO2 refrigeration systems in supermarkets," Master thesis, Royal Institute of Technology - Division of Applied Thermodynamic and Refrigeration, Stockholm, 2007.

[21] P. Neksa, "CO2 as refrigerant for systems in transcritical operation principles and technology," *EcoLibrium,* October 2004.

[22] N. Réhault and D. Kalz, "Aldi 2010 - Hocheffizienter Supermarkt mit Geothermiegestützdem Kälteverbund," Abschlussbericht, Fraunhofer ISE; Aldi Süd, 2013.

[23] U. Lindberg, M. Axell and L. Rolfsman, "Energy Efficiency in Supermarkets – Implication of EU Efficiency Directives," in *International Conference of Refrigeration*, Prague, 2011.

[24] M. Titze, F. Frydenlund and A. Heafner, "Energy Efficient Ventilation of Supermarkets," in *Clima 2013*, Prague, 2013.

[25] Office of the Deputy Prime Minister, "The building regulations 2000 - Ventilation," Approved document F, 2006.

[26] Deutsches Institut für Normung, "DIN EN 13779: Lüftung von Nichtwohngebäuden – Allgemeine Grundlagen und Anforderungen für Lüftungs- und Klimaanlagen und Raumkühlsysteme," 2007.

[27] U. Lindberg, “Indoor Thermal Environment in Supermarkets. A study of measured and perceived comfort parameters,” Technical Report, Chalmers University of Technology - Department of Building Technology, Sweden, 2009.

[28] M. Orphelin and D. Marchio, “Computer-Aided Energy Use Estimation in Supermarkets,” in *Building Simulation Conference*, Prague, 1997.

[29] Y. T. Ge and S. A. Tassou, “Performance evaluation and optimal design of supermarket refrigeration systems with supermarket module ‘supersim’, Part I: Model description and validation,” *International Journal of Refrigeration, 34,* pp. 540 - 549, December 2010.

[30] Carbon Trust, “Heat recovery - A guide to key systems and applications,” London, 2012.

[31] Energy Star, “Putting Energy into Profits. Guide for Small Business,” Washington, D. C., 2003.

[32] G. Cortella, P. D’Agaro, O. Saro and M. Franceschi, “Prediction of the energy consumption of a supermarket refrigeration system,” in *International Conference of Refrigeration*, Prague, 2011.

[33] S. Girotto, S. Minetto and P. Nekså, “Commercial refrigeration system using CO2 as the refrigerant,” *International Journal of Refrigeration,* pp. 717 - 723, November 2004.

[34] O. Finckh, R. Schrey and M. Wozny, “Energy and efficiency comparison between standard HFC and CO2 transcritical systems for supermarket applications,” in *International Conference on Refrigeration*, Prague, Czech Republic, 2011.

[35] Y. T. Ge and S. A. Tassou, “Performance evaluation and optimal design of supermarket refrigeration systems with supermarket model “SuperSim”. Part II: Model applications,” *International Journal of Refrigeration,* pp. 540 - 549, November 2010.

[36] S. Sawalha, “Carbon Dioxide in Supermarket Refrigeration,” Doctoral thesis, Royal Institute of Technology (KTH), Stockholm, Sweden, 2008.

[37] V. Sharma, B. Fricke and P. Bansal, “Comparative analysis of various CO2 configurations in supermarket refrigeration systems,” *International Journal of Refrigeration,* pp. 86 - 99, July 2014.

[38] A. Mikhailov and H. O. Matthiesen, “System efficiency for natural refrigerants,” *ASHRAE Journal,* pp. 66 - 71, August 2013.

[39] N. Réhault and D. Kalz, “Ongoing commissioning of a high efficiency supermarket with a ground coupled carbon dioxide refrigeration plant,” in *International Conference for Enhanced Building Operations (ICEBO)*, Manchester, England, 2012.

[40] C. Lucas and J. Köhler, "Experimental investigation of the COP improvement of a refrigeration cycle by use of an ejector," *International Journal of Refrigeration,* pp. 1595 - 1603, May 2012.

[41] A. Hafner, S. Försterling and K. Banasiak, "Multi-ejector concept for R-744 supermarket refrigeration," *International Journal of Refrigeration,* pp. 1-13, April 2014.

[42] U. Lindberg, M. Axell and P. Fahlén, "Vertical display cabinets with doors - Influence of the dooropening frequency on storage temperature and cooling demand," in *Sustainable Refrigeration and Heat Pump Techn. Conference*, Stockholm, Sweden, 2010.

[43] R. T. Faramarzi and D. H. Walker, "Investigation of secondary loop supermarket refrigeration systems," Consultant report, California Energy Comission, 2004.

[44] M. S. Spyrou, K. Shanks, M. J. Cooka, J. Pitcher and J. Lee, "An empirical study of electricity and gas demand drivers in large food retail buildings of a national organisation," *Energy and Buildings,* p. 172–182, April 2014.

[45] P. Lundqvist and J. Arias, "Heat recovery and floating condensing in supermarkets," *Energy and Buildings,* pp. 73 - 81, February 2006.

[46] E. Mayer, "Energieeffizienz im Einzelhandel: Intelligente Regelungstechnik in einem Supermarkt," *Heizungsjournal,* 2012.

[47] R. H. Howell, "Effects of store relative humidity on refrigerated display case performance," *ASHRAE Transactions,* pp. 667 - 678, 1993.

[48] A. Campbell and R. Oliver, "Building services for low carbon supermarkets," The Insitute of Refrigeration, 2009.

[49] N. Narendran, J. Brons and J. Taylor, "Energy efficient lighting alternative for commercial refrigeration - Report prepared for the New York State energy research and development Authority," Ransselaer Polytechnic Institute, 2006.

[50] GE Consumer Industrial, "Wal-Mart Uses GE LED Refrigerated Display Lighting," 2006. [Online]. Available: http://www.businesswire.com/news/home/20061116005286/en/Wal-Mart-GE-LED-Refrigerated-Display-Lighting-Save. [Accessed 24 03 2016].

[51] Irish Energy Centre, "Energy efficient lighting in shops," Dublin, 1995.

[52] L. Edwards and P. Torcellini, "A Literature Review of the Effects of Natural Light on Building Occupants," National Renewable Energy Laboratory, Golden, Colorado, 2002.

[53] The Chartered Institution of Building Services Engineers, "Guide A: Environmental Design," London, 2007.

[54] US EPA, “Profile of an Average U.S. Supermarket’s Greenhouse Gas Impacts from Refrigeration Leaks Compared to Electricity Consumption,” http://www.epa.gov/greenchill/downloads/GC AverageStoreProfile FINALJUNE 2011 REVISED.pdf, 2011.

[55] S. Tassou, “Potential for solar energy in food manufacturing, distribution and retail,” Final report, Department for Environment, Food and Rural Affairs , London, 2007.

[56] M. Atzberger, “Energieeffizienz im Einzelhandel. Ergebnisse,” in *DENA Energieeffizienzkongress*, Berlin, 2015.

[57] European Parliament and the Council of the EU, Directive 2002/91/EC of 16 December 2002 on the energy performance of buildings, 2002.

[58] European Parliament and the Council of the EU, Directive 2010/31/EC of 19 May 2010 on the energy performance of buildings (recast), 2010.

[59] The Air Tightness Testing & Measurement Association, Technical standard L2. measuring air permeability of building envelopes (non-dwellings), Northampton, 2010.

[60] Department for Environment, Food and Rural Affairs, “Economic Note on UK Grocery Retailing,” London, 2006.

[61] EnergyStar, “Supermarkets: An overview of energy use and energy efficiency opportunities,” [Online]. Available: https://www.energystar.gov/sites/default/files/buildings/tools/SPP%20Sales%20Flyer%20for%20Supermarkets%20and%20Grocery%20Stores.pdf. [Accessed 24 03 2016].

[62] Department for Environment, Food and Rural Affairs, “Economic note on UK grocery retailing,” London, 2006.

[63] Institute of Grocery Distribution, “UK Grocery Retailing,” [Online]. Available: http://www.igd.com/our-expertise/Retail/retail-outlook/3371/UK-Grocery-Retailing/#2. [Accessed 11 03 2013].

[64] W. Chung, Y. Hui and Y. Lam, “Benchmarking the energy efficiency of commercial buildings,” *Applied Energy,* pp. 1 - 14, 03 2005.

[65] M. Sankar, V. P. I. S. R. Ramakrishna, V. Sarangan and A. Vasan, “Comparing Apples to Oranges: Energy Benchmarking of Supermarkets with Limited Data,” in *International Conference on Future Energy Systems*, Cambridge, 2014.

[66] BizEE Software Limited, “Degree days,” 2012. [Online]. Available: http://www.degreedays.net/. [Accessed 24 03 2016].

[67] Carbon Trust, “Refrigeration Road Map,” London, 2010.

[68] Target Zero, “Guidance on the design and Construction of sustainable, low carbon supermarket buildings,” Report V 2.0, 2011.

[69] S. Sawalha, “Theoretical evaluation of trans-critical CO2 systems in supermarket refrigeration. Part I: modeling, simulation and optimization of two system solutions,” *International Journal of Refrigeration,* pp. 516 - 524, August 2007.

[70] S. Sawalha, “Theoretical evaluation of trans-critical CO2 systems in supermarket refrigeration. Part II: system modifications and comparisons of different solutions,” *International Journal of Refrigeration,* pp. 525 - 534, August 2007.

[71] S. Sawalha, “Investigation of heat recovery in CO2 trans-critical solution for supermarket refrigeration,” *International Journal of Refrigeration,* pp. 145 - 156, October 2012.

[72] M. Karampour and S. Sawalha, “Performance and control strategies analysis of a CO2 trans-critical booster system,” in *International Conference on Sustainability and the Cold Chain*, London, 2014.

[73] A. Abdi, “Analysis of heat recovery in supermarket refrigeration using carbon dioxide as refrigerant,” Master thesis , Royal Institute of Technology - School of Industrial Engineering and Management, Stockholm, 2014.

[74] S. Sawalha, M. Karampour and J. Rogstam, “Field measurements of supermarket refrigeration systems. Part I: Analysis of CO2 trans-critical refrigeration systems,” *Applied Thermal Engineering,* pp. 633 - 647, May 2015.

[75] Y. T. Ge and S. Tassou, “Thermodynamic analysis of transcritical CO2 booster refrigeration systems in supermarket,” *Energy Conversion and Management,* pp. 1868 - 1875, January 2011.

[76] S. Maxwell and G. Shrestha, “Empirical validation of building energy simulation software: Energyplus. In Proceedings of Building Simulation,” in *Conference of International Building Performance Simulation Association*, Sydney, 2011.

[77] US Department of Energy, “EnergyPlus Energy Simulation Software,” 2015. [Online]. Available: http://apps1.eere.energy.gov/buildings/energyplus/. [Accessed 17 02 2016].

[78] US Department of Energy, “EnergyPlus Features,” 2015. [Online]. Available: https://energyplus.net/features. [Accessed 24 03 2016].

[79] NASA, “Researcher news,” 2010. [Online]. Available: http://www.nasa.gov/centers/langley/news/researchernews/rn_RETscreen.html. [Accessed 17 02 2016].

[80] The University of Wisconsin Madison, “A TRaNsient SYstems Simulation Program,” 2013. [Online]. Available: http://sel.me.wisc.edu/trnsys/. [Accessed 24 03 2016].

[81] N. Fidoora, A. Hafner, N. Lemke and J. Köhler, “SuperSmart-Energiebenchmarktool für Supermärkte,” in *DKV Tagung*, Hannover, 2013.

[82] W. Tegethoff, J. N. Jäschke, C. Schulze and N. Fidorra, “Verschaltung von Functional-Mockup-Units (FMUs) mit physikalischen Konnektoren am Beispiel der thermischen Simuation,” in *ASIM-Treffen STS/GMMS*, Lippstadt, 2016.

[83] TLK Thermo, “Softwareprodukte,” 2016. [Online]. Available: http://www.tlk-thermo.com/index.php/de/softwareprodukte. [Accessed 19 02 2016].

[84] SkyscraperCity, [Online]. Available: http://www.skyscrapercity.com/showthread.php?t=1473380&page=5.

[85] TLK-Thermo GmbH, “TILMedia Add-In for Microsoft Excel Version 3.3.1,” 2015.

[86] Norwegian Meteorological Insitute, “eKlima,” [Online]. Available: http://eklima.met.no. [Accessed 22 02 2016].

[87] J. D. Pleil and A. B. Lindstrom, “Collection of a single alveolar exhales breath for volatile organic compounds analysis,” *American Journal of Insustrial Medicine,* pp. 109 - 121, July 1995.

[88] K. Paech, “Biologische Grundlagen der Frischhaltung pflanzlicher Lebensmittel,” in *Handbuch der Kältetechnik*, 1 ed., vol. 9, Berlin, Göttingen, Heidelberg, Springer Verlag, 1952, p. 252.

[89] Umweltbundesamt, “Gesundheitliche Bewertung von Kohlendioxid in der Innenraumluft,” *Bundesgesundheitsblatt - Gesundheitsforschung - Gesundheitsschutz,* pp. 1358 - 1369, 2008.

[90] A. Schälin, “Gebäudeeingänge mit grossem Publikumsverkehr,” AFC Air Flow Consulting, April, Zürich, 1998.

[91] Verein Deutscher Ingenieure, Richtlinie VDI 2078: Berechnung der thermischen Lasten und Raumtemperaturen (Auslegung Kühllast und Jahressimulation), Düsseldorf, 2015.

[92] W. Glaubitt and J. Probst, “Klarer Durchblick - Optimierung der Lichttransmissionseigenschaften von Verglasungen (presentation),” in *Forum Building Science*, Krems, 2013.

[93] C. Buratti and E. Moretti, “Glazing systems with silica aerogel for energy savings in buildings,” *Applied Energy,* p. 396 – 403, April 2012.

[94] J. Köhler, “Wärme- und Stoffübertragung - Skriptum zur Vorlesung,” Technische Universität Braunschweig - Insittut für Thermodynamik.Braunschweig.

[95] TLK Thermo GmbH and Institut für Thermodynamik, “TIL 3.3.1: User's Guide,” 2015.

[96] Modelica, “A unified object-oriented language for systems modeling,” Language specification, 2012.

[97] TLK Thermo GmbH and Institut für Thermodynamik, “TILMedia 3.3.1: User's Guide,” 2015.

[98] C. Kaiser, S. Försterling, W. Tegethoff and J. Köhler, “Untersuchungen von Regelstrategien für die Omnibusklimatisierung mit Hilfe einer Gesamtfahrzeugsimulation,” in *ASIM-Tagung STS/GMMS*, Wolfenbüttel, 2012.

[99] C. Kaiser, S. Försterling, C. Strupp, N. Lemke, M. Sonnekalb and J. Köhler, “Simulation zur verbrauchsorientierten Bewertung von Omnibus-Klimatisierungskonzepten,” in *Wärmemanagement des Kraftfahrzeugs VIII - Energiemanagement. Haus der Technik Fachbuch Band 125*, Renningen, Expert-Verlag, 2012.

[100] J. Averdam, “Erstellung eines dynamischen Gebäude-Modells zur Simulation von Supermärkten,” Study thesis, Technische Universität Braunschweig - Insitut für Thermodynamik, Braunschweig, 2015.

[101] T. Alpögger, “Dynamische Simulation solarer Kraft-Wärme-Kopplung mittels ORC für kleine Leistungen,” Master thesis, Technische Universität Braunschweig - Institut für Thermodynamik, Braunschweig, 2012.

[102] C. Baak, “Dynamische Simulation und energetische Betrachtung eines Solartrockners als Teil eines Heizungssystems,” Master thesis, Technische Universität Braunschweig - Institut für Thermodynamik, Braunschweig, 2015.

[103] J. Lüer, “Erstellung eines dynamischen Erdwärmesondenmodells in Modelica,” Bachelor thesis, Technische Universität Braunschweig - Institut für Thermodynamik, Braunschweig, 2014.

[104] W. Wagner, Strömung und Druckverlust, 6 ed., Würzburg: Vogel Buchverlag, 2008.

[105] Verein Deutscher Ingenieure, “Wärmeübergang bei Ströhmung durch Rohre,” in *VDI Wärmeantlas*, 10 ed., Berlin, Heidelberg, Springer Verlag, 2006.

[106] G. Cerbe and G. Wilhelms, Technische Thermodynamik, 15 ed., München: Carl Hanser Verlag, 2008.

[107] D. Becker and D. Wang, “Green Roof Heat Transfer and Thermal Performance Analysis,” Civil and Environmental Engineering, Carnegie Mellon University - Civil and Environmental Engineering, Carnegie Mellon University, 2011.

[108] N. Carroll, “The Thermal and Rainwater Runoff Performance of an Extensive Green Roof System,” Master thesis, University of Strathclyde - Department of Mechanical Engineering, Glasgow, 2010.

[109] Verein Deutscher Ingenieure, “Druckverlust und Wärmeübergang in Plattenwärmeübertragern,” in *VDI Wärmealtas*, 11 ed., Berlin, Heidelberg, Springer Verlag, 2013.

[110] H. D. Baehr and K. Stephan, Heat and Mass Transfer, vol. 2, Berlin, Heidelberg, New York: Springer Verlag, 2006.

[111] G. Quaas, “Vergleich makroökonomische Modelle - Fehlermaße,” [Online]. Available: http://www.georg-quaas.de/modellvergleich.pdf. [Accessed 23 01 2016].

[112] H. Kuchling, Taschenbuch der Physik, 12 ed., Thun and Frankfurth/ Main: Verlag Harri Deutsch, 1989, p. 577.

[113] M. NDoye and S. Mousset, “Experimental study of the cold aisle phenomenon in supermarket display cabinet,” in *International Conference of Refrigeration*, Prague, 2011.

[114] Danfoss, *Temperature sensors, type AKS 21 - Data Sheet,* Baltimore, 2006.

[115] Bernt Messtechnik, *Monicon S500-IR NDIR Gas Sensor - Data sheet,* Düsseldorf, 2006.

[116] PCE Instruments, *Thermo-Hygrometer RH-2 - Data Sheet,* Meschede.

[117] Eltako Electronics, *Technische Daten Wechselstromzähler, Drehstromzähler und Energieverbrauchsanzeige - Data Sheet,* Fellbach, 2012.

[118] Y. T. Ge and S. A. Tassou, “Control optimisation of CO2 cycles for medium temperature retail food refrigeration systems,” *International Journal of Refrigeration,* pp. 1376 - 1388, January 2009.

[119] S. M. Liao, T. S. Zhao and A. Jacobsen, “A correlation of heat rejection pressures in transcritical carbon dioxide cycles,” *Applied Thermal Engineering,* pp. 831 - 841, June 2000.

[120] Y. Chen and J. Gu, “The optimum high pressure for CO2 transcritical refrigeration systems with internal heat exchangers,” *International Journal of Refrigeration,* pp. 1238 - 1249, December 2005.

[121] L. Cecchinato, M. Chiarello, M. Corradi, E. Fornasieri, S. Minetto, P. Stringari and C. Zilio, “Thermodynamic analysis of different two-stage transcritical carbon dioxide cycles,” *International Journal of Refrigeration,* pp. 1058 - 1067, October 2008.

[122] F. Kauf, “Determination of the optimum high pressure for transcritical CO2-refrigeration cycles,” *International Journal of Thermal Sciences,* pp. 325 - 330, April 1999.

[123] M. Titze, N. Lemke, A. Hafner and J. Köhler, “Entwicklung und Simulation Luftaufbereitungs- und Kälteanlageanlage im Supermarkt mit Wärmerückgewinnung,” in *DKV Tagung*, Hannover, 2013.

[124] M. Titze, “Dynamische Simulation einer Kälte- und Lüftungsanlage mit Abwärmenutzung im Supermarkt (Presentation),” in *DKV Tagung*, Hannover, 2013.

[125] Deutsches Institut für Normung, “DIN EN 13053: Lüftung von Gebäuden – Zentrale raumlufttechnische Geräte – Leistungskenndaten für Geräte, Komponenten und Baueinheiten,” 2012.

[126] M. Orphelin, D. Marchio and S. Bech, “Significant parameters for energy consumption in frozen food area of large supermarkets,” in *Clima 2000*, Brussels, 1997.

[127] A. Bahman, L. Rosario and M. M. Rahman, “Analysis of energy savings in a supermarket refrigeration/HVAC system,” *Applied Energy,* pp. 11 - 21, April 2012.

[128] Eurostat, “Energiepreise in der EU - Strompreise für Haushalte in der EU stiegen 2014 um 2,9%,” Press release, European Comission, Brussels, 2015.

[129] Eurostat, “Energy, transport and environment indicators,” European Comission, Brussels, 2014.

[130] Forschungsstelle für Energiewirtschaft e. V., “Basisdaten zur Bereitstellung und Umwandlung von Brennstoffen,” München, 2010.

[131] Statistisk sentralbyrå - statistics Norway, “Electricity, annual figures,” 2013. [Online]. Available: https://www.ssb.no/en/energi-og-industri/statistikker/elektrisitetaar/aar/2015-03-25. [Accessed 25 03 2016].

[132] UK Government, “Gov.uk,” [Online]. Available: https://www.gov.uk/government/uploads/system/uploads/attachment_data/file/487838/Electricity.pdf. [Accessed 25 03 2016].

Appendix A

Evaluation of the measurement data

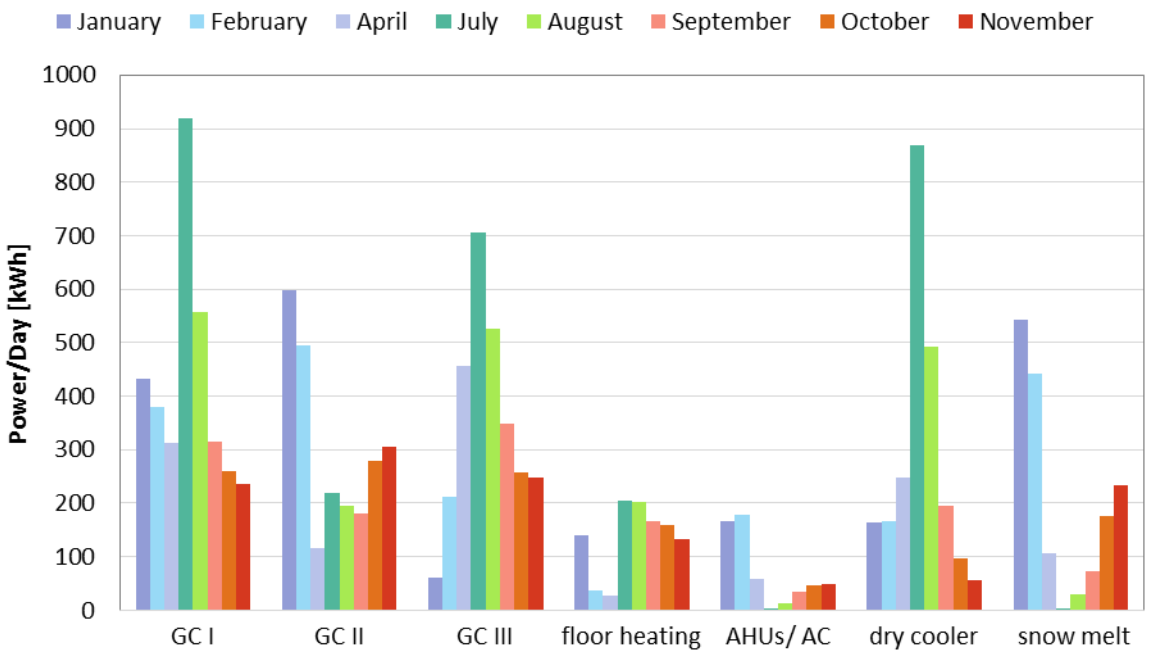

Measured waste heat and use of the waste heat

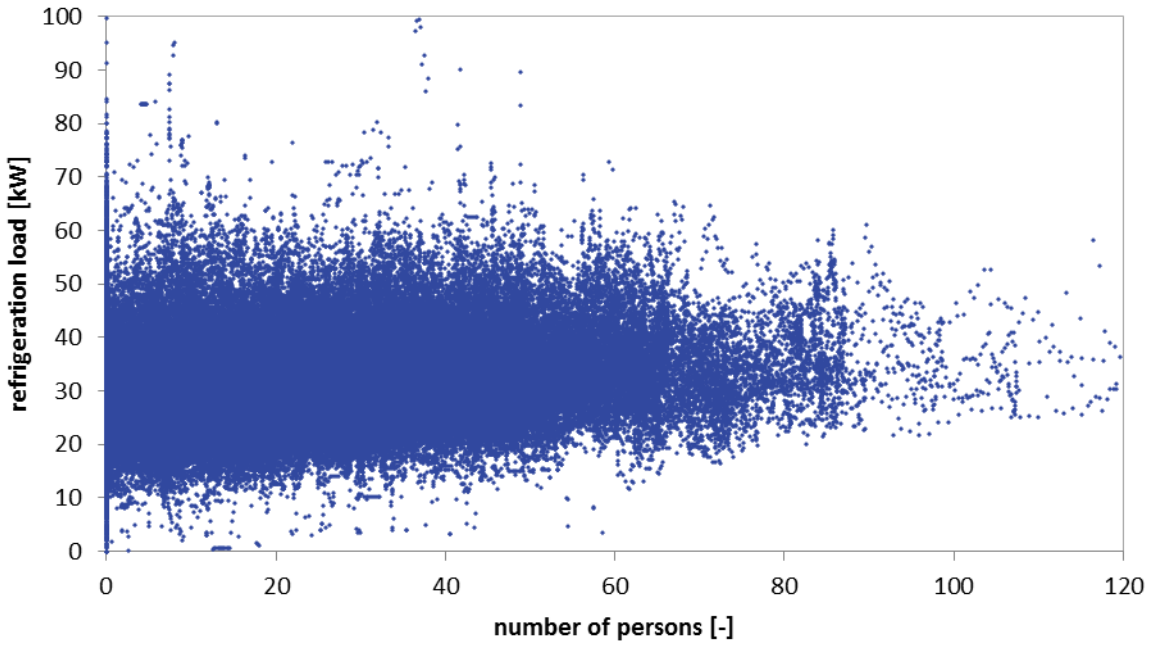

Dependence of the refrigeration load on the number of persons in the shop

Appendix B

Validation of the simulation model

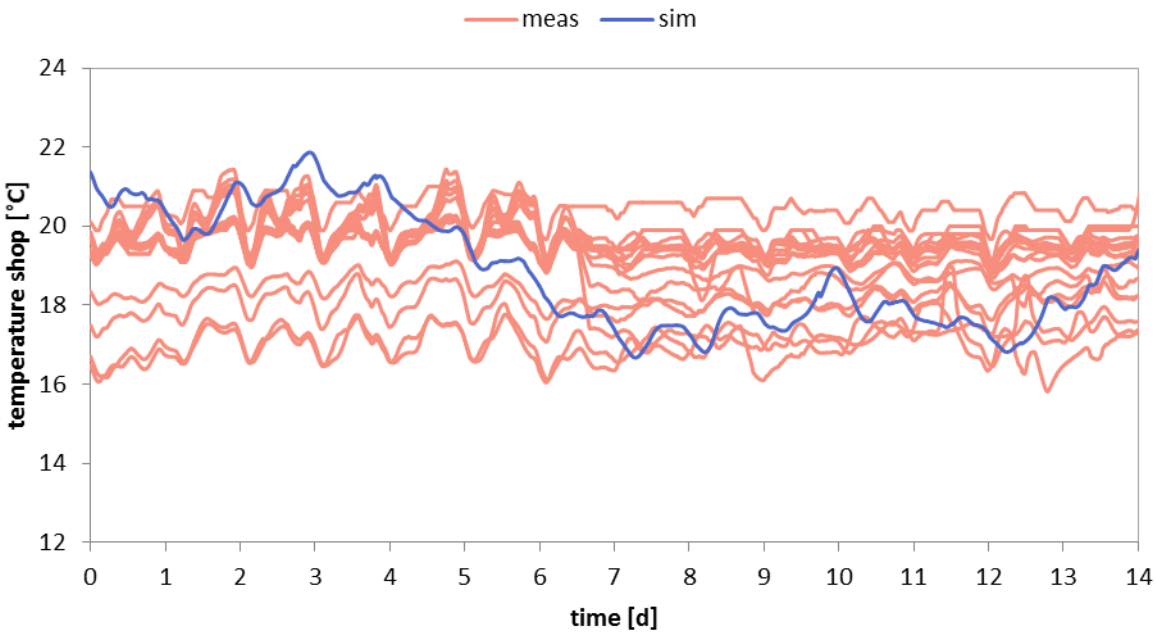

January: all shop temperatures

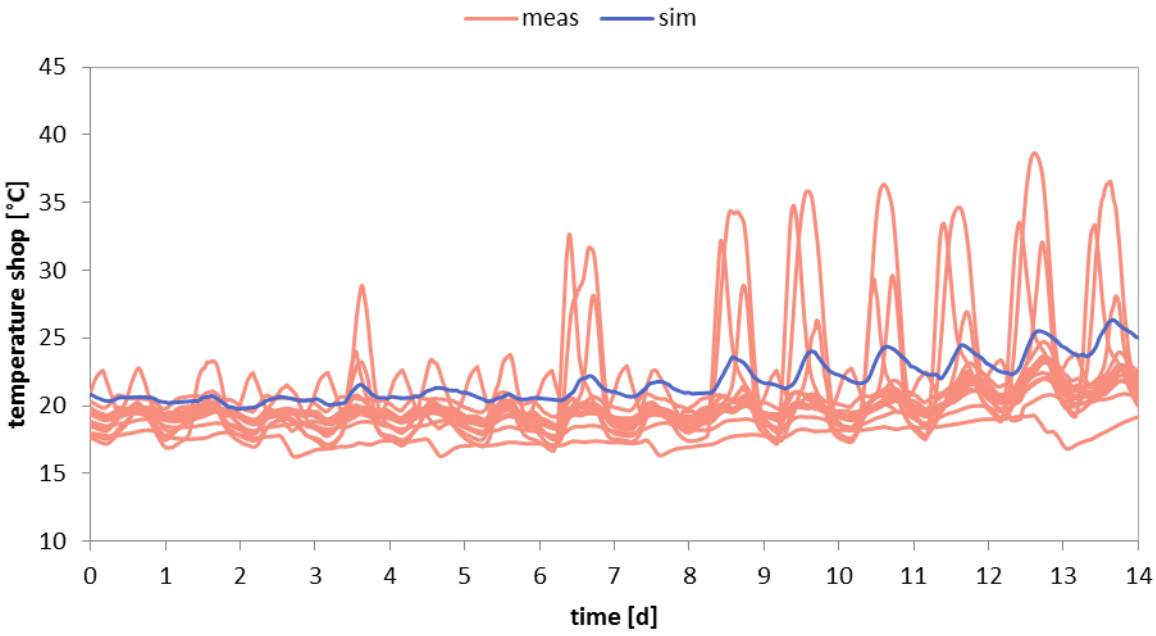

April: all shop temperatures

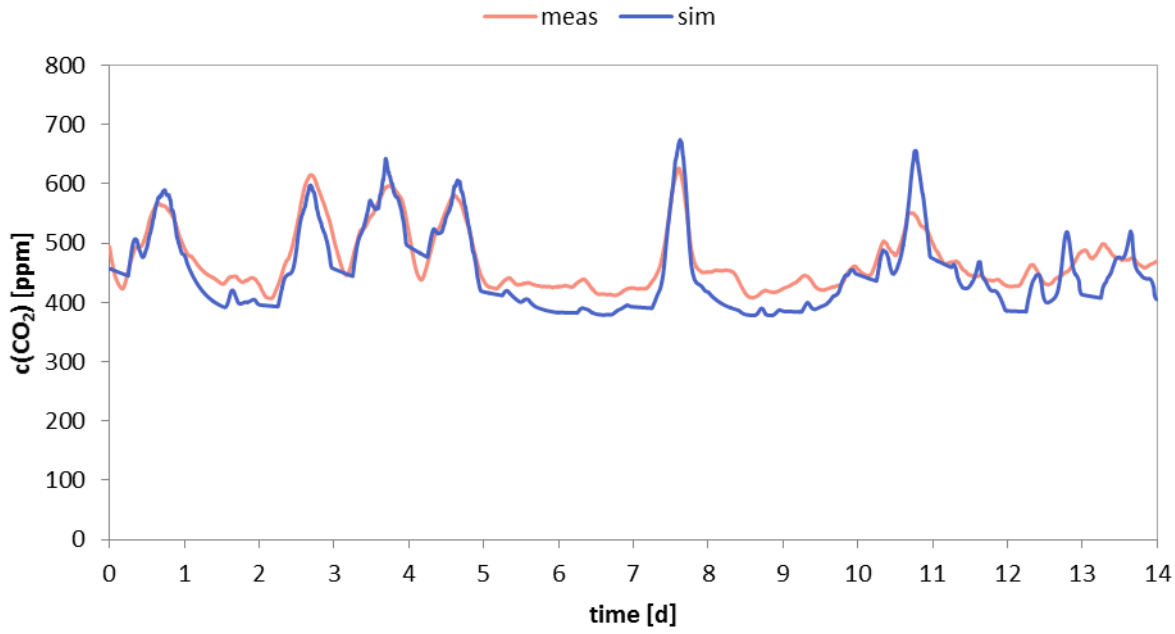

April: CO2 content shop

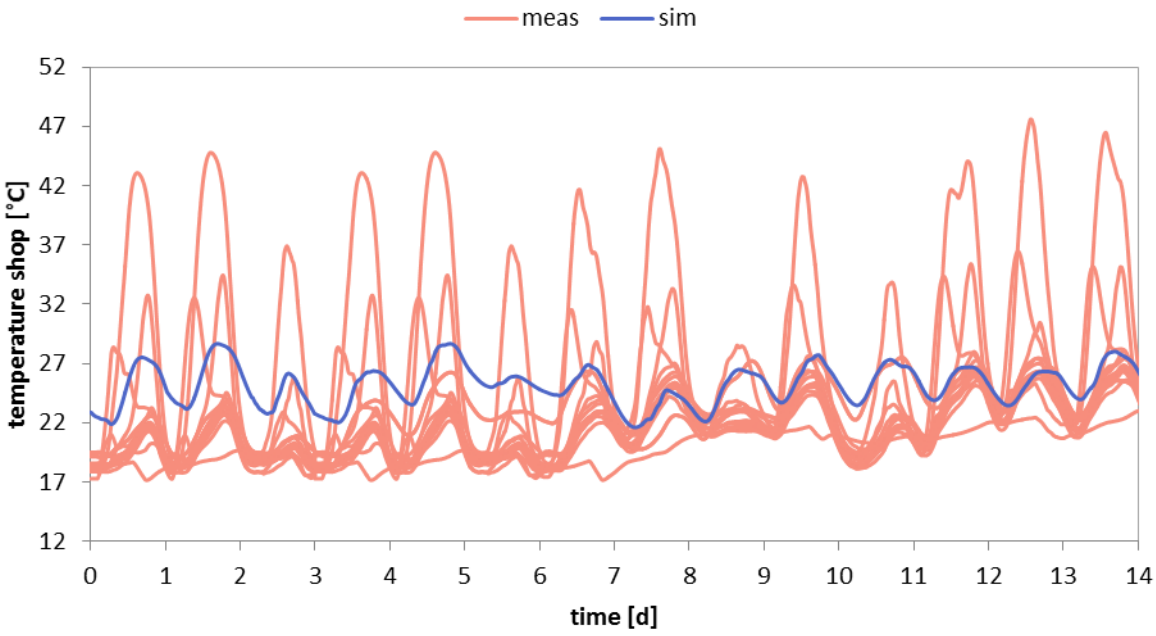

July: all shop temperatures

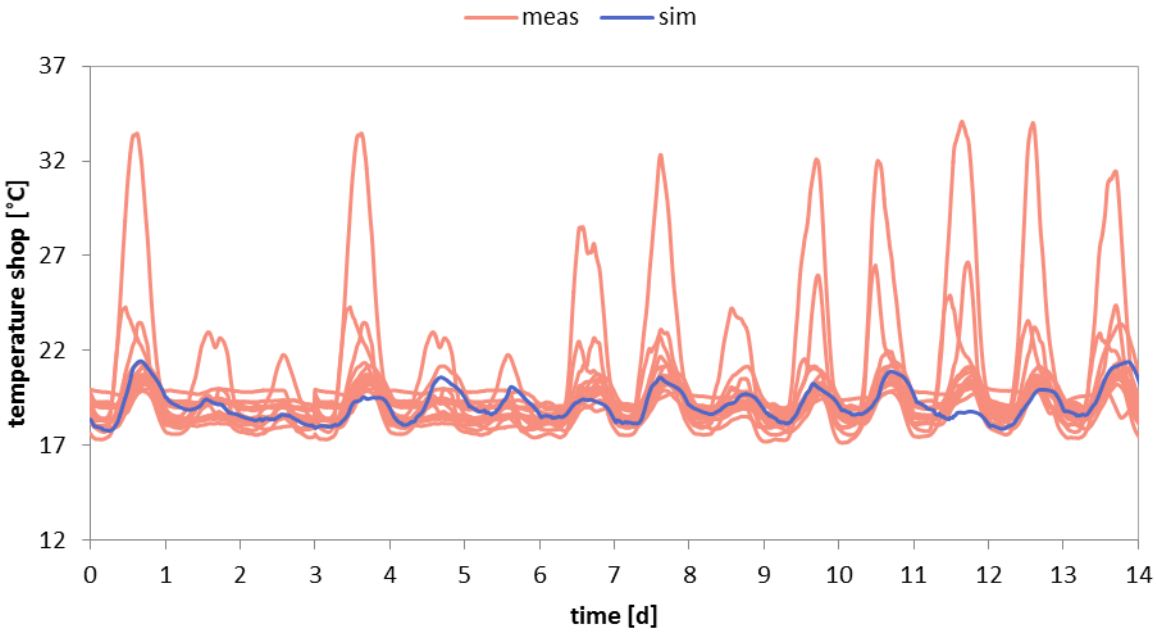

August: all shop temperatures

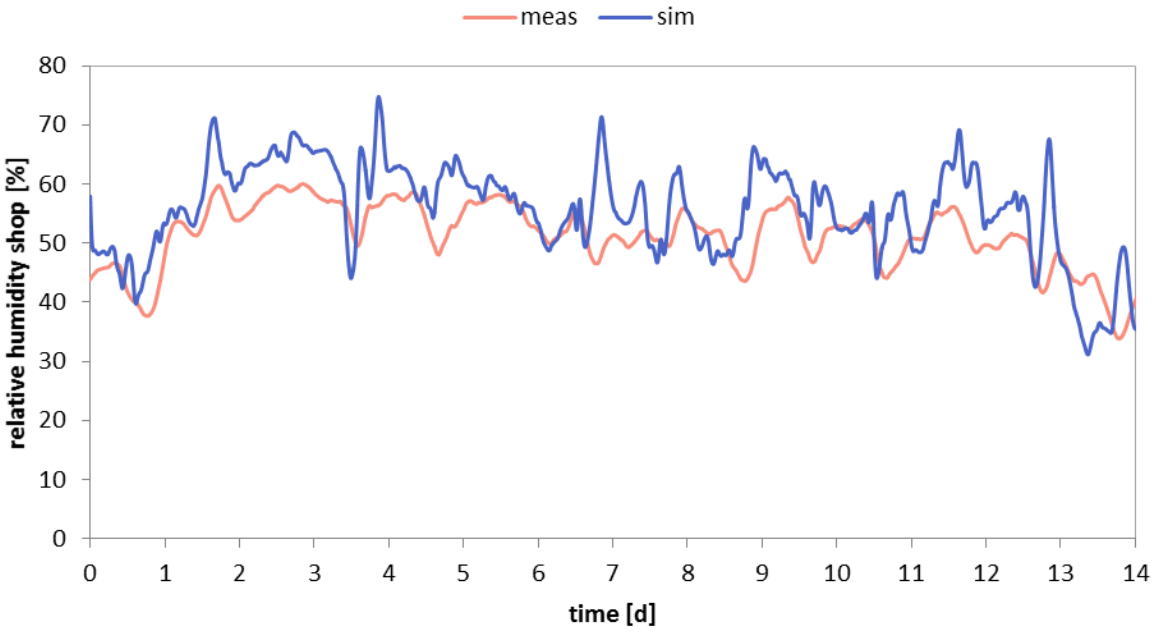

August: relative humidity shop

Appendix C

Simulation results

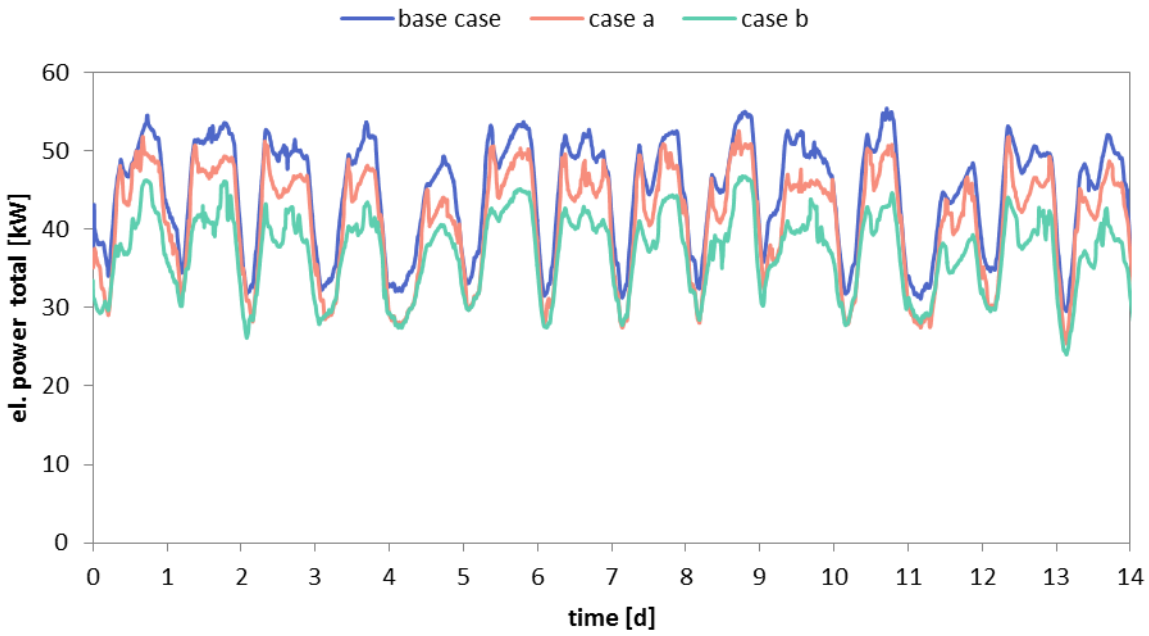

January: power consumption total

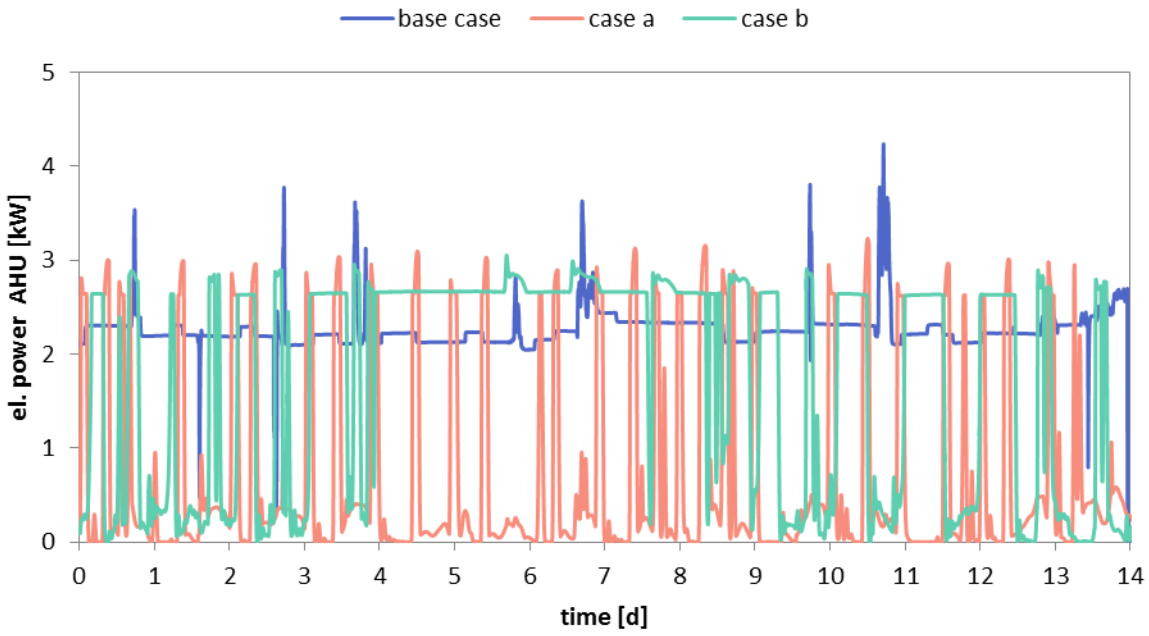

January: power consumption AHU

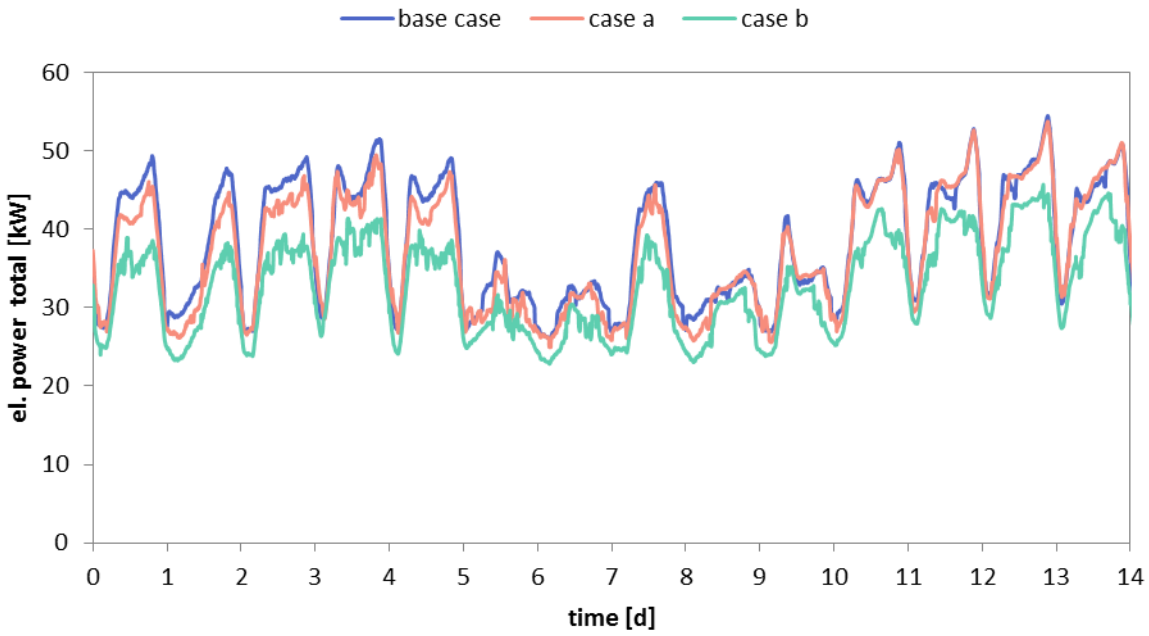

April: power consumption total

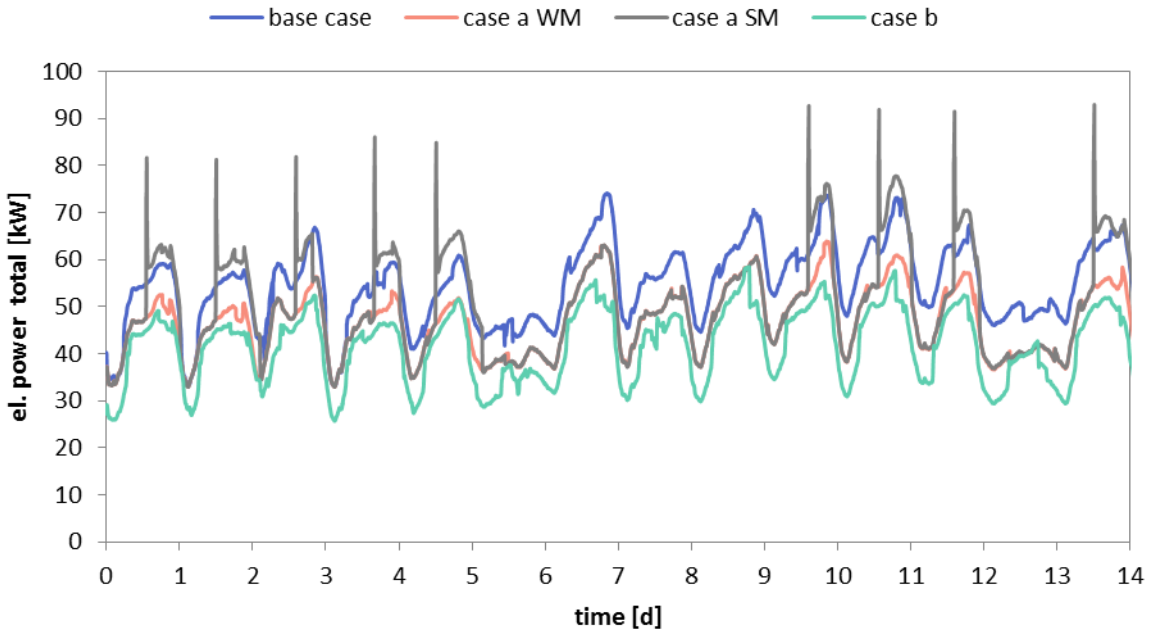

July: power consumption total

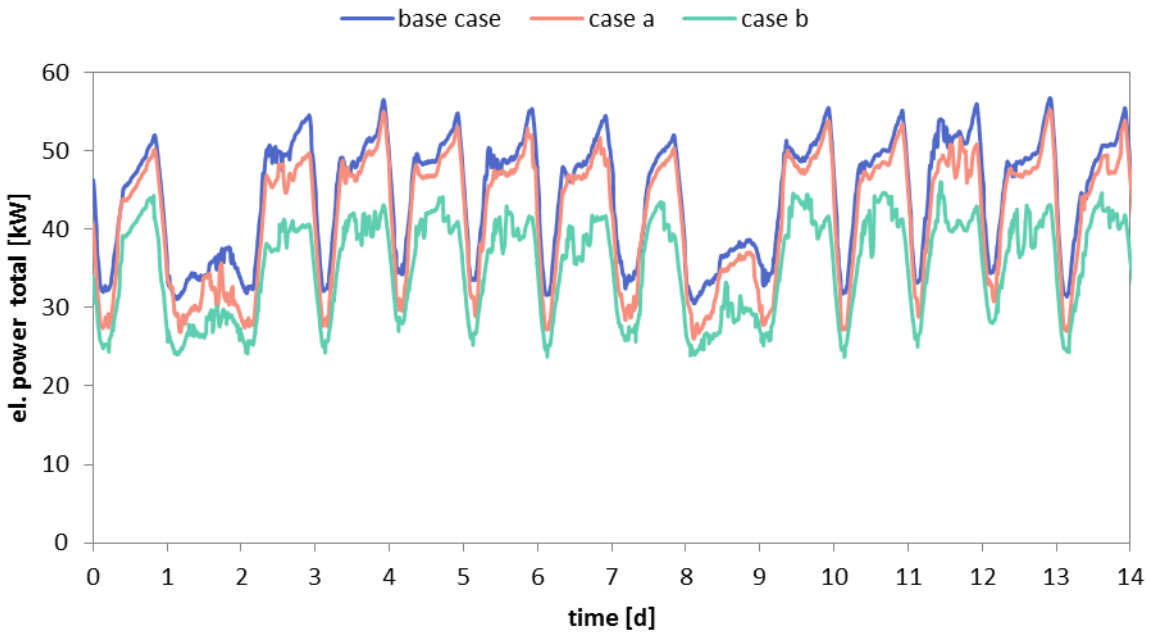

August: power consumption total

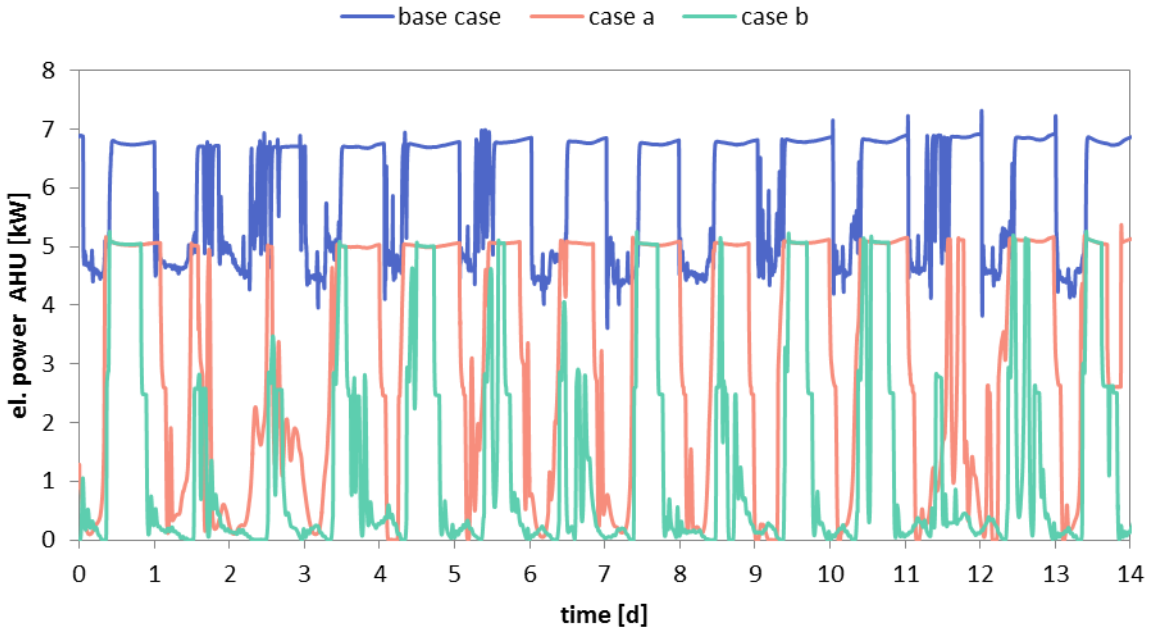

August: power consumption AHU